



UNIVERSITÀ DEGLI STUDI DI TRIESTE

**XXVII CICLO DEL DOTTORATO DI RICERCA IN
FISICA**

**TESTING NEW PHYSICS
WITH BOTTOM QUARKS
AT LHC:
A PRAGMATIC APPROACH.**

Settore scientifico-disciplinare: Fisica Nucleare e Subnucleare (FIS04)

Ph.D. STUDENT

GIANCARLO PANIZZO

DIRECTOR

PROF. PAOLO CAMERINI

SUPERVISORS

PROF. CLAUDIO VERZEGNASSI

PROF.SSA MARINA COBAL

ACADEMIC YEAR 2013 / 2014

Dedicated to

Φύσις

**Testing New Physics
with bottom quarks at LHC:
a pragmatic approach.**

Giancarlo Panizzo

Submitted for the degree of PhD
February 19, 2015

Abstract

This work discusses how Bottom-quark physics at the Large Hadron Collider (LHC) can be used as a probe to hint to Beyond the Standard Model Physics from a phenomenological point of view. In this context, the calculation of three observables is presented, all related to the production of one boson (Z , or a Higgs particle of Beyond the Standard Model nature) in association with a bottom-quark.

The Polarization Asymmetry of the Z -boson produced in association with a b -quark is computed at Leading Order, using the 5-flavours number scheme, assuming it is measured at the LHC with a center of mass energy of 14 TeV. It is shown how this observable can be used for an accurate determination of the A_b parameter, measured at the Stanford Linear Collider (and, indirectly, at the Large Electron Positron), and known to be in tension with its Standard Model prediction: this strongly motivates its new, independent, determination at the LHC. As an estimate of the theoretical uncertainties affecting the prediction of the Polarization Asymmetry, this is re-computed varying both the renormalization/factorization scale and the Parton Density Function set, showing its strong stability against such effects.

The Forward-Backward asymmetry of the b -quark produced in association with a leptonically decaying Z -boson, firstly defined by the candidate, is computed at LO in the 5-flavours number scheme. It is here shown that this observable inherits, from the Polarization Asymmetry of the Z -boson in the same process, stability

under factorization/renormalization scale variations and PDF-set choice. For this observable, directly accessible by the LHC experimental collaborations, a complete feasibility study is presented in this work, simulating, with modern tools (MadGraph, PYTHIA, Delphes), both the showering/hadronization processes and the detector response, assuming a final integrated luminosity of 400 fb^{-1} with 14 TeV in the center of mass of the colliding proton beams. This allows to determine, for the Forward-Backward asymmetry, an upper bound on the leading experimental systematic and statistical uncertainties at the next LHC run.

Finally, the production cross section of a light Higgs boson in association with one b -quark is computed at Next-to-Leading Order in α_{em} in the framework of the Next-to-Minimal Supersymmetric Standard Model. The calculation has been done in the 5FNS, using, respectively, the $\overline{\text{DR}}$ renormalisation scheme to manage Ultraviolet divergencies, and the soft-photon approximation to treat consistently Infrared divergencies. This is the first calculation of the Electromagnetic NLO effect in the NMSSM, which shows a relevant relative magnitude respect to the LO determination of genuinely NMSSM nature.

Declaration

The work in this thesis is based on research carried out at the Trieste University and ATLAS Udine group, the Department of Physics, Italy. No part of this thesis has been submitted elsewhere for any other degree or qualification and it is all my own work unless referenced to the contrary in the text.

Copyright © 2014 by Giancarlo Panizzo.

“The copyright of this thesis rests with the author. No quotations from it should be published without the author’s prior written consent and information derived from it should be acknowledged”.

Acknowledgements

Thanks to my supervisors prof. Claudio Verzegnassi and prof. Marina Cobal. Thanks to my colleagues both of the Phd School and of ATLAS Udine Group, and in particular to Dr. Michele Pinamonti and Dr. Rachik Soualah.



Contents

Abstract	III
Declaration	IV
Acknowledgements	v
Introduction	1
1 Framework	3
1.1 The Standard Model	3
1.2 LHC and the ATLAS experiment	5
1.3 The ATLAS detector	8
1.3.1 Electrons	10
1.3.2 Muons	11
1.3.3 Jets	11
1.3.4 b -jets reconstruction	13
1.4 Bottom production in association with massive neutral bosons	15
2 The Z-boson Polarization Asymmetry in the bZ-associated production at LHC	17
2.1 A “LEP Paradox”	17
2.2 The Z polarization asymmetry at tree-level	20
2.3 Impact of the scale/PDF choices and radiative corrections	25
2.4 Conclusions	28

3	New Physics constraints from A_{FB}^b at LHC	29
3.1	Introduction	29
3.2	Helicity amplitudes for the process $bg \rightarrow b\bar{l}\bar{l}$	30
3.3	Definition of $A_{FB}^{b,\text{LHC}}$	34
3.4	Testing New Physics through $A_{FB}^{b,\text{LHC}}$	38
3.4.1	Corrections to \mathcal{A}_b in the (N)MSSM	38
3.4.2	Corrections to \mathcal{A}_b in models with additional bottom partners	42
3.5	Jet charge determination and Q_{FB} at LHC	44
3.6	Feasibility study	45
3.6.1	MadGraph 5	46
3.6.2	The study	46
3.6.3	Impact of $A_{FB}^{b,\text{LHC}}$	48
4	bH_{light} associated production in the NMSSM at LHC at One-Loop Order	51
4.1	Motivations for the NMSSM	51
4.2	The NMSSM Higgs Sector	57
4.3	Motivations for a study of the NMSSM bH_{light} associated production	61
4.4	Born Level cross section	62
4.5	One-Loop structure	63
4.5.1	Relevant Counterterms	64
4.6	Numerical Analysis	68
4.6.1	Numerical Checks	68
4.6.2	Benchmarks	70
4.6.3	Results	73
	Conclusions	77
	Appendix	79
A	Useful results	79

B	The code <i>Beauty</i>	81
B.1	FeynArts Model file [147]	81
B.1.1	Checks of the model	82
B.1.2	Counterterms implementation	82
B.1.3	Restrictions	84
B.2	Fortran Model files	84
B.2.1	Basic Parameters	85
B.2.2	Intrinsic NMSSM parameters	85
B.2.3	Higgs sector masses and mixings	85
B.2.4	Gauginos masses and mixings	87
B.2.5	Sfermions, soft SUSY breaking parameters	87
B.2.6	Sfermions, masses and mixings	88
B.2.7	Routines description	88
B.3	Change of variables in <code>lumi_hadron.F</code>	89
	Bibliography	91
	Bibliography	91



List of Figures

1.1	A schematic view of the CERN experiments. The Large Hadron Collider (grey) has four intersection points at which sit the corresponding experiments.	6
1.2	Peak and integrated luminosities registered by the four LHC experiments as a function of the 8 TeV pp collision data taking day in 2012.	7
1.3	The ATLAS detector.	9
1.4	Flow chart of the generic clustering procedure.	12
1.5	Schematic view of a b -hadron decay inside a jet [16], resulting in a secondary vertex with three charged particle tracks. The vertex is significantly displaced with respect to the primary vertex, thus the decay length is macroscopic and well measurable. The track impact parameter, which is the distance of closest approach between the extrapolation of the track and the primary vertex, is shown in addition for one of the secondary tracks.	13
1.6	Charm rejection rates [16] as a function of the b -tagging efficiency for jets stemming from simulated $t\bar{t}$ events produced according to the SM predictions. The performance of several b -tagging algorithms (the MVb, blue line, and the MVbCharm, gray line) is compared to the one of the MV1 (black line) and the MV1c (green line) algorithm. . .	14
1.7	Feynman diagrams for $gb \rightarrow bX_0$ production.	15

2.1	Born diagrams for the associated production of a Z -boson and a single b -quark.	20
2.2	Polarization asymmetry $A_Z^{pol,b}$ in b - Z production at LHC with $\sqrt{s}=7$ TeV. The green band displays the $\pm 1\sigma$ bounds [23] for the measured asymmetry parameter \mathcal{A}_b while the SM prediction [23] is shown in red. . .	25
2.3	Polarization asymmetry $A_Z^{pol,b}$ as a function of \mathcal{A}_b for three different choices of factorization and renormalization scales, respectively μ_F and μ_R , $\mu_F = \mu_R = k\mu_0$ with $\mu_0 = M_Z$ and $k=1, 3$ and $1/3$	26
2.4	$A_Z^{pol,b}$ as a function of \mathcal{A}_b , for three different choices of pdf sets, as described in the text.	27
3.1	5FNS LO Feynmann diagrams for the process $bg \leftrightarrow b\bar{l}$	30
3.2	The coordinate system defined in the text. In blue the colliding partons momenta. The polar axis of the helicity frame coincides with the momentum of the outgoing b' (green arrow). Momenta of lepton and antilepton are represented by the red and orange arrows.	32
3.3	Event level (<i>i.e.</i> without parton showering) dependence of the asymmetry defined in the text on A_{FB}^b , in a ficticiously wide range of A_{FB}^b values, aiming to prove the direct proportionality also in the presence of typical kinematic cuts [63] on decay products pseudorapidities and transverse momenta. The uncertainty on k is only numerical, <i>i.e.</i> related to MC statistics (see the text for other uncertainties).	36
3.4	Comparison between the LO $\mu_F = \mu_R = kM_Z$ scale variation dependencies of the total cross section and our asymmetry.	37
3.5	Comparison of different pdf set LO asymmetry predictions taking CTEQ6L1 as a reference.	37
3.6	Higgs loop contributions to $\delta\rho_{b,v}$ and $\delta\kappa_{b,v}$. M_S is a common mass scale for light squark generations, on which however results are not quite sensitive. The green band represents the 95% C.L. exclusion from [32]. The green straight line gives the exact limit contour, while the dashed one is an extrapolation, since results of [27] are not sufficient to draw the net 95% limit contour.	39

3.7	The MSSM, NMSSM and SM predictions for ρ_b and $\sin^2 \theta_{eff}^b$, compared with the LEP/SLD data at 68%, 95.5% and 99.5% confidence level. The MSSM predictions are from a scan over the parameter space.	41
4.1	Latest combined 95 % C.L. exclusion limits for direct production of electroweakinos from the ATLAS and CMS experiments, as presented at the 37th International Conference on High Energy Physics (ICHEP 2014). Proceedings of this conference will be published in Nuclear Physics B - Proceedings Supplements (NUPHBP)).	53
4.2	Relevant Feynman graphs at Born Level.	63
4.3	Internal Self Energies. Scalars, Fermions and Vectors are labelled as S , F and V	64
4.4	s -channel triangular diagrams contributing to EW one-loop corrections.	65
4.5	u -channel triangular diagrams contributing to EW one-loop corrections.	66
4.6	Boxes.	67
4.7	Soft photon radiation from external charged particles.	69
4.8	Results for case A.1 in terms of K factors. The dependence of the single virtual and real contributions on the soft photon mass regulator λ cancel in the total, UV and IR finite one-loop complete EW correction, shown in black.	74
4.9	Results for case A.2 in terms of K factors.	75
4.10	Results for case D.2 in terms of K factors.	76

List of Figures

List of Tables

1.1	The SM field content.	3
3.1	Generated events and input parameters. Systematic errors on flavour fractions and δ_f are irrelevant given the estimated statistical uncertainty on the final results, while they should be taken into account (comprising possible effects giving $\delta^f \neq -\delta^{\bar{f}}$) in a possible HL-LHC upgrade.	47
3.2	Results (times a factor 10^4) for an integrated luminosity of 400 fb^{-1} for both electron and muon channels, assuming lepton universality. . .	48
4.1	Relevant parameters defining scenario A.1. The values $ \mathcal{R}_{H_1 h_s}^S ^2, \mathcal{R}_{A_1 a_s}^{P\star} ^2$ should be intended here, with a slight abuse of notation, as one-loop quantities, <i>i.e.</i> the absolute squares of the rotation matrices which relates tree level states to <i>one-loop corrected</i> states.	71
4.2	Relevant parameters defining scenario A.2.	72
4.3	Relevant parameters defining scenario D.2.	73
4.4	Predictions for the semi inclusive NMSSM h_1^0 production cross sections in association with a $p_T > 25 \text{ GeV}$ b -jet at 13 TeV LHC, both at LO and EW NLO for benchmark points defined in the text.	73

Introduction

The Higgs Boson discovery has been only the last of the successful predictions of the Standard Model of Particle Physics. Before its discovery, its mass range, compatible with SM predictions of several observables was indeed calculable by global fits [3], in which the model was considered as a function of its parameters and fitted to the measured values of these quantities by means of minimization of an appropriate χ^2 . It is well known that the measured value of the Higgs mass has fallen amazingly well not only in the resulting allowed 95% Confidence Level region, but also in the 68% one. What is intriguing is that bottom quark observables entering the global fit are known to be in some tension with their SM prediction, increasing the *value* of the minimum χ^2 found. The attitude and motivation of this work is to take this as a starting fact, beyond its interpretation, to understand how much New Physics can be tested at future runs of the Large Hadron Collider (LHC), using bottom-quark physics as a probe.

This thesis in fact describes recent developments concerning new definitions and accurate predictions of measurable observables involving bottom-quarks at LHC. It is opinion of the author that these observables have good chances to become little cornerstones in New Physics (NP) searches at the next Run of LHC, being intimately related either to well known discrepancies in Standard Model (SM) precision tests or to direct searches of Supersymmetric particles.

Chapter 1 is a short presentation of the SM as the most general $SU(3)_c \times SU(2)_L \times U(1)_Y$ gauge invariant Lagrangian with a definite particle content, with a brief discussion about what are nowadays considered its weaknesses both from the theoretical (Hierarchy problem, Naturalness) and the experimental point of view

(neutrino masses, Dark Matter). It describes also the general framework of the thesis.

In **Chapter 2** a Large Electron Positron (LEP) paradox is introduced, as a motivation to define the Polarization Asymmetry of the Z boson in the bZ associated production at LHC, including a detailed description of its theoretical properties and predictions at LHC. The candidate original work in this part has been the numerical computation of the prediction of this observable and of its theoretical uncertainties.

In **Chapter 3** the Forward-Backward asymmetry in the bZ associated production at LHC is defined as found by the candidate, explaining its connection with the Polarization Asymmetry of the Z boson described in the previous chapter. All experimental methods needed for its precise measurement at the next LHC Runs are explained in details, in particular the ones first defined by the candidate (like Q_{FB}^b , adapted from LEP). A complete original feasibility study at LHC and at future colliders ends this chapter.

Chapter 4 is dedicated to NP. It describes the first one-loop calculation of the associated production of bottom-light (non standard) Higgs cross section in the Next to Minimal Supersymmetric Standard Model (NMSSM) at LHC, as computed by the candidate.

Chapter 1

Framework

1.1 The Standard Model

One of the powerful features of gauge theories, besides that of describing surprisingly well particle physics, is that, to have a complete description of their phenomenology, it suffices to define the gauge group under which the associated Lagrangian is invariant and the relative transformation properties of its field content (we *assume* Lorentz invariance of the theory). This fix unambiguously mutual particles interactions, and consequently the described phenomena. As an example, the most general

Field	Lorentz	$SU(3)_c$	$SU(2)_L$	$U(1)_Y$
g	(1,1)	8	1	0
W	(1,1)	1	3	0
B	(1,1)	1	1	adj.
Q_i	$(0, \frac{1}{2})$	3	2	1/6
u_i^c	$(0, \frac{1}{2})$	$\bar{3}$	1	-2/3
d_i^c	$(0, \frac{1}{2})$	$\bar{3}$	1	1/3
L_i	$(0, \frac{1}{2})$	1	2	-1/2
e_i^c	$(0, \frac{1}{2})$	1	1	1
H	(0,0)	1	2	1/2

Table 1.1. The SM field content.

$SU(3)_c \otimes SU(2)_L \otimes U(1)_Y$ invariant (renormalizable) Lagrangian with field content

given in Table 1.1 defines univocally¹ the general features of the so-called *Standard Model* (SM), the modern theory describing amazingly well most of the known particle physics. From the theoretical point of view, the particular field content choice is somewhat arbitrary: this is immediately fixed once we agree that our theory should eventually describe Nature. This will simultaneously fix also the *phase* characterising the theory under consideration: in the SM in fact the gauge group is actually *softly broken* down to $SU(3)_c \otimes U(1)_{em}$ by the vacuum expectation value of the Higgs field H , which constitutes the minimal field choice able to simultaneously brake the gauge group to the phenomenologically correct pattern and preserve the so-called *custodial* symmetry [5]. Remarkably, the (renormalizable) SM predicts neutrinos as massless, since no $SU(2)_L$ singlet is present with appropriate $U(1)_Y$ charge to allow the needed Yukawa interaction and the derived Dirac mass term (curiously, or suggestively depending on the point of view, such a field would be *sterile* as seen from the SM gauge group). This has been historically imposed ab initio since neutrinos were introduced in the weak interactions exactly with the phenomenological requirement of being massless. Today it is well known [6] that neutrinos cannot be exactly massless. The only way to allow Majorana masses for neutrinos without altering the SM field content could be to allow also non-renormalizable terms in the Lagrangian, in which case also their smallness might be understood in terms of the magnitude of an associated high mass scale. This is one of the reasons why the SM is now-a-days considered an *effective theory* of a more complete, renormalizable one, valid at higher energies. This however introduces a deeper issue related to the magnitude of the electroweak scale, the so-called *hierarchy* problem. Phenomenologically it is indeed clear that, whatever particular choice of fundamental, “parent” theory we choose (neutrino mass is only one example of phenomenon calling for an underlying theory), its scale should be decisively higher than the electroweak scale (with a magnitude depending of course on the underlying theory). This kind of *hierarchy* between scales poses a theoretical enigma, namely how it is possible to

¹The *form* of the several interactions is univocally fixed, experiments will *measure* the actual couplings.

achieve such a separation of scales, possibly in a *natural* way. Both (partial) composite Higgs models and Supersymmetric theories try to answer one aspect of this problem. Possibly, a satisfactory extension of the SM should also take into account another modern intriguing puzzle: cosmological observations suggest in fact that ordinary matter, *i.e.* the one described by the SM, constitutes only roughly 4% of the gravitationally interacting content of the universe. A stable, possibly only weakly interacting new particle could explain at least part of this problem, constituting the so-called *dark matter* candidate. Regarding this, one should mention also the fact that another possible direction toward which the SM (as well as its supersymmetric versions) could be extended, this time in a renormalizable way, is to realize that also a *scalar* singlet could be easily embedded, since this would equally be custodial symmetry preserving.

1.2 LHC and the ATLAS experiment

The Large Hadron Collider (LHC [7]) is presently the largest and highest-energy particle accelerator in the world. It is located at CERN, inside a 27 km long circular tunnel at a depth varying between 50 and 175 meters below the ground, which also housed the Large Electron Positron collider (LEP).

The LHC can provide both proton-proton (pp) and heavy ion (HI) collisions. For pp collisions, the design luminosity is $10^{34} \text{ cm}^{-2}\text{s}^{-1}$ and the design centre-of-mass energy for the collisions is 14 TeV. The LHC started its operations in 2008, and during 2010 and 2011 runs, collisions at 7 TeV centre-of-mass energy have been provided. After a short shut-down period, on February 2012 the beam energies have been raised to get to the final run at 8 TeV in the center-of-mass. The maximum instantaneous luminosity reached in 2010 is slightly higher than $2 \times 10^{32} \text{ cm}^{-2}\text{s}^{-1}$, while during the 2011 run a peak of $\sim 4 \times 10^{33} \text{ cm}^{-2}\text{s}^{-1}$ has been achieved. The maximum instantaneous luminosity in 2012 has been $\sim 8 \times 10^{33} \text{ cm}^{-2}\text{s}^{-1}$.

The LHC is mainly composed by superconducting magnets, operating at a temperature of 1.9 K, provided by a cryogenic system based on liquid Helium. The LHC is equipped with a 400 MHz superconducting cavity system and it is made of

the Standard Model (BSM). LHCb has instead been designed especially to study b -physics, and ALICE to study the formation of the so-called quark-gluon plasma through HI collisions. Colliding particles are grouped together into a number of bunches, each containing $\sim 10^{11}$ protons. The design number of bunches is 2808, so that interactions happen every 25 ns. During the commissioning phase, the number of colliding bunches has been progressively increased to reach the design value. At the end of 2010 the maximum number of colliding bunches has been 348, while 1092 has been then reached in June 2011. In April 2012, after the increase in beam energies from 3.5 TeV to 4 TeV, the maximum number of colliding bunches reached 1380. Before being injected into the LHC, particles are accelerated step by step up to the energy of 450 GeV, by a series of accelerators. For protons, the first system is the linear accelerator LINAC2, which generates them at an energy of 50 MeV. A chain of subsequent accelerating steps follows: through the Proton Synchrotron Booster (PSB), protons reach 1.4 GeV; the Proton Synchrotron (PS), brings them to 26 GeV and, finally, the Super Proton Synchrotron (SPS) is used to further increase their energy to 450 GeV.

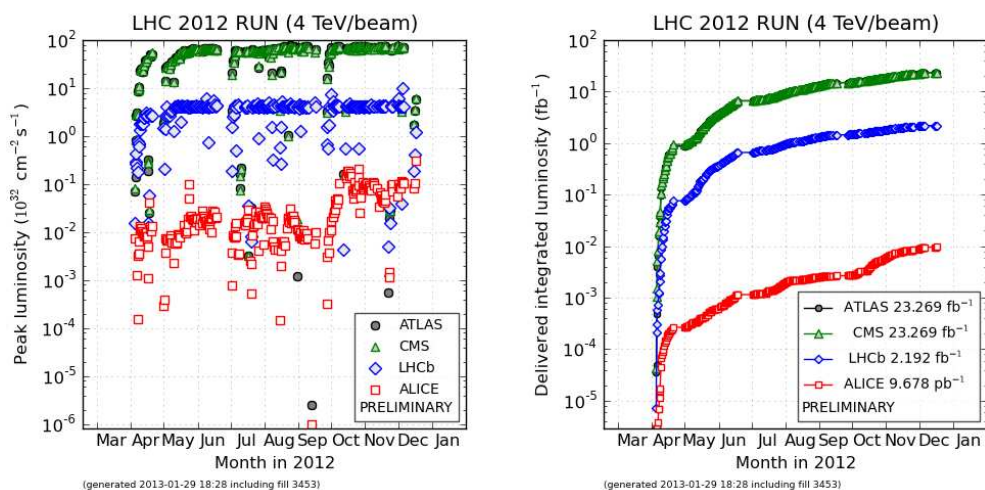


Figure 1.2. Peak and integrated luminosities registered by the four LHC experiments as a function of the 8 TeV pp collision data taking day in 2012.

The LHC started its operations on September 10th 2008, with the first beams

circulating into the rings, in both directions, without collisions. After a commissioning phase, the first collisions were expected few days later. Unfortunately, on September 19th a major accident happened, causing a long stop of the machine. During Autumn 2009, after more than one year, the operations started again, with the first collisions at a centre-of-mass energy of 900 GeV recorded by the four experiments on 23 November 2009. First collisions at 7 TeV were registered on March 2010, reaching the total delivered integrated luminosity at this energy of 5.46 fb^{-1} at the end of 2011. The 8 TeV run started in 2012, delivering a total integrated luminosity of 22.8 fb^{-1} at this energy.

1.3 The ATLAS detector

The ATLAS experiment is positioned at Point 1, in a cavern at a depth of 100 m. With its height of 25 m and its length of 44 m, it is one of the biggest detectors ever built. It weights about 7000 tons and it is cylindrically symmetric. After the cavern was completed, the construction started in 2003 and it went on until July 2007. Since 2009 it has been recording cosmic-ray events and, since November 2009, pp collision events at rates of up to 200 Hz.

The ATLAS detector is composed of different sub-detectors, as shown in Figure 1.3. Each of them plays an important role in the particles reconstruction. The sub-detectors are arranged in cylindrical layers around the interaction point. Closest to the beam pipe is the Inner Detector (ID), used to reconstruct the trajectory of charged particles. The ID is enclosed by a solenoidal magnet, which provides a strong magnetic field to bend the charged particles and measure their momentum and charge. The Electromagnetic (EM) Calorimeter surrounds the ID and is designed to precisely measure the energy of electrons and photons. Outside the EM Calorimeter there is the Hadronic (Had) Calorimeter, which measures the energy of hadronic particles. Finally, the calorimeters are enclosed by the Muon Spectrometer (MS), designed to reconstruct and identify muons, which usually escape the previous detector layers. The MS is embedded in a toroidal magnetic field and consists in tracking chambers, to provide precise measurements of momentum and charge, and

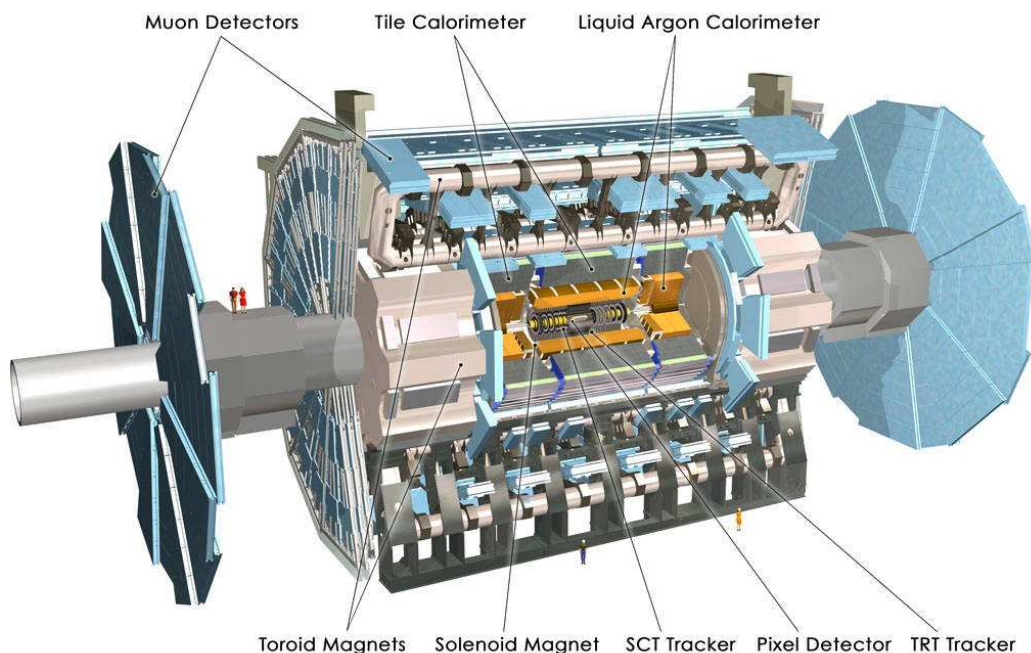


Figure 1.3. The ATLAS detector.

detectors used for fast triggering. ATLAS includes a three-level trigger system for evaluating and recording only the most interesting events during a run. The trigger is configurable at every level to provide a constant stream of data under any beam conditions.

The coordinate system is defined taking the nominal interaction point as the origin. The z -axis is parallel to the beam and the x - and y - axes belongs to the plane perpendicular to the beam, forming a right-handed cartesian coordinate system, where x points towards the centre of the LHC ring and y points upward. The x - y plane is called the transverse plane. The azimuthal angle, ϕ , is measured around the z -axis, while the polar angle, θ , is measured from the z -axis. The *pseudorapidity* is defined as

$$\eta = -\ln \tan(\theta/2),$$

and it is often preferable as a polar coordinate than the angle θ itself, since pseudorapidity spectra are invariant under Lorentz boosts along z -axis for massless particles. The distance ΔR in η - ϕ space is defined as $\Delta R = \sqrt{\Delta\eta^2 + \Delta\phi^2}$. Particles are often

described by their transverse momentum p_T and transverse energy E_T (projections onto the transverse plane), as these variables are a better indicator of interesting physics than the standard energy and momentum, and since they are assumed to vanish for the colliding partons in the initial state.

In the following, the way the physics objects are reconstructed in ATLAS is briefly described.

1.3.1 Electrons

Electron reconstruction and identification algorithms are designed to achieve both a large background rejection and a high and uniform efficiency for isolated high-energy ($E_T > 20$ GeV) electrons over the full acceptance of the detector. Isolated electrons need to be separated from hadron decays in QCD jets and from secondary electrons originating mostly from photon conversions in the tracker material. Electron reconstruction is based on the identification of a set of clusters in the EM Calorimeter [12]. For each reconstructed cluster, the reconstruction algorithm tries to find a matching track in the ID. While the energy of the electron is determined using the calorimeter information, the more precise angular information from the ID track is used. The corrections applied to the measured cluster energy are based on precise Monte Carlo (MC) simulations, validated by comprehensive measurements with 900 GeV data [13]. The baseline ATLAS electron identification algorithm relies on variables which deliver good separation between isolated electrons and fake signatures from QCD jets. These variables include information from the calorimeter, the tracker and the matching between tracker and calorimeter. Cuts are applied on the energy in the Had Calorimeter inside the electron cone, on the shape of the electromagnetic shower, on the track impact parameter, on the number of hits in the different layers of the ID, on the difference between the calorimeter cluster and the extrapolated track positions in η and ϕ , on the ratio of the cluster energy to the track momentum ratio. Electrons passing all the identification requirements are called *tight* electrons, while *loose* and *medium* electrons pass only some of the above listed requirements.

1.3.2 Muons

Muon reconstruction is based on information from the MS, the ID and the calorimeters. Different kinds of muon candidates can be built, depending on how the detector information is used in the reconstruction. In the analyses described in this thesis, the so-called *combined* muons are used. The information from the MS and from the ID is combined through a fit to the hits in the two sub-detectors to derive the muon momentum and direction.

1.3.3 Jets

Hadronic particles deposit their energies mainly in the calorimeter system. In an attempt to resolve particles coming from the hard scatter, these energy deposits may be grouped into objects called jets. The mapping from partons to jets is a complex problem and it depends strongly on which one is the jet algorithm used. Many solutions have been used or proposed to define jets. In ATLAS the so-called anti- k_T algorithm [14] has been adopted as default. It is part of the wider class of “Cluster Algorithms”, based upon pair-wise clustering of the initial constituents. Two “distances” are defined: d_{ij} between entities (particles, proto-jets) i and j and d_{iB} between entity i and the beam (B):

$$d_{ij} = \min(k_{T,i}^{2p}, k_{T,j}^{2p}) \frac{\Delta R_{ij}^2}{\Delta R^2}, \quad d_{iB} = k_{T,i}^{2p}, \quad (1.3.1)$$

with $\Delta R_{ij}^2 = (y_i - y_j)^2 + (\phi_i - \phi_j)^2$, and respectively $k_{T,i}$, y_i and ϕ_i the transverse momentum, the rapidity and the azimuthal angle of particle i . The generic clustering procedure is explained in the flow chart depicted in Fig. 1.4. What characterises the particular algorithm are the two real parameters ΔR and p . To intuitively understand their meaning, one may first realize that, from inspection of Eq. (1.3.1), it is clear that, for large values of ΔR , the d_{ij} are smaller, and thus more merging takes place before jets are complete. The p parameter, instead, causes a preferred ordering of clustering: if the sign of p is positive, clusters with lower energy will be merged first, while if it’s negative the clustering will start from higher energy clusters. In the anti- k_T algorithm $p = -1$, meaning that objects with high relative

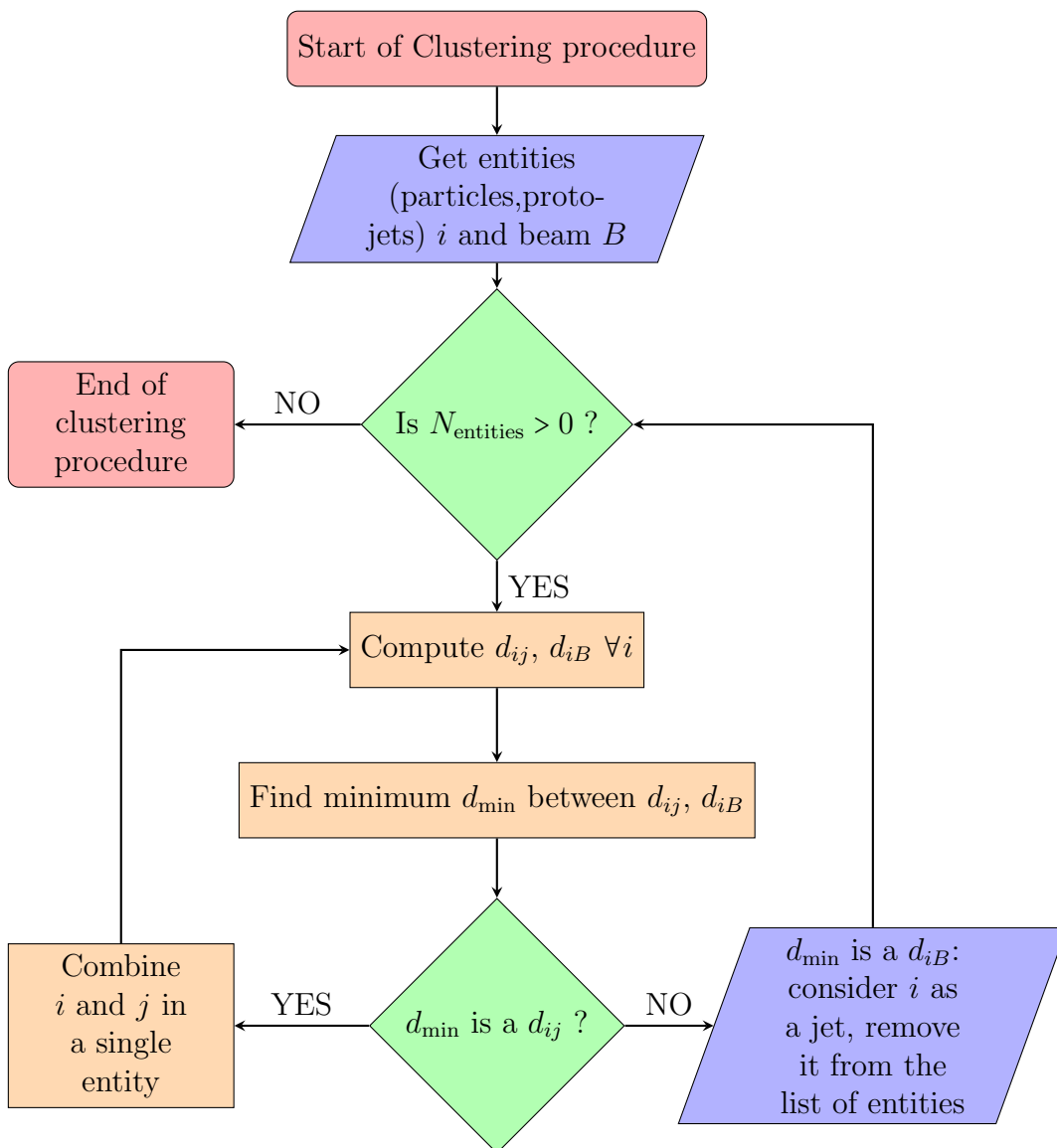


Figure 1.4. Flow chart of the generic clustering procedure.

momentum k_T are merged first. Compared to other jet algorithms (*cf.* [15] and references therein), anti- k_T is less sensitive to low energy constituents, its clustering procedure is faster, there is no need of introducing new parameters to decide whether two jets have to be split or merged (the “split & merge” procedure, present in the so-called Cone Algorithms) and the resulting jet area is more regular. The choice of the ΔR parameter is analysis dependent: the typical default values used in ATLAS

are $\Delta R = 0.4, 0.6$. For physical processes analysed in this thesis, characterized by medium-low QCD activity in the final state, the larger cone size is more suitable, so that $\Delta R = 0.6$ has been chosen.

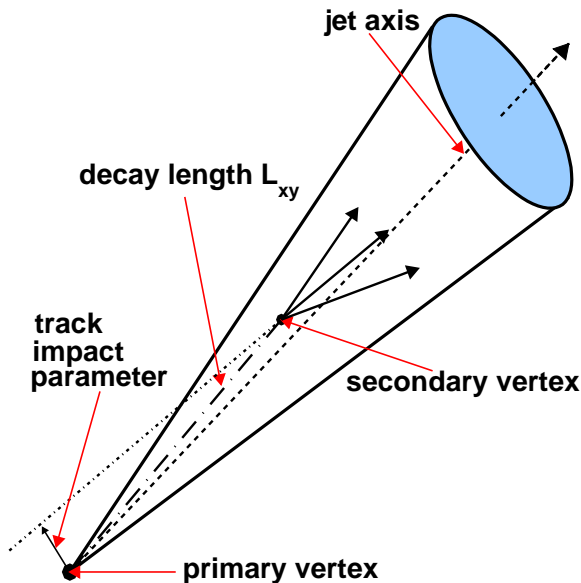


Figure 1.5. Schematic view of a b -hadron decay inside a jet [16], resulting in a secondary vertex with three charged particle tracks. The vertex is significantly displaced with respect to the primary vertex, thus the decay length is macroscopic and well measurable. The track impact parameter, which is the distance of closest approach between the extrapolation of the track and the primary vertex, is shown in addition for one of the secondary tracks.

1.3.4 b -jets reconstruction

The aim of b -tagging algorithms is to identify jets containing b -flavoured hadrons. To each selected jet they assign some measure of probability that it originates from a b -quark. The discrimination of b -quark jets from light quark jets takes advantage mainly of the relatively long life time of b -flavoured hadrons, resulting in a significant flight path length $L \sim \text{mm}$. This leads to measurable secondary vertices and impact parameters of the decay products, as shown in Figure 1.5. The transverse impact

parameter d_0 is the distance in the transverse plane (x,y) between the point of the closest approach of a track to the primary vertex; the longitudinal impact parameter z_0 is the z -coordinate of this point. Various b -tagging algorithms (or “taggers”) can be defined, based on these discrimination variables (L , d_0 and z_0), on secondary vertex properties and on the presence of leptons within b -quark jets. Each tagging algorithm defines a “weight” w , associated to the probability for a given jet to have been originated from a b -quark. For each tagging algorithm, different “working points”, i.e. different threshold on the w variable cut to define a “tagged” jet, can be used. The choice of the working point sets the tagging efficiencies for b -, c - and light quark jets. Figure 1.6 shows the charm quark rejection rates (defined as

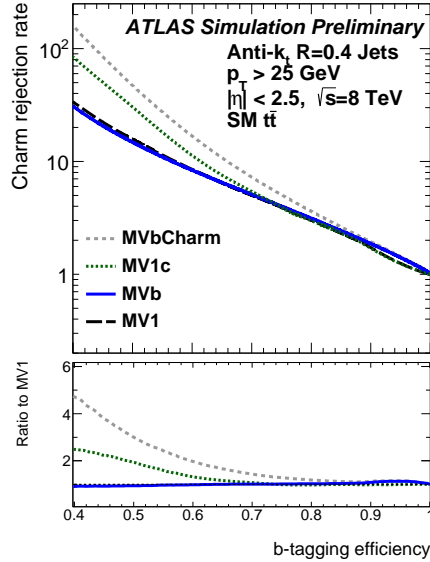


Figure 1.6. Charm rejection rates [16] as a function of the b -tagging efficiency for jets stemming from simulated $t\bar{t}$ events produced according to the SM predictions. The performance of several b -tagging algorithms (the MVb, blue line, and the MVbCharm, gray line) is compared to the one of the MV1 (black line) and the MV1c (green line) algorithm.

the inverse of the charm quark jet tagging efficiency) as a function of the b -quark jet tagging efficiency (also called simply b -tagging efficiency), obtained varying the working point for the different considered taggers.

1.4 Bottom production in association with massive neutral bosons

In a four-flavour scheme with no b -quarks in the initial state, the lowest order processes for associated production of a massive neutral boson X_0 in association with bottom quarks receive at tree level contributions from $gg \rightarrow b\bar{b}X_0$ and $q\bar{q} \rightarrow b\bar{b}X_0$. The inclusive cross section for $gg \rightarrow b\bar{b}X_0$ develops potentially large logarithms proportional to $\log(Q^2/m_b^2)$ which arise from splitting of gluons into $b\bar{b}$ pairs. Since $Q \gg m_b$, the splitting is intrinsically of order $\mathcal{O}(\alpha_s \log(Q^2/m_b^2))$, undermining convergence of the perturbative expansion. To improve the convergence one can sum the collinear logarithms at all orders in perturbation theory through the use of b -quark parton distributions (the five-flavours number scheme [4,17,18], 5FNS) at the factorization scale $\mu_F = Q$. This approach is based on the approximation that the outgoing b -quarks, for which one does not ask for a tag (from which the attribute *inclusive*), are at small transverse momentum. Thus the incoming b -partons are given zero transverse momentum at leading order, acquiring a transverse component at higher orders. In the 5FNS the counting of perturbation order involves both α_s and $1/\log(Q^2/m_b^2)$. In this scheme, the lowest order *semi*-inclusive process, *i.e.*

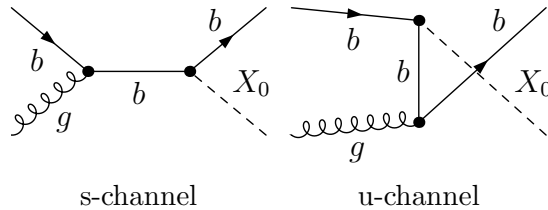


Figure 1.7. Feynman diagrams for $gb \rightarrow bX_0$ production.

when one requires exactly one b -tagged jet at high p_T , is $bg \rightarrow bX_0$, see Fig. 1.7. This process is sub-leading compared to the related inclusive one, dominated by the

tree level contribution $b\bar{b} \rightarrow X_0$, but is experimentally more appealing due to the presence in the final state of an high p_T b -jet, which in turns prevails by an order of magnitude [19] against the completely exclusive channel $gg \rightarrow b\bar{b}X_0$ (*i.e.* when both final b -jets are tagged). Of course in the case of the Z -boson ($X_0 = Z$) also light quarks fusion has a sizeable rate, but in this case the semi-inclusive choice has the additional, intriguing virtue of providing the possibility to inspect the flavour of the parton involved in the hard scattering.

Chapter 2

The Z -boson Polarization Asymmetry in the bZ -associated production at LHC

Introduction

The SM is confirmed up to per mil precision by collider data [20]; one of the latest (and biggest) successes is certainly the Higgs boson discovery [1,2], which continues to satisfy SM constraints the more experimental data are analysed [21] [22], with a mass consistent with predictions based on global fits to electroweak data [20].

The question arises of whether all the theoretical SM predictions are confirmed by the related experimental measurements. Nowadays the answer to this fundamental question is that at least one experimental result still appears in some tension (roughly, at 3σ level) with the SM, i.e. the measurement of A_{FB}^b , the forward-backward asymmetry of $b\bar{b}$ production at the Z peak [23].

2.1 A “LEP Paradox”

The polarized b - Z forward-backward asymmetry has been defined several years ago [53], and considered to be the best way of measuring, in a theoretical SM approach,

a combination of the polarized b - Z couplings. The definition of this quantity was chosen as

$$A_{FB}^{b,pol} = \frac{(\sigma_{e_L^- b_F} - \sigma_{e_R^- b_F}) - (\sigma_{e_L^- b_B} - \sigma_{e_R^- b_B})}{\sigma_{e_L^- b_F} + \sigma_{e_R^- b_F} + \sigma_{e_L^- b_B} + \sigma_{e_R^- b_B}}, \quad (2.1.1)$$

where $b_{F,B}$ indicates forward and backward outgoing bottom quarks respectively (a polarization degree of the incoming beam = 1 is for simplicity assumed). At the Z peak one may easily verify that

$$A_{FB}^{b,pol} = \frac{3 g_{Lb}^2 - g_{Rb}^2}{4 g_{Lb}^2 + g_{Rb}^2}, \quad (2.1.2)$$

where $g_{L,Rb}$ are the couplings of a left and right handed bottom to the Z . Calling

$$\mathcal{A}_b = \frac{g_{Lb}^2 - g_{Rb}^2}{g_{Lb}^2 + g_{Rb}^2}, \quad (2.1.3)$$

one finds that

$$A_{FB}^{b,pol} = \frac{3}{4} \mathcal{A}_b. \quad (2.1.4)$$

The quantity \mathcal{A}_b appears also in an unpolarized transition from an electron-positron to a $b - \bar{b}$ pair. One finds in that case that the unpolarized forward-backward b -asymmetry at the Z peak can be written as

$$A_{FB}^b = \frac{3}{4} \mathcal{A}_e \mathcal{A}_b, \quad (2.1.5)$$

where \mathcal{A}_e is the longitudinal electron polarization asymmetry [54]

$$\mathcal{A}_e = \frac{g_{Le}^2 - g_{Re}^2}{g_{Le}^2 + g_{Re}^2} \quad (2.1.6)$$

and equations Eq. (2.1.5) Eq. (2.1.6) can be extended to a different final quark-antiquark couple $f\bar{f}$, giving

$$A_{FB}^f = \frac{3}{4} \mathcal{A}_e \mathcal{A}_f, \quad (2.1.7)$$

where \mathcal{A}_f is the analogue of \mathcal{A}_b eq Eq. (2.1.3) with f replacing b . The direct measurement of \mathcal{A}_b , which requires the use of initially longitudinally polarized electrons, was performed with the Stanford Linear Collider (SLC) at the Stanford Linear Accelerator Center (SLAC) [55, 56], and the result was found to be in good agreement with the SM prediction [57]

$$\mathcal{A}_b^{SM, th} = 0.93464_{-0.00007}^{+0.00004}.$$

Later, LEP1 performed a number of unpolarized measurements at the Z peak from which the value of \mathcal{A}_b was derived. This was obtained from Eq. (2.1.7) and found to be in remarkable disagreement, at the 3σ level, with the SM prediction [58]. This result was in a certain sense unexpected, since the relative decay rate of the Z into bottom pairs $R(b) = \Gamma(Z \rightarrow b\bar{b})/\Gamma(Z \rightarrow \text{hadrons})$ provided a value

$$R_b \simeq g_{Lb}^2 + g_{Rb}^2 \quad (2.1.8)$$

in perfect agreement with the SM prediction [58]. Accepting the LEP1 result for \mathcal{A}_b , a search started of possible new physics models that might have cured the disagreement. In particular, it was concluded that a conventional MSSM was unable to save the situation [27]. This conclusion remained problematic, since no extra measurements of \mathcal{A}_b were eventually performed, and the emerging picture seems definitely unclear: that is what will be called here a “LEP paradox”, for obvious reasons¹.

In fact, a number of models have been proposed that might cure the discrepancy (see [24–26] and references therein). In particular, a slightly embarrassing fact for Supersymmetric models is the difficulty that simplest minimal versions, (N)MSSM, would face to eliminate the discrepancy, as exhaustively discussed in Ref. [27] (for a short review see next chapters).

The aim of this chapter is to show that a specific observable can be defined at LHC which can provide essentially a re-measurement of the LEP1 A_{FB}^b one, despite of having a completely different final state. This quantity is defined in the production of a b - Z pair as the ratio of the difference of production cross sections with different (left, right) Z polarizations (Z_L, Z_R) divided by the corresponding sum.

It will first be shown in Section 2 that this quantity is directly proportional to A_{FB}^b at the partonic Born level, providing a possible ten percent deviation from its SM prediction if the relevant parameters are chosen to reproduce the experimental LEP1 result for the asymmetry. In Section 3 some special properties of this new observable will be derived, *i.e.* the fact that its value remains stable against variations of the strong scales and of the adopted parton distribution functions (pdfs)

¹This should not be confused with the well known LEP paradox defined in [28].

as well as by electroweak corrections. This would represent a strong motivation to perform an accurate measurement of the asymmetry at LHC in a near future, as qualitatively discussed in the final conclusions.

2.2 The Z polarization asymmetry at tree-level

The process of associated production of a Z -boson and a single b -quark, as represented in Figure 2.1, is defined at parton level by two subprocesses $bg \rightarrow bZ$, involving Born diagrams with bottom quark exchange in the s -channel and in the u -channel.

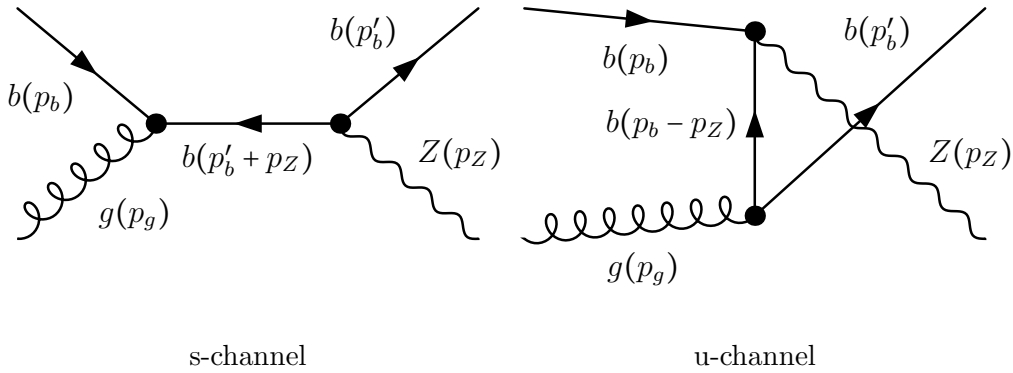


Figure 2.1. Born diagrams for the associated production of a Z -boson and a single b -quark.

This process has been calculated at next-to-leading order (NLO) in QCD in a previous paper [35] where the theoretical uncertainties assessment on cross section calculation have been addressed as well.

For the purposes of this work it is though needed a derivation of the expressions of the polarized cross sections. This requires a number of formulae that will briefly be shown in what follows, starting from the calculation of the various quantities performed at the Born level.

The interaction vertices involved in the diagrams of Figure 2.1 are defined as

$$gq\bar{q}: ig_s \not{\epsilon} \left(\frac{\lambda^l}{2} \right) \quad Zbb: -ie \not{\epsilon} (g_{Lb} P_L + g_{Rb} P_R) \quad , \quad (2.2.9)$$

Therefore, the Born invariant amplitude is given by

$$\begin{aligned} A^{Born}(gb \rightarrow Zb) &= eg_s \left(\frac{\lambda^l}{2} \right) \bar{u}(b') (\not{\epsilon} (g_{Lb} P_L + g_{Rb} P_R) \frac{(\not{q} + m_b) \not{\epsilon}}{s - m_b^2} \\ &\quad + \frac{\not{\epsilon} (\not{q}' + m_b) \not{\epsilon}}{u - m_b^2} (g_{Lb} P_L + g_{Rb} P_R)) u(b) \quad , \end{aligned} \quad (2.2.10)$$

where e, λ^l are the gluon polarization vector and colour matrix, ϵ is the Z polarization vector and $q = p_b + p_g = p_Z + p'_b$, $s = q^2$, $q' = p'_b - p_g = p_b - p_Z$, $u = q'^2$ with the kinematical decompositions

$$p_b = (E_b; 0, 0, p) \quad , \quad p'_b = (E'_b; p' \sin \theta, 0, p' \cos \theta) \quad , \quad (2.2.11)$$

$$p_g = (p; 0, 0, -p) \quad , \quad p_Z = (E_Z; -p' \sin \theta, 0, -p' \cos \theta) \quad , \quad (2.2.12)$$

$$e(g) = \left(0; \frac{\mu}{\sqrt{2}}, -\frac{i}{\sqrt{2}}, 0 \right) \quad , \quad \epsilon(Z_T) = \left(0; \frac{\mu' \cos \theta}{\sqrt{2}}, \frac{i}{\sqrt{2}}, \frac{-\mu' \sin \theta}{\sqrt{2}} \right) \quad , \quad (2.2.13)$$

$$\epsilon(Z_0) = \left(-\frac{p'}{M_Z}; \frac{E_Z}{M_Z} \sin \theta, 0, \frac{E_Z}{M_Z} \cos \theta \right) \quad . \quad (2.2.14)$$

The decomposition of Dirac spinors and polarization vectors leads to 24 helicity amplitudes denoted as $F_{\lambda\mu\tau\mu'}$ with $\lambda = \pm\frac{1}{2}$, $\mu = \pm 1$, $\tau = \pm\frac{1}{2}$, $\mu' = \pm 1, 0$ referring to b, g, b', Z respectively.

However, in order to quickly explore the properties of this subprocess, m_b/M_Z and m_b/\sqrt{s} terms can be neglected, considering only the following eight non-vanishing amplitudes: six transverse ones

$$F_{++++} = \frac{2eg_s g_{Rb} \sqrt{\beta'}}{\cos \frac{\theta}{2}} \quad , \quad F_{----} = \frac{2eg_s g_{Lb} \sqrt{\beta'}}{\cos \frac{\theta}{2}} \quad , \quad (2.2.15)$$

$$F_{+--+} = 2eg_s g_{Rb} \frac{\cos \frac{\theta}{2}}{\sqrt{\beta'}} \quad , \quad F_{-+-+} = 2eg_s g_{Lb} \frac{\cos \frac{\theta}{2}}{\sqrt{\beta'}} \quad , \quad (2.2.16)$$

$$F_{++++} = 2eg_s g_{Rb} \cos \frac{\theta}{2} \cdot \frac{M_Z^2}{s} \cdot \frac{\tan^2 \frac{\theta}{2}}{\sqrt{\beta'}} , \quad F_{----} = 2eg_s g_{Lb} \cos \frac{\theta}{2} \cdot \frac{M_Z^2}{s} \cdot \frac{\tan^2 \frac{\theta}{2}}{\sqrt{\beta'}} , \quad (2.2.17)$$

and two longitudinal ones

$$F_{++0} = -2\sqrt{2}eg_s g_{Rb} \frac{\sin \frac{\theta}{2}}{\sqrt{\beta'}} \cdot \frac{M_Z}{\sqrt{s}} , \quad (2.2.18)$$

$$F_{--0} = 2\sqrt{2}eg_s g_{Lb} \frac{\sin \frac{\theta}{2}}{\sqrt{\beta'}} \cdot \frac{M_Z}{\sqrt{s}} , \quad (2.2.19)$$

having defined

$$\beta' = \frac{2p'}{\sqrt{s}} \simeq 1 - \frac{M_Z^2}{s} . \quad (2.2.20)$$

For the present analysis, it is instructive to consider the Z density matrix

$$\rho^{ij} = \sum_{\lambda\mu\tau} F_{\lambda\mu\tau i} F_{\lambda\mu\tau j}^* . \quad (2.2.21)$$

A priori there are nine independent Z density matrix elements. However with the above Born terms and neglecting again the subleading terms in m_b they reduce to only five ones:

$$\rho^{++} = 4e^2 g_s^2 \left(\frac{g_{Rb}^2}{\cos^2 \frac{\theta}{2}} \left(\beta' + \frac{\sin^4 \frac{\theta}{2}}{\beta'} \left(\frac{M_Z^2}{s} \right)^2 \right) + g_{Lb}^2 \frac{\cos^2 \frac{\theta}{2}}{\beta'} \right) , \quad (2.2.22)$$

$$\rho^{--} = 4e^2 g_s^2 \left(\frac{g_{Lb}^2}{\cos^2 \frac{\theta}{2}} \left(\beta' + \frac{\sin^4 \frac{\theta}{2}}{\beta'} \left(\frac{M_Z^2}{s} \right)^2 \right) + g_{Rb}^2 \frac{\cos^2 \frac{\theta}{2}}{\beta'} \right) , \quad (2.2.23)$$

$$\rho^{00} = 8e^2 g_s^2 (g_{Rb}^2 + g_{Lb}^2) \sin^2 \frac{\theta}{2} \left(\frac{M_Z^2}{s\beta'} \right) , \quad (2.2.24)$$

$$\rho^{+0} = \rho^{0+} = -4e^2 g_s^2 g_{Rb}^2 \frac{\sin^3 \frac{\theta}{2}}{\cos \frac{\theta}{2}} \left(\frac{M_Z^3 \sqrt{2}}{\beta' s \sqrt{s}} \right) , \quad \rho^{-0} = \rho^{0-} = 4e^2 g_s^2 g_{Lb}^2 \frac{\sin^3 \frac{\theta}{2}}{\cos \frac{\theta}{2}} \left(\frac{M_Z^3 \sqrt{2}}{\beta' s \sqrt{s}} \right) . \quad (2.2.25)$$

With these powerful but extremely simple mathematical expressions at hand, some physical observables of the process under consideration which keep informations of the underlying Zb vertex structure can be explored. Let's stick for the

moment at the partonic level. The first obvious quantity that one can inspect is the subprocess unpolarized angular distribution: with the colour sum $\sum_{col} Tr(\frac{\lambda^i}{2} \frac{\lambda^i}{2}) = 4$, the unpolarized subprocess angular distribution (averaged on the gluon and b -quark spins and colours) is given by

$$\frac{d\sigma}{d\cos\theta} = \frac{\beta'}{768\pi s\beta} \sum_{\lambda\mu\tau\mu'} |F_{\lambda\mu\tau\mu'}|^2 . \quad (2.2.26)$$

One sees that it is proportional to

$$\frac{d\sigma}{d\cos\theta} \propto (\rho^{++} + \rho^{--} + \rho^{00}) \quad (2.2.27)$$

and, summing the above density matrix expressions, solely depends on $(g_{Rb}^2 + g_{Lb}^2)$:

$$\sum_{\lambda\mu\tau\mu'} |F_{\lambda\mu\tau\mu'}|^2 = (g_{Rb}^2 + g_{Lb}^2) C_{diff} , \quad (2.2.28)$$

with

$$C_{diff} = 4e^2 g_s^2 \beta' \cos^2 \frac{\theta}{2} \left(\frac{1}{\cos^4 \frac{\theta}{2}} + \frac{1}{\beta'^2} + \left(\frac{M_Z^2 \tan^2 \frac{\theta}{2}}{s \beta'} \right)^2 + \frac{2M_Z^2}{s\beta'^2} \tan^2 \frac{\theta}{2} \right) . \quad (2.2.29)$$

In order to separate the g_{Zb}^R and g_{Zb}^L contributions, and therefore to check their possible anomalous behaviours, one needs to be sensitive to different density matrix combinations besides the one just found in the unpolarized distribution, Eq. (2.2.27). This can be achieved only keeping track of the final Z polarization. The general procedure of its measurement has been described in [36, 37] for Tevatron processes. The Z polarization can be analysed by looking at the distributions of the Z decays, for example in lepton pairs. It is there shown that, appropriately defined a reference frame in which the leptons has azimuthal and polar angles θ_l, ϕ_l , each density matrix element is associated to a specific θ_l, ϕ_l dependence. The polarized quantities, therein called σ^P and σ^I , respectively proportional to $(\rho^{++} - \rho^{--})$ and to $(\rho^{+0} - \rho^{-0})$ are the only ones in which the combination $(g_{Rb}^2 - g_{Lb}^2)$ appears, as one can check by using the above expressions (2.2.22-2.2.25) of the density matrix elements. They respectively produce lepton angular dependencies of the types $\cos\theta_l$ and $\sin 2\theta_l \cos\phi_l$ as compared

to the unpolarised part proportional to $(1 + \cos^2 \theta_l)$. The specific generalization of that analysis to the LHC case is sketched in [29].

From this brief discussion, the Z -boson polarization asymmetry $A_Z^{pol,b}$ in b - Z production rises naturally by the definition:

$$A_Z^{pol,b} \equiv \frac{\sigma(Z_R) - \sigma(Z_L)}{\sigma(Z_R) + \sigma(Z_L)} = \frac{g_{Rb}^2 - g_{Lb}^2}{g_{Rb}^2 + g_{Lb}^2} C_{pol} \quad , \quad (2.2.30)$$

where C_{pol} is given as a convolution involving the bottom quark (b and \bar{b}) and gluon (g) pdfs:

$$C_{pol} = \frac{(bg + \bar{b}g) \otimes \left(\frac{1}{\cos^4 \frac{\theta}{2}} - \frac{1}{\beta'^2} + \left(\frac{M_Z^2}{s} \cdot \frac{\tan^2 \frac{\theta}{2}}{\beta'} \right)^2 \right)}{(bg + \bar{b}g) \otimes \left(\frac{1}{\cos^4 \frac{\theta}{2}} + \frac{1}{\beta'^2} + \left(\frac{M_Z^2}{s} \cdot \frac{\tan^2 \frac{\theta}{2}}{\beta'} \right)^2 \right)} \quad . \quad (2.2.31)$$

As one can see, Eq. (2.2.30) is simply proportional to the asymmetry parameter \mathcal{A}_b (Eq. (2.1.3)), the same quantity that is measured in the forward-backward $b\bar{b}$ asymmetry in e^+e^- annihilation at the Z pole A_{FB}^b [23] (*cf.* Eq. (2.1.7)). In order to exhibit the relation between $A_Z^{pol,b}$ and \mathcal{A}_b without any approximations, a numerical calculation of the full helicity amplitude has been implemented, retaining the bottom mass effects; in the present calculation it has been required a final state b -quark with $p_T > 25$ GeV and rapidity $|y| < 2$, to reproduce the typical experimental phase space cuts. The gluon and bottom quark in the initial state have been folded with CTEQ6 [38] parton distribution functions. The polarization asymmetry $A_Z^{pol,b}$ in b - Z production at LHC with $\sqrt{s} = 7$ TeV is shown in Figure 2.2 as a function of \mathcal{A}_b along with the SM prediction [23] (red band) and the measured LEP1 value [23] (green band).

As can be argued by looking at Figure 2.2, provided that a $\sim 8\%$ precision will be achieved on the $A_Z^{pol,b}$ measurement at LHC, it could be sufficiently sensitive to \mathcal{A}_b in order to discriminate between the LEP1 measurement and the SM prediction. To better realize if such required precision could be reached in the $A_Z^{pol,b}$ calculation, an assessment about the effect of its dominant theoretical uncertainties is now needed.

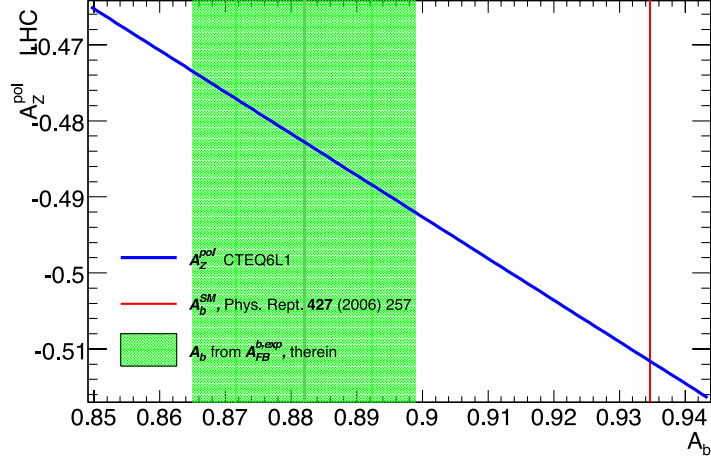


Figure 2.2. Polarization asymmetry $A_Z^{pol,b}$ in b - Z production at LHC with $\sqrt{s} = 7$ TeV. The green band displays the $\pm 1\sigma$ bounds [23] for the measured asymmetry parameter \mathcal{A}_b while the SM prediction [23] is shown in red.

2.3 Impact of the scale/PDF choices and radiative corrections

The previous discussion has been performed at the simplest Born level. The next step is to verify whether the expression of $A_Z^{pol,b}$ remains essentially identical when possible sources of theoretical uncertainties or NLO corrections are considered.

It has been proceeded in the following way. First, possible effects of either strong scales or pdf variations have been taken into account; as shown in Ref. [35], these variations generate a sensible effect, of the almost ten percent relative size, in the total cross section. Next, the possible contribution of NLO electroweak radiative corrections have been considered; their effect on the total and angular cross section have been determined in [39] and found to be possibly relevant.

The dependence of $A_Z^{pol,b}$ on factorization and renormalization scales, μ_F and μ_R respectively, is evaluated by varying their values simultaneously by a conservative

factor of four with respect to the central value; $A_Z^{pol,b}$ is shown in Figure 2.3 as a function of \mathcal{A}_b for $\mu_F = \mu_R = k\mu_0$ with $\mu_0 = M_Z$ and $k = 1, 3$ and $1/3$. As can be observed from Figure 2.3 the scales variation effect on $A_Z^{pol,b}$ is below 1%. However it is worth noting that the total cross section dependence on μ_R could be strongly reduced by using the “Principle of Maximum Conformality” scale-setting (see for instance [40]).

The asymmetry dependence on the pdf is examined performing the numerical calculation with different pdf sets. In Figure 2.4, $A_Z^{pol,b}$ values are shown as a function of \mathcal{A}_b for three different LO pdf sets: CTEQ [38]; MSTW2008 [41] and NNPDF [42]. As can be seen, the dependence on the pdf set is below 2% while the total cross section can be affected by large variations of order 7% [43]. The NLO EW effects

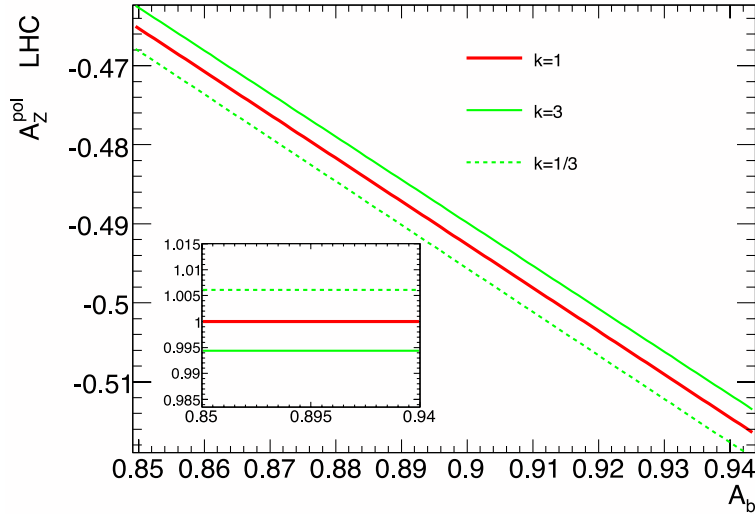


Figure 2.3. Polarization asymmetry $A_Z^{pol,b}$ as a function of \mathcal{A}_b for three different choices of factorization and renormalization scales, respectively μ_F and μ_R , $\mu_F = \mu_R = k\mu_0$ with $\mu_0 = M_Z$ and $k = 1, 3$ and $1/3$.

on $A_Z^{pol,b}$ deserve a rather different discussion. In principle, these effects should not introduce any appreciable theoretical uncertainty, since the values of the involved parameters are all known and with great accuracy. The purpose of their calculation would simply be to offer a more complete theoretical prediction for $A_Z^{pol,b}$. In fact, it is well known that electroweak corrections can have sizable effects on processes

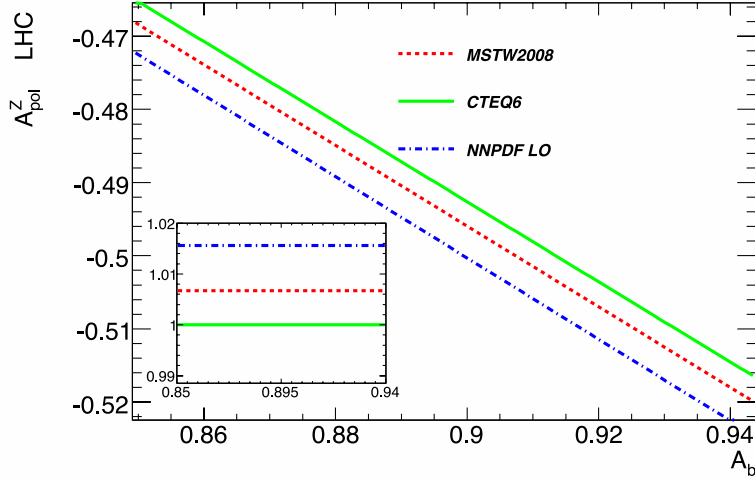


Figure 2.4. $A_Z^{pol,b}$ as a function of A_b , for three different choices of pdf sets, as described in the text.

involving W - or Z -boson production at LHC. We have observed it in associated top-quark and W -boson production [44, 45] and papers on W +jet or Z +jet production had also mentioned it, see [39, 46]. These effects can reach the several percent size and even more than ten percent on the subprocess cross sections. This can be immediately understood by looking at the simple Sudakov (squared and linear) logarithmic terms which affect the amplitudes at high energy [47, 48]. To estimate the size of this type of effect at lower energies one also can use the so-called “augmented Sudakov” terms, in which constant terms have been added to the logarithmic ones [49]. Using this approach, one can be convinced that the polarization asymmetry $A_Z^{pol,b}$ will be essentially unaffected by these EW corrections. Actually, looking at the transverse Born amplitudes, one can first notice that, since $g_{Lb} \sim 5g_{Rb}$, the dominant amplitudes are F_{-+++} and F_{----} . The other ones will contribute to the total cross section via terms which are suppressed by a factor $1/25$. Then, applying the Sudakov rules of Ref. [44, 45, 47–49], one can see that the leading logs associated to the b_L and Z states are very similar for these two amplitudes. A raw estimate gives effects of several percents in the 1 TeV range which should directly affect the cross section.

However for $A_Z^{pol,b}$, dominated by the $(|F_{-+++}|^2 - |F_{----}|^2)/(|F_{-+++}|^2 + |F_{----}|^2)$ ratio, the common EW corrections to each of these amplitudes in the numerator and in the denominator will cancel out. So a small non zero effect will only come from the smaller amplitudes (which contribute by a factor 25 less) and from the small differences due to the subleading (mass suppressed) terms.

Using the augmented Sudakov expressions written in ref. [49], it has been checked that the effects on $A_Z^{pol,b}$ reach at most the 1% level. In this spirit, it is here argued that the SM NLO electroweak corrections are probably irrelevant. A more complete determination of their numerical effect will be given in a forthcoming paper.

2.4 Conclusions

In this first chapter it has been shown that the Z -polarization asymmetry ($A_Z^{pol,b}$) in bZ associated production at the LHC is strictly connected to the well known forward-backward $b\bar{b}$ asymmetry at the Z -pole, A_{FB}^b , measured at LEP1. Results of this study indicate that $A_Z^{pol,b}$ is almost free from theoretical uncertainties related to QCD scale variations as well as to pdf set variations; this property strongly suggests a measurement of $A_Z^{pol,b}$ at LHC as a unique candidate to possibly clarify the long standing puzzle related to the A_{FB}^b measurement at LEP1.

More generally, it can be noticed that polarization asymmetries would be quite relevant theoretical observables at LHC, as shown by [50], where a polarization asymmetry was studied in the context of polarized top production in association with a charged Higgs boson, as a possible way of determining the $\tan\beta$ parameter in the Minimal Supersymmetric Standard Model (MSSM). A rather general conclusion which can be drawn from this chapter is therefore that polarisation measurements at LHC would represent a tough but possibly quite rewarding experimental effort.

Chapter 3

New Physics constraints from the Forward–Backward asymmetry in bZ associated production at LHC

3.1 Introduction

In the previous chapter the $A_Z^{pol,b}$ polarization asymmetry has been defined, and it has been shown that this would represent a unique possibility of measuring the \mathcal{A}_b quantity. It has been proved that, from a theoretical point of view, this asymmetry exhibits the remarkable properties of being QCD scale and PDF set choice independent, which represents a quite remarkable feature. Though feasible, its experimental determination does not convince specialists. Indeed it is well known that its measure, being derived from the experimental determination of the so-called *polarization fractions* (see for example [60] and references therein) of the Z -boson in bZ associated production, would be affected by intrinsically large *systematic* uncertainties. To this, one should add the implicit (but not less important) uncertainty coming from the b -quarks charge determination, resulting in poor chances to obtain a precise measurement of $A_Z^{pol,b}$. Last but not least, the definition of $A_Z^{pol,b}$ does not refer directly to an experimental recipe for its determination, since the polarization of the Z -boson, as widely discussed, has to be inferred by its decay products angular

distributions, thus separating the experimental level from the theoretical observable it should inspect. The aim of this chapter is exactly to study in deeper details the associate production of a bottom quark with a Z -boson, now taking into account the subsequent leptonic decay $Z \rightarrow l\bar{l}$. This will be done with the explicit intention of trying to build the definition of an alternative quantity that should inherit from $A_Z^{pol,b}$ the proportionality to \mathcal{A}_b , but which should be experimentally cleaner and usable, and possibly reminiscent of observables already measured in past experiments, such that past techniques could help present and future physicists. We will see that this is the case for what has been named the *Forward-Backward Asymmetry of the bottom quark in bZ associated production at LHC* ($A_{FB}^{b,LHC}$). The chapter ends with a discussion on how a measurement of $A_{FB}^{b,LHC}$ can influence searches for New Physics at the LHC.

3.2 Helicity amplitudes for the process $bg \rightarrow bl\bar{l}$

As a first step for the above sketched program, one has to start with the study of the parton level process of associated production of a single b -quark and a Z -boson and its subsequent decay into a lepton-antilepton pair. In a 5FNS approach it is defined at LO by subprocesses $bg \rightarrow bl\bar{l}$ involving two Born diagrams with a b -quark exchange in the s -channel and in the u -channel, as shown in Figure 3.1. The

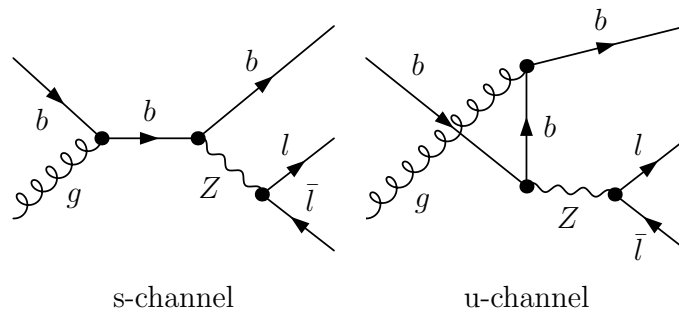


Figure 3.1. 5FNS LO Feynmann diagrams for the process $bg \leftrightarrow bl\bar{l}$

interaction vertexes involved in these two diagrams are defined as follows

$$gqq : ig_s \not{\epsilon} \left(\frac{\lambda_c^k}{2} \right)$$

$$Zff : -ie\gamma^\mu [g_{Lf}P_L + g_{Rf}P_R] \equiv -ie\gamma^\mu [g_{(a)f}P_a].$$

Therefore, defining the two Lorentz vectors H^μ , L^μ as

$$\begin{aligned} H^\mu &= g_s \left(\frac{\lambda_c^k}{2} \right) \bar{u}(b') \left[\gamma^\mu \{g_{(a)b}P_a\} \frac{(\not{q} + m_b)}{s - m_b^2} \not{\epsilon} + \right. \\ &\quad \left. + \not{\epsilon} \frac{(\not{q}' + m_b)\gamma^\mu}{u - m_b^2} \{g_{(a)b}P_a\} \right] u(b), \\ L^\mu &= \bar{u}(l) \gamma^\mu \{g_{(a)l}P_a\} v(\bar{l}) \end{aligned} \quad (3.2.1)$$

the Born invariant amplitude is given by

$$A^{Born}(bg \rightarrow bZ \rightarrow b\bar{l}) = 4\pi\alpha D_Z(p_Z^2) H^\mu L_\mu, \quad (3.2.2)$$

where ϵ , λ_c^k are the gluon polarization vector and colour matrix, $p_l + p_{\bar{l}} \equiv p_Z$, $D_Z(p_Z^2)$ is the usual Z effective propagator, $q = p_b + p_g = p_Z + p'_b$, $s = q^2$, $q' = p'_b - p_g = p_b - p_Z$, $u = q'^2$ and with the kinematic decompositions in the center of mass frame (all fermion massless)

$$\begin{aligned} p_b &= (p; 0, 0, p), & p_g &= (p; 0, 0, -p), \\ p'_b &= (p_1; 0, p_1 \sin \theta_1, p_1 \cos \theta_1)^1, \\ p_l &= (p_2; p_2 \sin \theta_2 \sin \phi_2, p_2 \sin \theta_2 \cos \phi_2, p_2 \cos \theta_2), \\ p_{\bar{l}} &= (p_3; p_3 \sin \theta_3 \sin \phi_3, p_3 \sin \theta_3 \cos \phi_3, p_3 \cos \theta_3), \\ \epsilon(g) &= \left(0; \frac{\lambda_g}{\sqrt{2}}, -\frac{i}{\sqrt{2}}, 0 \right), \end{aligned} \quad (3.2.3)$$

where $\lambda_g = \pm 1$ stands for the gluon polarization and the variables p_i , θ_i , ϕ_i do not yet satisfy momentum conservation, for clarity of notation. A more appropriate set

¹An additional azimuthal angle for b' would manifest itself only through overall phase factors in the amplitudes.

of variables more cleanly fulfilling the center of mass condition $p_b + p_g = p'_b + p_l + p_{\bar{l}}$ will be improperly called here ‘helicity frame’²: this is defined as the coordinate system in which the polar axis coincides with the direction and versus of b' , while

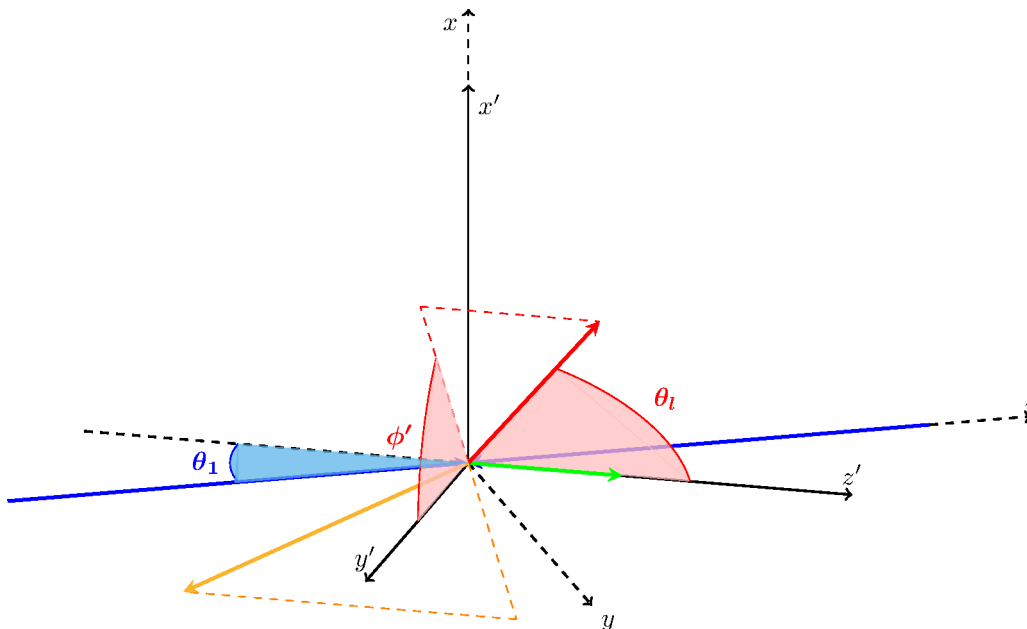


Figure 3.2. The coordinate system defined in the text. In blue the colliding partons momenta. The polar axis of the helicity frame coincides with the momentum of the outgoing b' (green arrow). Momenta of lepton and antilepton are represented by the red and orange arrows.

azimuthal angles are measured with respect to the normal to the production plane (i.e. the one spanned by the colliding and decaying bottom quarks momenta³). The rotation matrix between the two coordinate systems

$$R_{\theta_1} = \begin{pmatrix} 1 & 0 & 0 \\ 0 & \cos \theta_1 & -\sin \theta_1 \\ 0 & \sin \theta_1 & \cos \theta_1 \end{pmatrix} \quad (3.2.4)$$

²Properly this ‘helicity frame’ is not a different *frame* from the center of mass one, but it’s just a different *coordinate system*, still in the center of mass frame.

³The ambiguity coming from the orientation of the normal to the production plane will be cancelled after integration over the azimuthal angle in the definition of observable quantities.

can be used to relate the new polar and azimuthal angles $\theta_l, \theta_{\bar{l}}$ and ϕ'

$$\begin{aligned} p_l^{hf} &= (p_2; p_2 \sin \theta_l \sin \phi', p_2 \sin \theta_l \cos \phi', p_2 \cos \theta_l) , \\ p_{\bar{l}}^{hf} &= (p_3; -p_3 \sin \theta_{\bar{l}} \sin \phi', -p_3 \sin \theta_{\bar{l}} \cos \phi', p_3 \cos \theta_{\bar{l}}) \end{aligned}$$

with the old variables Eq. (3.2.3). In this frame the coplanarity of the final particles is clearly shown by the dependence on the same variable ϕ' of both leptons: the reader may already have noticed that this angle is related to the conventional azimuthal angle of the lepton l by $\phi_l = \pi/2 - \phi'$. The reason for this choice of variables in the formulas resides in the physical meaning of ϕ' , corresponding to the angle between the production plane (spanned by \vec{p}_b, \vec{p}_g and $\vec{p}_{b'}$) and the decay plane (spanned by $\vec{p}_{b'}, \vec{p}_l$ and $\vec{p}_{\bar{l}}$). Energy conservation leads, in this frame and for massless particles, to simple formulas for the energies of the final particles ($\{\theta_l, \theta_{\bar{l}}\}^h \equiv \{\theta_l, \theta_{\bar{l}}\}/2$):

$$p_1 = p \left(1 - \cot(\theta_{\bar{l}}^h) \cot(\theta_l^h) \right), \quad (3.2.5)$$

$$p_2 = p \cos(\theta_{\bar{l}}^h) \csc(\theta_l^h) \csc(\theta_{\bar{l}}^h + \theta_l^h), \quad (3.2.6)$$

$$p_3 = p \csc(\theta_{\bar{l}}^h) \cos(\theta_l^h) \csc(\theta_{\bar{l}}^h + \theta_l^h), \quad (3.2.7)$$

which make manifest the (maximal) domain of integration

$$\theta_l \in [0, \pi], \quad \theta_{\bar{l}} \in [\pi - \theta_l, \pi] .$$

Besides that, the introduction of this reference frame cleans and simplifies greatly the form which the matrix elements assume there. Due to the massless assumption, the helicity amplitudes can be expressed as

$$\mathcal{M}_{\lambda_b \lambda_g; \lambda_{b'} \lambda_l \lambda_{\bar{l}}} \equiv \delta_{\lambda_b \lambda_{b'}} \delta_{\lambda_l \lambda_{\bar{l}}} \mathcal{M}_{\lambda_g; \lambda_{b'} \lambda_l} ,$$

where $\lambda_f = \pm \frac{1}{2} \equiv \pm$, $\lambda_g = \pm 1 \equiv \pm$ and $\lambda_i \equiv -\bar{\lambda}_i$. Modulo a common term

$$\mathcal{M}_{\lambda_g; \lambda_{b'} \lambda_l} \equiv \left(D_Z(p_Z^2) 16\sqrt{2} \pi \alpha g_s \lambda_c^k \sqrt{\frac{p_1 p_2 p_3}{p}} \right) F_{\lambda_g; \lambda_{b'} \lambda_l} ,$$

the non vanishing helicity amplitudes factors read:

$$F_{+++} = -i (g_{Rb}g_{Rl}) e^{i\phi'} \frac{\cos \theta_l^h \sin \theta_l^h}{\cos \theta_1^h}, \quad (3.2.8)$$

$$F_{++-} = i (g_{Rb}g_{Ll}) e^{i\phi'} \frac{\cos \theta_l^h \sin \theta_l^h}{\cos \theta_1^h}, \quad (3.2.9)$$

$$F_{-++} = i (g_{Rb}g_{Rl}) \frac{\sin \theta_l^h}{\cos(\theta_l^h + \theta_l^h)} \frac{\cos \theta_l^h}{\cos \theta_1^h} \left(e^{-i\phi'} \cos \theta_1^h \sin \theta_l^h - \sin \theta_1^h \cos \theta_l^h \right)^2, \quad (3.2.10)$$

$$F_{--+} = -i (g_{Rb}g_{Ll}) \frac{\sin \theta_l^h}{\cos(\theta_l^h + \theta_l^h)} \frac{\cos \theta_l^h}{\cos \theta_1^h} \left(e^{-i\phi'} \cos \theta_1^h \sin \theta_l^h + \sin \theta_1^h \cos \theta_l^h \right)^2, \quad (3.2.11)$$

while the other four can be derived from these by parity conjugation, that in our conventions is represented by complex conjugation together with the switch $g_{Lf} \leftrightarrow g_{Rf}$. As an example

$$F_{---} = i (g_{Lb}g_{Ll}) e^{-i\phi'} \frac{\cos \theta_l^h \sin \theta_l^h}{\cos \theta_1^h}.$$

Note that formulas which are related by the switch of the lepton helicities are related one to each other by the replacements

$$(\theta_l \leftrightarrow \theta_{\bar{l}}, \phi' \rightarrow \phi' + \pi) \equiv l \leftrightarrow \bar{l}, \quad (3.2.12)$$

$$g_{Ll} \leftrightarrow g_{Rl}. \quad (3.2.13)$$

From these formulas one can build the total cross section by introducing the usual flux factor and the convolution with the relevant partons density functions for the proton.

3.3 Definition of $A_{FB}^{b,\text{LHC}}$

For our purposes it suffices to define the squared amplitude summed over the initial state helicities as

$$\rho_{\lambda_{b'}\lambda_l} \equiv \sum_{\lambda_g} |\mathcal{M}_{\lambda_g; \lambda_{b'}\lambda_l}|^2$$

and to identify

$$\rho_{++} + \rho_{--} \equiv (g_{Lb}^2 g_{Ll}^2 + g_{Rb}^2 g_{Rl}^2) f(\theta_l^h, \theta_{\bar{l}}^h, \theta_1, \phi')$$

(one can check that actually in the sum in the RHS the couplings factorize out). The complete unpolarized squared amplitude can now be simply written as

$$\begin{aligned} |\mathcal{M}|^2 &= (g_{Lb}^2 g_{Ll}^2 + g_{Rb}^2 g_{Rl}^2) f(\theta_l^h, \theta_{\bar{l}}^h, \theta_1, \phi') + (g_{Lb}^2 g_{Rl}^2 + g_{Rb}^2 g_{Ll}^2) \bar{f}(\theta_l^h, \theta_{\bar{l}}^h, \theta_1, \phi') \\ &\equiv c_+ \frac{f+\bar{f}}{2} + c_- \frac{f-\bar{f}}{2}, \end{aligned} \quad (3.3.14)$$

where $\bar{f} \equiv f|_{l \leftrightarrow \bar{l}}$. In the last line Eq. (3.3.14), the two terms have definite symmetry properties under $l \leftrightarrow \bar{l}$, with coefficients

$$\begin{aligned} c_+ &= (g_{Lb}^2 + g_{Rb}^2)(g_{Ll}^2 + g_{Rl}^2), \\ c_- &= (g_{Lb}^2 - g_{Rb}^2)(g_{Ll}^2 - g_{Rl}^2), \\ \frac{c_-}{c_+} &= \mathcal{A}_b \mathcal{A}_l. \end{aligned}$$

This allows us to extract (c_-) c_+ simply measuring (anti-)symmetrized combination of cross sections in kinematic domains related one to each other under exchange of the two leptons angles. The simplest choice in the CM frame is

$$\mathcal{D}_\pm \equiv \theta_l \gtrless \theta_{\bar{l}}. \quad (3.3.15)$$

To be more explicit, note that the condition $\theta_l \gtrless \theta_{\bar{l}}$ translates in the Z rest frame to the experimentally simpler condition of Forward/Backward lepton momentum respect to the b -quark momentum versor. This finally leads to the definition of $A_{FB}^{b,\text{LHC}}$

$$A_{FB}^{b,\text{LHC}} \equiv \frac{\sigma(\mathcal{D}_F) - \sigma(\mathcal{D}_B)}{\sigma(\mathcal{D}_F) + \sigma(\mathcal{D}_B)}, \quad (3.3.16)$$

where the reference axis is the b -quark momentum in the Z -rest frame. From Eq. (3.3.14) this quantity will be proportional, modulo a kinematic factor k , to the LEP A_{FB}^b

$$A_{FB}^{b,\text{LHC}} = k A_{FB}^b, \quad (3.3.17)$$

where FB , as already emphasized, has different meaning in the two expressions.

A theoretical prediction of $A_{FB}^{b,\text{LHC}}$ (and, in particular, of the numerical value of the kinematical constant k) has to take into account several experimental issues, thus needing a realistic simulation of the detector features, and in particular of its geometrical properties and of intrinsic cuts applied to the event reconstruction. In

such a context, kinematic cuts on transverse momentum and pseudorapidity of the decaying particles introduce some subtleties in the derivation of a direct connection of $A_{FB}^{b,LHC}$ to the LEP asymmetry A_{FB}^b . To prove the validity of Eq. (3.3.17) also in

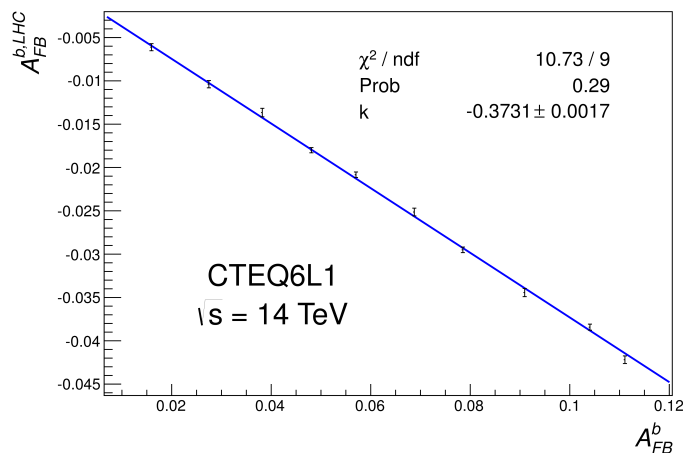


Figure 3.3. Event level (*i.e.* without parton showering) dependence of the asymmetry defined in the text on A_{FB}^b , in a ficticiously wide range of A_{FB}^b values, aiming to prove the direct proportionality also in the presence of typical kinematic cuts [63] on decay products pseudorapidities and transverse momenta. The uncertainty on k is only numerical, *i.e.* related to MC statistics (see the text for other uncertainties).

the presence of a realistic event selection, one can vary ficticiously $g_{L,Rb}$ in a wide range of values, determining the corresponding values of $A_{FB}^{b,LHC}$ with usual kinematic cuts. Figure 3.3 shows the results of a simulation with ten different choices of $g_{L,Rb}$, including the SM one (for the events simulation we have used CalcHEP [62] and checked good agreement with different event generators). The particular choice of selection criteria closely follows the one used by ATLAS for the Z - b -jets cross section analysis [63]. With these assumptions, the kinematical constant k is found to be -0.37 at LO. Its QCD scale dependence has been inspected varying simultaneously the renormalization and factorization scales and computing the corresponding $A_{FB}^{b,LHC}$ values, Figure 3.4. Similarly the PDF set choice dependence is depicted in Figure 3.5. The total theoretical uncertainty in both cases is at the 1% level.

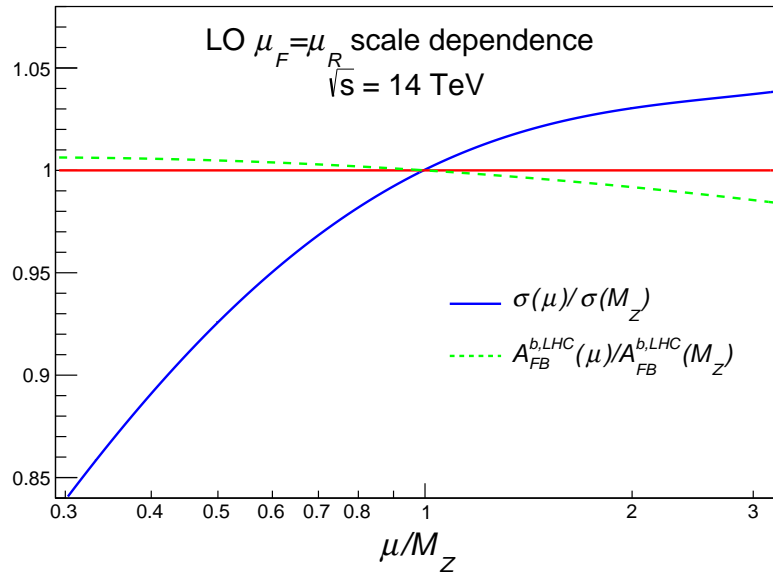


Figure 3.4. Comparison between the LO $\mu_F = \mu_R = kM_Z$ scale variation dependence

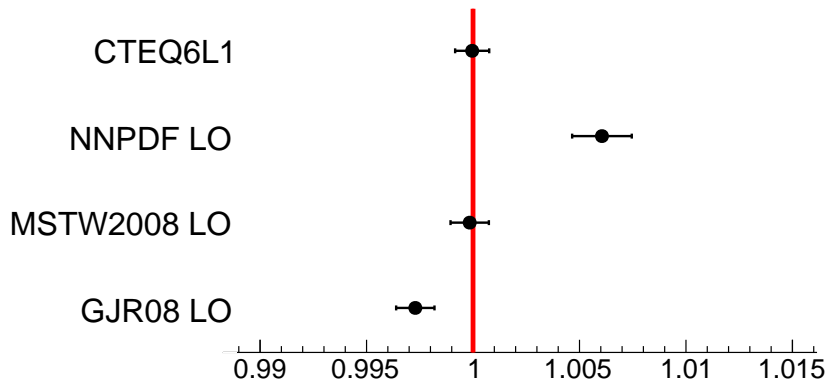


Figure 3.5. Comparison of different pdf set LO asymmetry predictions taking CTEQ6L1 as a reference.

3.4 Testing New Physics through $A_{FB}^{b,\text{LHC}}$

Now that we have at hand the concrete possibility to test the SM prediction for the parameter \mathcal{A}_b through $A_{FB}^{b,\text{LHC}}$, is it time to have a brief digression on the theoretical side, to understand in a pragmatic way (*i.e.* neutrally and blindly) what kind of models can predict some possible discrepancy on the measured value of \mathcal{A}_b with respect to the SM well known and familiar case. This not being the main aim of this work, it has been chosen to report two different NP models as cases of study, taken as examples of theories with opposite behaviours for what concerns a possible deviation from the LEP measurement of \mathcal{A}_b .

3.4.1 Corrections to \mathcal{A}_b in the (N)MSSM

Supersymmetric corrections both in the MSSM and in the NMSSM have been studied in [27]. In that work the authors scrutinized the full one-loop supersymmetric effects on $Zb\bar{b}$ coupling, considering all constraints at disposal at that time: precision electroweak measurements, direct searches for sparticles and Higgs bosons, the stability of Higgs potential, the dark matter relic density, and the muon $g - 2$ measurement. They analysed the characters of each type of corrections and searched for the SUSY parameter regions where the corrections could be sizeable.

Their choice was to parametrize the $Zf\bar{f}$ interaction at Z -pole in term of the parameter ρ_f and the effective electroweak mixing angle $\sin^2\theta_{eff}^f$ [30, 31]:

$$\Gamma_{Zf\bar{f}}^\mu = (\sqrt{2}G_\mu\rho_f)^{\frac{1}{2}}m_Z\gamma^\mu [-2Q_f\sin^2\theta_{eff}^f + I_3^f(1 - \gamma_5)] \quad (3.4.18)$$

This parametrization is preferred from the experimental point of view because all the measured asymmetries, included also the ones here studied, are only dependent on $\sin^2\theta_{eff}^f$, whose value can be directly determined with their precise measurements. The corrections to these parameters are indeed connected to the ones of the chiral fermions couplings to the Z -boson:

$$\rho_f = 1 + \delta\rho_{se} + \delta\rho_{f,v}, \quad (3.4.19)$$

$$\sin^2\theta_{eff}^f = (1 + \delta\kappa_{se} + \delta\kappa_{f,v})s_W^2, \quad (3.4.20)$$

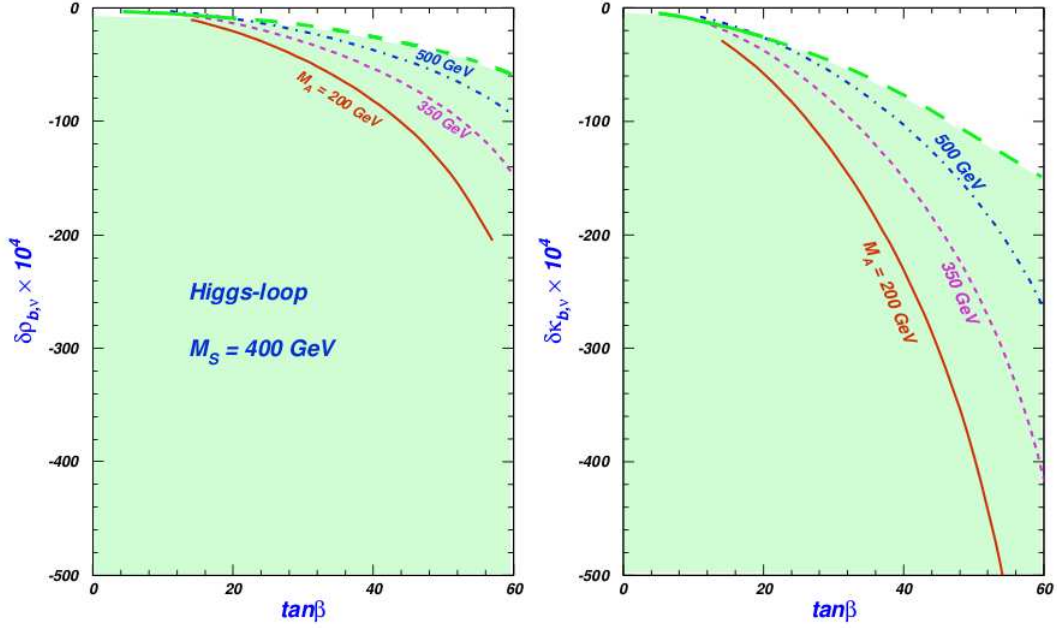


Figure 3.6. Higgs loop contributions to $\delta\rho_{b,v}$ and $\delta\kappa_{b,v}$. M_S is a common mass scale for light squark generations, on which however results are not quite sensitive. The green band represents the 95% C.L. exclusion from [32]. The green straight line gives the exact limit contour, while the dashed one is an extrapolation, since results of [27] are not sufficient to draw the net 95% limit contour.

where the subscript ‘*se*’ stands for universal, flavour independent contributions from gauge boson self-energies, and ‘*f,v*’ denotes the contribution from the vertex correction to $Zf\bar{f}$ interaction, with

$$\delta\rho_{f,v} = 2\frac{\delta g_{Lf} - \delta g_{Rf}}{g_{Lf} - g_{Rf}} - 2\delta^v - \delta^b; \quad \delta\kappa_{f,v} = \frac{1}{2Q_f s_W^2} \frac{g_{Rf}\delta g_{Lf} - g_{Lf}\delta g_{Rf}}{g_{Lf} - g_{Rf}} \quad (3.4.21)$$

and, finally, $\delta g_{L,R}^f$ are the corrections to the chiral Zf couplings $g_{L,Rf}$. The authors have found that the *potentially* sizeable corrections come from the Higgs sector with light m_A and large $\tan\beta$ (Fig. 3.6), which can reach -2% and -6% for ρ_b and $\sin^2\theta_{eff}^b$, respectively. However, such sizable negative corrections are just opposite to what needed to solve the anomaly, being potentially even larger in the NMSSM case. This is also reflected in the statistical global analysis they did, scanning over the allowed parameter space to investigate to what extent supersymmetry could narrow the discrepancy: they indeed found that, under all constraints they took into

account, the potentially large supersymmetric effects are instead quite restrained and cannot significantly ameliorate the anomaly of $Zb\bar{b}$ coupling, Fig. 3.7. Compared with $\chi^2/dof = 9.62/2$ in the SM, the MSSM and NMSSM can only improve it to $\chi^2/dof = 8.77/2$ in the allowed parameter space. Their conclusion is that, if the anomaly of $Zb\bar{b}$ coupling is not a statistical or systematic problem, it would suggest new physics beyond the MSSM or NMSSM. It is quite reassuring that recent direct exclusions from ATLAS and CMS experiments [32] indeed forbid exactly the “large-corrections” region that was there found to badly deviate from the SM prediction for ρ_b and $\sin^2\theta_{eff}^b$.

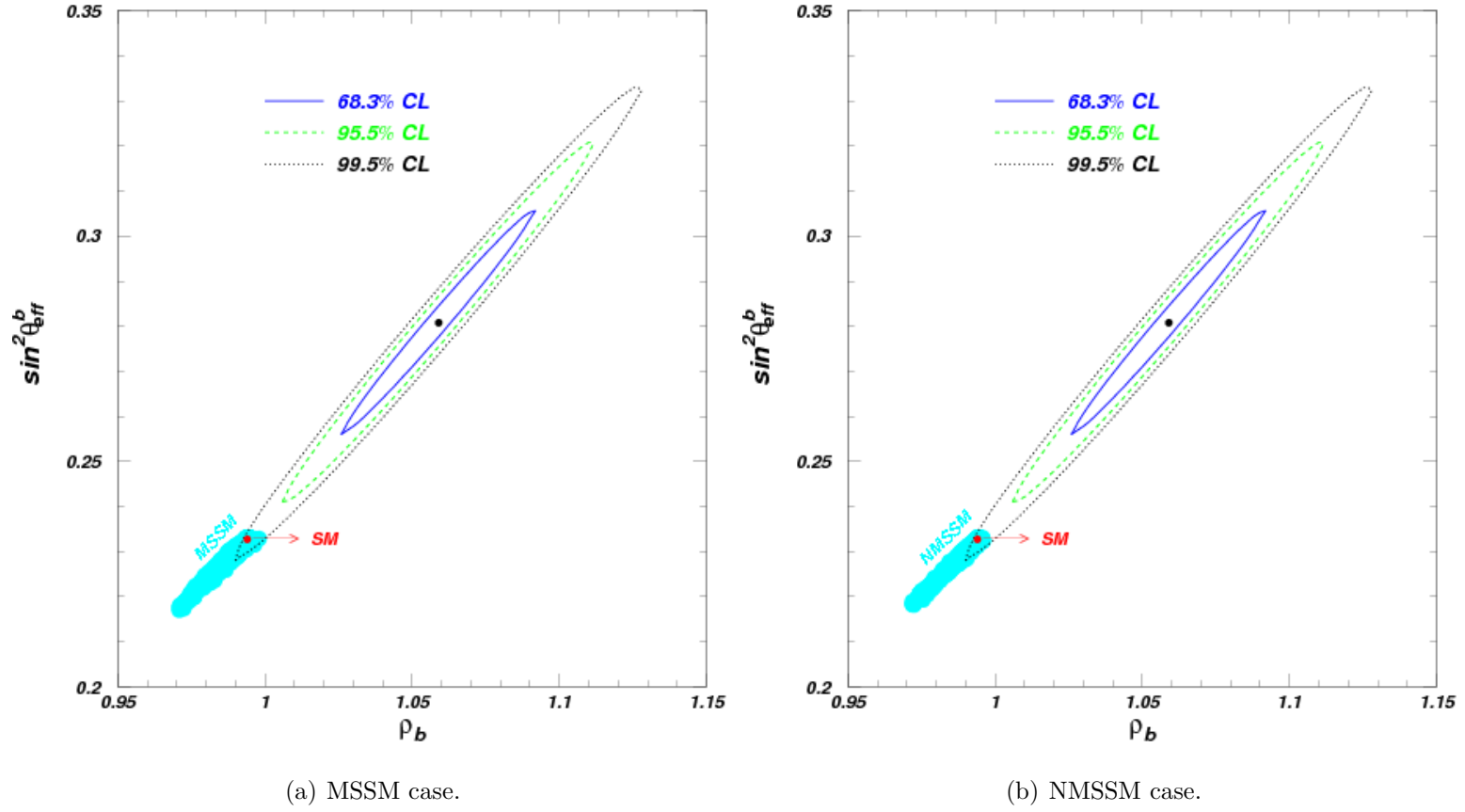


Figure 3.7. The MSSM, NMSSM and SM predictions for ρ_b and $\sin^2 \theta_{eff}^b$, compared with the LEP/SLD data at 68%, 95.5% and 99.5% confidence level. The MSSM predictions are from a scan over the parameter space.

3.4.2 Corrections to \mathcal{A}_b in models with additional bottom partners

A large class of models that can address the LEP paradox is the one quite generally characterised by the introduction of vector-like quarks (*cf.* [81, 82] and references citing that). These are Dirac fermions whose Weyl left and right components are in the same representation of the SM gauge group. The peculiarity of such kind of fields is that they are allowed to possess an explicit SM gauge group invariant mass term, thus not directly related to the Electroweak scale. Experimentally their mass is starting to be constrained from below only after LHC direct searches [83]. After EWSB, they can mix with ordinary quarks, giving rise to striking modifications of their couplings to the Higgs and gauge bosons. They can be analysed in a model-independent approach in terms of just a few free parameters, as *e.g.* in [82], where it is revisited, in a simplified version, the possibility [85] of adding to the SM field content just a single, vector-like, $SU(2)_L$ doublet,

$$\Psi_{L,R} = \{B, X\}_{L,R} \doteq (3, 2, -5/6) \quad (3.4.22)$$

with hypercharge $Y = -5/6$, able to explain the LEP paradox. Of course this is only one of the several different theoretical motivations of this kind of models, but it is here interesting just to sketch what are the main features of this particular topic, especially regarding the bottom sector. The $Q_{\text{em}} = -1/3$ component B of the additional vector-like doublet mixes with the other three down quarks to give four $Q_{\text{em}} = -1/3$ mass eigenstates. One expects dominant mixing with the b -quark, given the usual Yukawa coupling hierarchy in the mass matrices (this is the case, for instance, in models with fermion partial compositeness):

$$\begin{pmatrix} b_{L,R} \\ B_{L,R} \end{pmatrix} = \begin{pmatrix} \cos \theta_{L,R} & -\sin \theta_{L,R} e^{i\phi} \\ \sin \theta_{L,R} e^{-i\phi} & \cos \theta_{L,R} \end{pmatrix} \begin{pmatrix} b_{L,R}^0 \\ B_{L,R}^0 \end{pmatrix}. \quad (3.4.23)$$

where, imposing the b mass to its SM value, one gets

$$\tan \theta_L = \frac{m_b}{m_B} \tan \theta_R. \quad (3.4.24)$$

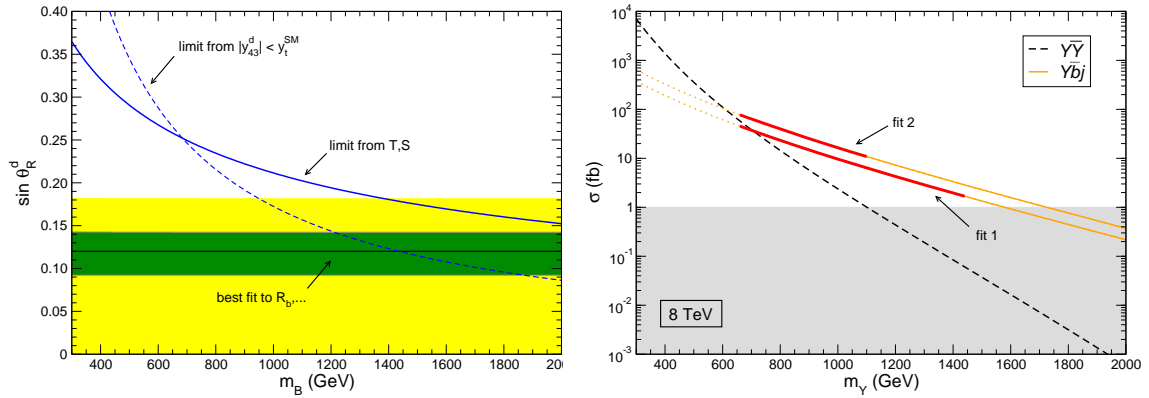
This mixing, together with the different Y assignment, is responsible of the modification of the b gauge couplings, in particular to the Z -boson:

$$g_{bR} = I_3^{B_L} \sin^2 \theta_R - Q \sin^2 \theta_W, \quad g_{bL} = I_3^{b_L} \cos 2\theta_L - Q \sin^2 \theta_W \quad (3.4.25)$$

where, using Eq. (3.4.24), one can substitute

$$\cos 2\theta_L = \frac{1 - \epsilon^2}{1 + \epsilon^2} \simeq 1 - 2\epsilon \quad (3.4.26)$$

with $\epsilon = m_b/m_B \tan \theta_R$. In [82] a simplified fit⁴ of SM values [34] to Z pole observables has been made, with free parameters the $b - B$ mixing angle θ_R and the partner mass m_B . Using this procedure, the best-fit value for the mixing is found to be $\sin \theta_R = 0.12$, reducing the χ^2 from $\chi^2 = 7.37/4 \text{ dof}$ in the SM to $\chi^2 = 4.16/3 \text{ dof}$, independently from the heavy B mass, since m_B and θ_R are independent parameters and the corrections to Zbb couplings depend approximately only on θ_R , see Eq. (3.4.24). However, imposing in addition a Yukawa off-diagonal y_{43}^d in the down



(a) Fit results.

(b) Y Cross sections for B single production at LHC with parameters set to the fit results.

squarks mass matrix not higher than the top Yukawa y_t , they obtained upper limits

⁴Two different sets of SM predictions were then used, but the one from [59] had a not yet fixed result on the calculation of R_b , which temporarily put it in disagreement with its measured value too, generating some new excitement (and works trying to explain it). The problem in the calculation of [59] was solved by the authors in Fall 2013, one year later the first publication.

on the partner mass $m_B \lesssim 1.4$ TeV, giving together with the value of $\sin\theta_R$ good chances of discovery/exclusion at LHC for the B $SU(2)_L$ partner, see Fig. 3.4.2.

This brief digression on the possibilities of sample models to address the LEP paradox, hopefully, has given at least the taste of how much an independent determination of the \mathcal{A}_b parameter can influence the confidence on modern examples of field theories. Supersymmetric extension of the SM, in their minimal versions, “mimic” too well their parent theory at low energy in the bottom sector: for this kind of theories, even a confirmation of the LEP measurement could be troublesome. On the other hand, very simple models with minimal vector-like field content addition, could solve so cleanly this issue that, at the opposite, they would be in trouble very fast⁵ as the \mathcal{A}_b discrepancy would be showered by a new measurement. It’s clear that a determination of $A_{FB}^{b,\text{LHC}}$ asks loudly to be performed. The rest of this chapter treats exactly this topic.

3.5 Jet charge determination and Q_{FB} at LHC

For a detector level simulation one has to choose an appropriate procedure to measure the b -jet charge, and in particular to connect it with the theoretical definition of $A_{FB}^{b,\text{LHC}}$: here the fact that this is intimately related to the LEP A_{FB}^b allows us to adapt the LEP procedure of measuring A_{FB}^b to the LHC case [64,65]. Here a weighting technique [66–68] is applied in which the b -jet charge is defined as a weighted sum of the b -jet track charges,

$$Q_{b\text{-jet}} \equiv \frac{\sum_i Q_i |\vec{j} \cdot \vec{p}_i|^k}{\sum_i |\vec{j} \cdot \vec{p}_i|^k} \quad (3.5.27)$$

where Q_i and \vec{p}_i are the charge and momentum of the i -th track, \vec{j} defines the b -jet axis direction, and k is a parameter which was set to 0.5 following literature (this value optimises the separation between b - and \bar{b} -jets mean charges). In addition, in events with muons with transverse momentum relative to the jet axis $p_T^{\text{rel}} > 0.8$ GeV

⁵Of course, as always, the higher the complications, the more the chance to escape constraints, don’t shoot the messenger.

(this value is known to maximise the b -purity times efficiency, see [72]), we have defined an effective jet charge as

$$Q_{b\text{-jet}}^\mu \equiv \left(\frac{p_T^{\text{rel}}}{m_b} \right)^k q_\mu \quad (3.5.28)$$

where q_μ is the reconstructed muon charge and k was set to 0.5 from optimisation. This method is a simplified version of similar ones present in literature [72] mixed with the tracks weighted one, from which it inherits the advantage of taking already into account the problem of the B^0 - \bar{B}^0 mixing. For both methods, one can then define

$$\langle Q_{FB} \rangle \equiv \langle (-1)^{FB} Q_{\text{jet}} \rangle,$$

where $(-1)^{FB}$ is computed event by event as the sign of $\vec{j}^* \cdot \vec{p}_{e^-}^*$, both taken in the Z rest frame. The mean b -jet charge $\delta^b \equiv \langle Q_b \rangle$ is obtained from the average value of Q_{jet} for events with a b -quark initiated jet (i.e. not a \bar{b}), and was here taken from simulations (but will be experimentally constrained in a real measurement). With these definitions, in a pure b/\bar{b} sample, the b -quark asymmetry $A_{FB}^{b,\text{LHC}}$ is proportional to $\langle Q_{FB} \rangle$:

$$\langle Q_{FB} \rangle = \delta^b A_{FB}^{b,\text{LHC}}. \quad (3.5.29)$$

With a non pure sample of jets originated from different quark flavours, Eq. (3.5.29) gets modified into:

$$\langle Q_{FB} \rangle = \sum_f \delta^f A_{FB}^{f,\text{LHC}} r_f, \quad (3.5.30)$$

where the sum runs over the quark flavours present in the sample, while r_f are the fractions of events with flavour f . For the purposes of this article, given the usual efficiencies and mistag rates of b -tagging algorithms on the market, it suffices to consider only the c -jet background (represented at LO from the process $p p \rightarrow c l \bar{l}$).

3.6 Feasibility study

Modern feasibility studies deeply rely on Monte Carlo (MC) simulation programs. Even if their history goes far in the past of particle physics, two genuinely contemporary features which starts to characterise an increasing fraction of MC generators

is their independence from experimental collaborations and their fastness, both regarding parton level processes and detector simulations.

3.6.1 MadGraph 5

The `MadGraph 5` software [69] is a matrix element generator, written in the Python programming language. It can generate matrix elements both at tree-level for any model Lagrangian and at one-loop order in QCD, with the corresponding helicity amplitudes. The process-specific commands that have to be passed to the software are contained in a card called `proc-card-mg5.dat`; also decay chains of particles in the final state can be specified. After this first step the user can edit the card `run-card.dat`, where features of the generated samples of events can be modified, plus a great variety of possible kinematic cuts. `MadGraph` generates all Feynman diagrams which contribute to the amplitude of the process and outputs the computer code necessary to evaluate the associated matrix elements. By mean of this code, it proceeds to generate the pseudorandom sample of desired events, showing an highly user-friendly `html` page with all relevant informations like the cross section, the theoretical model which have been used and the pictures of the Feynman diagrams. `MadGraph` is natively predisposed to be interfaced with other MC showers (`Pythia`, `Herwig`) and detector simulators (`Delphes`, `PGS`).

3.6.2 The study

The simulated samples were generated using `MadGraph 5` [69] interfaced with `PYTHIA 6.4` [70] for the showering and with `Delphes 3` [71] for the detector simulation (the `Delphes` card was modified for ATLAS updated parameters). The event selection criteria was taken from [63]. The number of events generated corresponds to a conservative estimate of a ten years luminosity of 400 fb^{-1} at 14 TeV, though results can also be extrapolated to a possible final integrated luminosity of 3 ab^{-1} , predicted for the (not yet approved) High Luminosity LHC (HL-LHC). Due to partial cancellation from opposite values of mean jet charges in Eq. (3.5.30), the b -tagging efficiency which optimises the relative uncertainty on $\langle Q_{FB} \rangle$ was found to be 55%

		b/\bar{b} sample		c/\bar{c} sample	
		Jet charge	Soft muon	Jet charge	Soft muon
Total number of events		8.96 10^6		10.08 10^6	
Flavour fractions	ϵ_b 50%	0.94	0.99	0.06	0.01
	ϵ_b 60%	0.88	0.97	0.12	0.03
δ^f		-0.0736	-0.3027	0.0721	0.535

Table 3.1. Generated events and input parameters. Systematic errors on flavour fractions and δ_f are irrelevant given the estimated statistical uncertainty on the final results, while they should be taken into account (comprising possible effects giving $\delta^f \neq -\delta^{\bar{f}}$) in a possible HL-LHC upgrade.

(see [73]): we present results at two different b -tagging efficiency working points ($\{\epsilon_b, \epsilon_c\} = \{50, 3\}\%$, $\{60, 8\}\%$), which, from inversion of Eq. (3.5.30), allows in principle also an independent determination of A_{FB}^c , taking as input the predicted flavour fractions and mean charges. Table 3.1 collects the number of generated events and computed input parameters, while results are presented in Table 3.2, and refers to a single experiment (ATLAS in this case). Systematic uncertainties from ISR/FSR has been inspected switching them separately off and taking, as the associated uncertainty, 20% of the total effect. While FSR has no impact at all, ISR gives a relative systematic uncertainty lower than 2%, and needs a deeper understanding of the source of this variation. The impact of pile-up⁶ (PU) effects has been inspected using the related `Delphes` PU module, setting the average amount of PU events per bunch-crossing to 50, and found to be negligible.

This simplified study shows that a relative overall uncertainty on the measured asymmetry value of less than 10% can be easily reached with 400 fb^{-1} of data from ATLAS and CMS. This value, extrapolated for an integrated luminosity of 3 ab^{-1} , can be lower than 4%, imposing at that level also a deeper study of systematic

⁶Pile-up is defined as the average number of particle interactions per bunch crossing μ , and is directly correlated with the instantaneous luminosity. The growing pile-up presents a challenge for LHC experiments during data taking.

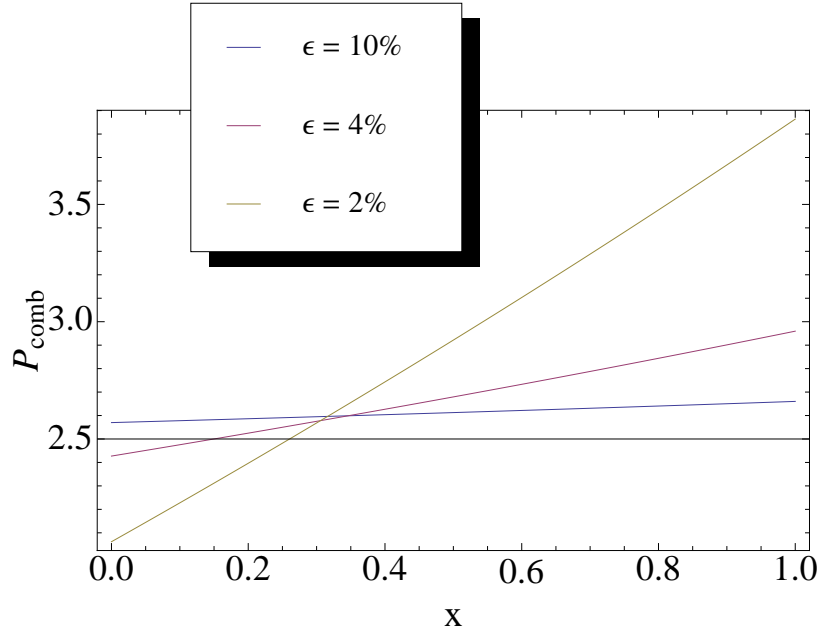
	ϵ_b 50%	ϵ_b 60%	$A_{FB}^{b,\text{LHC}}$	Combined value
$\langle Q_{\text{FB}} \rangle$	23.4 ± 2.3	21.3 ± 2.0	-343 ± 54	-347 ± 47
$\langle Q_{\text{FB}}^\mu \rangle$	104 ± 17	96 ± 15	-361 ± 95	

Table 3.2. Results (times a factor 10^4) for an integrated luminosity of 400 fb^{-1} for both electron and muon channels, assuming lepton universality.

uncertainties, out of the scopes of this work. One should also take into account that these values have to be intended as very conservative, and will most likely be lowered in a real experimental measurement, owing to the use of more sophisticated methods and improvements on b -purities and mean charges (e.g. from tagging and rejection of double b -hadron jets from ISR [74]).

3.6.3 Impact of $A_{FB}^{b,\text{LHC}}$

In the previous section a simplified study has put an upper bound on the relative uncertainty ATLAS and CMS can realistically obtain for a measurement of $A_{FB}^{b,\text{LHC}}$ at the (HL-)LHC. Of course, to give to these numbers some meaning, one should compare such quantities with the present relative uncertainty $\epsilon^{\text{WA}} = 1.6\%$ on the World Average (WA) value of $A_{FB}^{0,b}$, that results, as already discussed in Chapter 2, in a pull-value of 2.6 standard deviations from its Standard Model theoretical prediction (SM). To this aim let's call ϵ the relative uncertainty associated to a new determination of $A_{FB}^{0,b}$ through $A_{FB}^{b,\text{LHC}}$. Given the direct proportionality that connects the two quantities, it is fair to neglect additional sources of uncertainty coming from the unfolding procedure, such that it can be assumed an upper bound on ϵ certainly comparable to the one it has been here fixed on the relative uncertainty on $A_{FB}^{b,\text{LHC}}$. The impact of a new such experimental determination can be accordingly simulated given a probable outcome of the measurement itself. This can be *e.g.* left to vary in the range $\{\text{WA}(A_{FB}^{0,b}) - \sigma, \text{SM}(A_{FB}^{0,b})\}$, mapped linearly by a conventional parameter $x \in \{1,0\}$. For every value of x , it is thus possible to compute the combined



value of $A_{FB}^{0,b}$ and its uncertainty, here assumed to be

$$O_{\text{comb}} = \frac{\frac{O_{\text{WA}}}{\sigma_{\text{WA}}^2} + \frac{O_{\text{LHC}}}{\sigma_{\text{LHC}}^2}}{\sigma_{\text{WA}}^{-2} + \sigma_{\text{LHC}}^{-2}}, \quad \sigma_{\text{comb}} = \frac{\sigma_{\text{WA}} \sigma_{\text{LHC}}}{\sqrt{\sigma_{\text{WA}}^2 + \sigma_{\text{LHC}}^2}},$$

and for every probable outcome the resulting combined pull value P_{comb} (Figure 3.6.3). Under these simple but realistic assumptions, it is clear that the chances of a measurement of $A_{FB}^{b,\text{LHC}}$ not to have impact at all on the present situation are certainly poor. Indeed either it will solve the discrepancy (saving in this way theories like the SM or the MSSM in which, as we have already seen in section 3.4, no important deviation are allowed), or it will worsen the situation, opening the way to new NP models of mostly likely non supersymmetric origin.

Of course physics everyday brings in new surprises, and it may very well be that NP will knock on our doors with some new direct signal, like the discovery of a new particle, maybe just at the beginning of the next LHC Run II. The next chapter will treat precisely this eventuality.

Chapter 4

bH_{light} associated production in the NMSSM at LHC at One-Loop Order

Introduction

The pragmatic approach towards possible manifestations of NP at LHC leads us finally to this last chapter. We have already studied a significative example of indirect signal coming from ready-to-test observables. It is now time to take into account also the possibility of direct detection of NP, of which a relevant example chosen here is the associated production of bottom quarks and Higgs Bosons from the so-called Next to Minimal Supersymmetric Standard Model (NMSSM, see [86] and references therein).

4.1 Motivations for the NMSSM

The main motivations for SUSY extensions of the Standard Model (SM) are a solution of the hierarchy problem [87–91] through protection of the weak scale by SUSY and an automatic unification of the running gauge couplings at a Grand Unified (GUT) scale M_{GUT} [92–95] (as far as the SUSY-breaking scale is not too high). To

these one should add the possibility to explain the dark matter relic density in terms of a stable neutral particle [96,97], but only after the additional assumption that the SUSY extension has a certain global symmetry (called R-parity or matter-Parity, depending on the definitions) forbidding the lightest SUSY particle (LSP) to decay into ordinary matter.

Any SUSY extension of the Higgs sector of the SM [98,99] requires the introduction of two different Higgs $SU(2)$ -doublets, called H_u and H_d . This follows both from imposing the superpotential to be holomorphic in the fields and from the necessary mutual cancellation of the anomaly induced by the fermionic components of the two Superfields¹. The vacuum expectation values (VEVs) of H_u and H_d generate masses for up-type quarks and down-type quarks and charged leptons, respectively. The model with this minimal field content in the Higgs sector is denoted as the Minimal Supersymmetric Standard Model (MSSM) (for reviews see, e. g., [100–102]). Defining the MSSM Lagrangian to be the most general SUSY one invariant under the SM gauge group implies that it contains a SUSY mass term μ for H_u and H_d , which nevertheless seems constrained to be of the order of the SUSY-breaking scale M_{SUSY} for phenomenological reasons. In fact both complex Higgs scalars H_u and H_d of the MSSM have to be components of chiral Superfields which contain, in addition, fermionic $SU(2)$ -doublets ψ_u and ψ_d . The μ term in the Lagrangian of the MSSM generates identical positive masses squared μ^2 for $|H_u|^2$ and $|H_d|^2$, and a Dirac mass μ for ψ_u and ψ_d . On top of this, the presence of a SUSY mass term μ in the Lagrangian allows a soft SUSY-breaking mass term $m_{ud}^2 H_u H_d$ too, conventionally parametrized by $m_{ud}^2 = B\mu$, with B a parameter with dimensions of mass. This helps to understand how the μ parameter has both an upper and lower constraint.

μ cannot vanish. First, a Dirac mass μ for ψ_u and ψ_d is required for phenomenological reasons: both fermionic $SU(2)$ -doublets ψ_u and ψ_d contain electrically charged components. Together with the fermionic superpartners of the

¹It is not here the place to review the Superfields formalism [101]. For our purposes, it suffices to remember that, on-shell, they can be seen as multiplets containing usual fields as components differing by half units of spin, related one to each other by SUSY transformations.

W^\pm bosons, they constitute the so-called chargino sector of SUSY extensions of the SM (two charged Dirac fermions). Due to the fruitless searches for charginos at LEP [134] and LHC (Fig. 4.1), the lighter chargino has to have a mass above

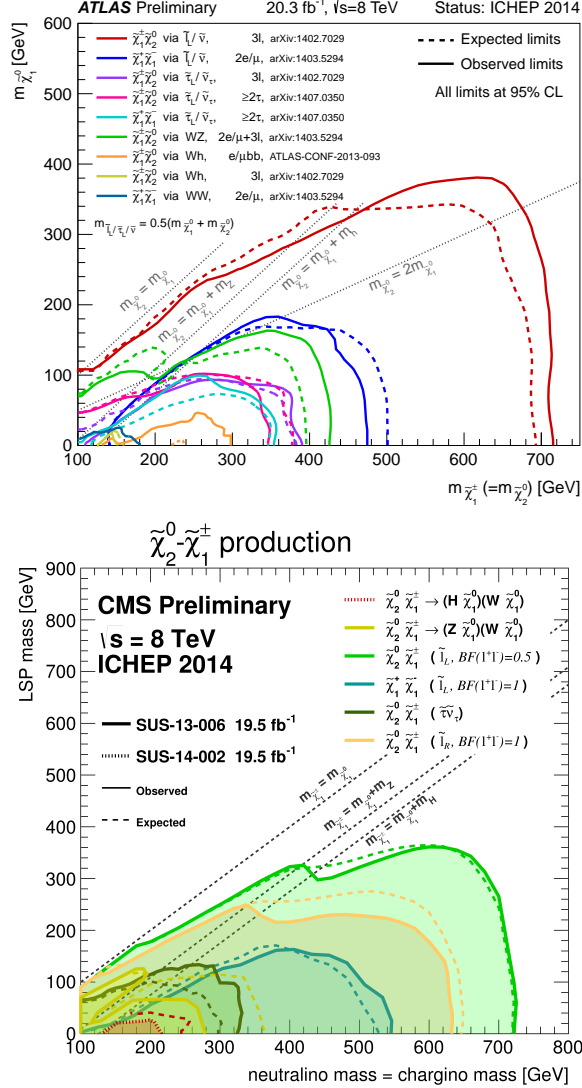


Figure 4.1. Latest combined 95 % C.L. exclusion limits for direct production of electroweakinos from the ATLAS and CMS experiments, as presented at the 37th International Conference on High Energy Physics (ICHEP 2014). Proceedings of this conference will be published in Nuclear Physics B - Proceedings Supplements (NUPHBP).

~ 270 GeV / 700 GeV depending on the particular assumptions of simplified models

used to extract exclusions from direct searches. Analysing the chargino mass matrix, one finds that this lower limit implies that the Dirac mass μ for ψ_u and ψ_d – for arbitrary values of the other parameters – has to satisfy the constraint $|\mu| \gtrsim 250$ GeV.

Additionally, an analysis of the Higgs potential shows that a non-vanishing term $m_{ud}^2 H_u H_d$ is a necessary condition for that *both* neutral components of H_u and H_d are non-vanishing at the minimum. This, in turn, is required in order to generate masses for up-type quarks, down-type quarks and leptons by the Higgs mechanism. Moreover, the numerical value of the product $B\mu$ should be roughly of the order of the electroweak scale (M_Z^2).

Finally, $\mu \simeq 0$ would generate a Peccei-Quinn symmetry in the Higgs sector, and hence an unacceptable massless axion [103].

$|\mu|$ must be not too large. The Higgs potential must be unstable at its origin $H_u = H_d = 0$ in order to generate the electroweak symmetry breaking. Whereas the soft SUSY-breaking mass terms for H_u and H_d (of the order of the SUSY-breaking scale M_{SUSY}) can generate such a desired instability, the μ -induced masses squared for H_u and H_d are always positive, and must *not* dominate the negative soft SUSY-breaking mass terms. Consequently the μ parameter must obey $|\mu| \lesssim M_{\text{SUSY}}$.

Hence, both “natural” values $\mu \simeq 0$ and very large μ ($\sim M_{\text{GUT}}$ or $\sim M_{\text{Planck}}$) are ruled out, and the need for an explanation of why $\mu \approx M_{\text{SUSY}}$ gives rise to the so-called μ -problem [103] of the MSSM. One of the simplest way to solve this problem consists in generating an effective (SUSY) mass term μ by spontaneous symmetry breaking from an additional scalar field: the mass term μ is replaced by a Yukawa coupling of H_u and H_d to this scalar, and its VEV $\langle S \rangle$ – induced by the soft SUSY-breaking terms – is of the desired order. Since the μ parameter carries no $SU(3) \times SU(2) \times U(1)_Y$ quantum numbers, the field to be introduced has to be a singlet S (the complex scalar component of a chiral Superfield \widehat{S}^2), and the resulting model is called the “general” NMSSM (NMSSM), sometimes also denoted as the (M+1)SSM. Of course, with no other symmetry assumptions, an *explicit* SUSY mixing between H_u and H_d could be also present, which motivates the introduction

²Here and in the following a “ $\widehat{}$ ” distinguishes *explicitly* the Superfield from its scalar component.

of a Z_3 discrete symmetry under which every chiral Superfield transforms multiplicatively by a common factor $e^{2\pi i/3}$. This discrete symmetry forbids terms even in \widehat{S} , \widehat{H}_u and \widehat{H}_d and in their scalar components, respectively in the superpotential and in the SUSY-breaking part of the Lagrangian. This is the so-called Z_3 or scale-invariant³ NMSSM, mostly called in literature simply NMSSM.

Within the NMSSM $\langle S \rangle$ is naturally of the order of M_{SUSY} , being induced by negative soft SUSY-breaking terms (squared masses or trilinear couplings). Then M_{SUSY} is the only scale in the theory. In this sense, the NMSSM is the simplest SUSY extension of the SM in which the weak scale is generated by the SUSY-breaking scale M_{SUSY} only.

From an historical point of view, it should be noticed that already the first attempts to construct SUSY extensions of the SM employed in fact such a singlet field [98, 99, 104]. A singlet was also present in most of the first globally SUSY GUT models [91, 105–108]. Then it has been realised that spontaneous SUSY-breaking in the framework of supergravity (SUGRA) leads in a simple way to the desired soft SUSY-breaking terms in the Lagrangian; see [100] for an early review. Within SUGRA, a μ term of the order of M_{SUSY} can actually be generated if one assumes the presence of a particular Higgs-dependent structure in the Kähler potential [109]: of course under this assumptions an *explicit* μ term is allowed too, and, in order to solve the μ problem, it must be forbidden by some additional mechanism. Still, the first locally SUSY extensions of the SM [110–112] as well as most GUT models within SUGRA [113–120] used a singlet field in the Higgs sector, leading to variants of the NMSSM at the weak or SUSY-breaking scale $\lesssim 1$ TeV (see also SUGRA models motivated by String theory [121–130]). Recently, the discovery of the new SM Higgs-like state with a mass of 125 GeV has renewed interest towards the NMSSM, especially due to its mitigation of fine tuning associated to this quite small mass compared to general MSSM predictions and to the lack of discovery of new SUSY states during the LHC Run I.

After electroweak symmetry breaking, the scalar components of \widehat{S} mix with

³Actually often the Z_3 discrete symmetry is seen as an accidental symmetry resulting by imposing scale-invariance to the superpotential.

the neutral scalar components of \widehat{H}_u and \widehat{H}_d leading, in the absence of complex parameters (corresponding to the absence of explicit CP violation), to three CP-even and two CP-odd neutral scalars (see [131–133] for some reviews). Likewise, the fermionic superpartner of \widehat{S} mixes with the neutral fermionic superpartners of \widehat{H}_u , \widehat{H}_d and the neutral electroweak gauginos, leading to five neutralinos. In this way the four additional degrees of freedom contained in the Superfield \widehat{S} enrich the scalar and fermionic sectors of the MSSM with three more mass eigenstates, rising the possibility of a distinct and peculiar phenomenology. In the Higgs sector, for example, important alterations with respect to the MSSM are a somehow lower tension with the measured mass value of the Higgs scalar with SM-like couplings to gauge bosons (or, equivalently, less tuning at fixed mass), and the yet open possibility of additional light states with reduced couplings to gauge-bosons. In fact the so-called LEP excess [135] around 98 GeV is still compatible with a NMSSM CP-even Higgs [136], contrary to earlier interpretations in the MSSM already excluded by LHC searches. Notably, a light CP-odd scalar with vanishing couplings to two gauge bosons (like all CP-odd scalars), but with even enhanced couplings to quarks and leptons can appear in the Higgs spectrum, allowing for new Higgs-to-Higgs decays. Under these circumstances, the detection of additional Higgs bosons at LHC or future colliders can become complicated (see e.g. [136]). In addition, a light CP-odd scalar can affect “low energy” observables in B -physics and Υ -physics, as well as and the anomalous magnetic moment of the muon.

The additional singlet-like neutralino can imply relevant modifications within the neutralino sector, especially if it is the lightest one and, simultaneously, the lightest SUSY particle (LSP). This would have an important impact on all decay chains of SUSY particles (sparticles), and hence on their signatures at colliders. For instance, the next-to-lightest SUSY particle (NLSP) can have a long life-time leading to displaced vertices. Also, the LSP relic density has to be reconsidered in this case.

4.2 The NMSSM Higgs Sector

The superpotential of the Minimal SUSY extension of the SM with both R-parity

$$R_P = (-1)^{(B-L)+2s} = (-1)^{2s} M \quad (4.2.1)$$

(B and L being barion and lepton numbers, s the spin of the field component of the Superfields) and Z_3 discrete symmetry acting on chiral Superfields Φ as

$$\Phi \rightarrow e^{2\pi i/3} \Phi \quad (4.2.2)$$

in terms of the quark and lepton Superfields $\hat{Q}, \hat{U}^c, \hat{D}^c, \hat{L}, \hat{E}^c$ reads

$$W_{MSSM}^{Z_3} = \epsilon_{ab} [y_e \hat{H}_d^a \hat{L}^b \hat{E}^c + y_d \hat{H}_d^a \hat{Q}^b \hat{D}^c - y_u \hat{H}_u^a \hat{Q}^b \hat{U}^c], \quad (4.2.3)$$

where $a, b = 1, 2$ are the $SU(2)_L$ fundamental representation indices and ϵ_{ab} denotes the totally antisymmetric tensor with $\epsilon_{12} = \epsilon^{12} = 1$. The addition of a complex scalar Superfield \hat{S} , neutral under the SM gauge group, allows for extra two terms involving Higgs S-fields $\hat{H}_u, \hat{H}_d, \hat{S}$, completing the NMSSM Superpotential in the form

$$W_{NMSSM} = W_{MSSM} - \epsilon_{ab} \lambda \hat{S} \hat{H}_d^a \hat{H}_u^b + \frac{1}{3} \kappa \hat{S}^3, \quad (4.2.4)$$

where the Higgs Superfield which couples to up-type (down-type) fermion Superfields is given by $\hat{H}_{u(d)}$. The parameters λ and κ are dimensionless and, working in the CP-invariant NMSSM, are chosen to be real.

The soft SUSY-breaking terms in the NMSSM in terms of the component fields H_u, H_d, S are given by

$$\mathcal{L}_{soft} = \mathcal{L}_{soft, MSSM} - m_S^2 |S|^2 + (\epsilon_{ab} \lambda A_\lambda S H_d^a H_u^b - \frac{1}{3} \kappa A_\kappa S^3 + h.c.), \quad (4.2.5)$$

with the MSSM soft SUSY-breaking Lagrangian

$$\begin{aligned} \mathcal{L}_{soft, MSSM} &= -m_{H_d}^2 H_d^\dagger H_d - m_{H_u}^2 H_u^\dagger H_u \\ &- m_Q^2 \tilde{Q}^\dagger \tilde{Q} - m_L^2 \tilde{L}^\dagger \tilde{L} - m_U^2 \tilde{u}^c \tilde{u}^{c*} - m_D^2 \tilde{d}^c \tilde{d}^{c*} - m_E^2 \tilde{e}^c \tilde{e}^{c*} \\ &- (\epsilon_{ab} [y_e A_e H_d^a \tilde{L}^b \tilde{e}^c + y_d A_d H_d^a \tilde{Q}^b \tilde{d}^c - y_u A_u H_u^a \tilde{Q}^b \tilde{u}^c] + h.c.) \\ &- \frac{1}{2} (M_1 \tilde{B} \tilde{B} + M_2 \tilde{W}_i \tilde{W}_i + M_3 \tilde{G} \tilde{G} + h.c.), \end{aligned} \quad (4.2.6)$$

where symbol “ $\tilde{}$ ” is used to denote the SUSY partner of the relative SM field (so that e.g. $\tilde{Q} = (\tilde{u}_L, \tilde{d}_L)^T$, $\tilde{L} = (\tilde{\nu}_L, \tilde{e}_L)^T$ are the scalar partners of the SM lepton and quark doublets, while in the last line the soft SUSY-breaking gaugino mass terms for the gaugino fields \tilde{B} , \tilde{W}_i ($i = 1, 2, 3$) and \tilde{G} are given). Often in literature one also finds the identification $\tilde{u}^c = \tilde{u}_R^*$, which here is avoided for the seek of clarity. All soft SUSY-breaking trilinear couplings A_k ($k = \lambda, \kappa, d, u, e$) and gaugino mass parameters M_i ($i = 1, 2, 3$) are assumed to be real, and squark and slepton mixing between the generations is neglected. Note also the absence of possible soft SUSY-breaking terms linear and quadratic in the scalar fields S , H_u and H_d (as e.g. the genuinely MSSM term $m_{ud}^2 \epsilon_{ab} H_d^a H_u^b$) due to imposition of Z_3 parity, in accordance with the majority of phenomenological NMSSM constructions.

The NMSSM scalar potential is derived through F terms contribution from the NMSSM superpotential W_{NMSSM} , the corresponding soft SUSY-breaking terms and the D term contributions. After spontaneous symmetry breaking, the neutral components of the Higgs fields acquire a vacuum expectation value, parametrised in terms of CP-even and CP-odd fluctuations as

$$H_d^1 = \frac{1}{\sqrt{2}}(v_d + h_d + ia_d), \quad H_u^2 = \frac{1}{\sqrt{2}}(v_u + h_u + ia_u), \quad S = \frac{1}{\sqrt{2}}(v_s + h_s + ia_s), \quad (4.2.7)$$

with the VEVs v_d , v_u , v_s chosen to be real and positive. From this it can be recognized the effective parameter μ_{eff} , which arises dynamically from the VEV of the singlet field *cf.* Eq. (4.2.4),

$$\mu_{\text{eff}} = \frac{\lambda v_s}{\sqrt{2}}. \quad (4.2.8)$$

The soft SUSY-breaking Higgs mass parameters $m_{H_u}^2, m_{H_d}^2, m_S^2$ can be replaced, through the minimisation conditions of the tree-level scalar potential, by combinations of λ , κ , the electroweak gauge couplings g and g' , the VEVs and the trilinear couplings A_λ , A_κ , so that the tree-level mass matrix M_S^2 of the neutral CP-even Higgs bosons obtained from the second derivative of the Higgs potential with respect to the fields in the vacuum, in the basis $h^S = (h_d, h_u, h_s)^T$, can be cast into the

form

$$M_S^2 = \begin{pmatrix} \bar{g}^2 v_d^2 + \frac{G_2 v_u v_s}{v_d} & (\lambda^2 - \bar{g}^2) v_u v_d - G_2 v_s & \lambda^2 v_d v_s - G v_u \\ (\lambda^2 - \bar{g}^2) v_u v_d - G_2 v_s & \bar{g}^2 v_u^2 + \frac{G_2 v_d v_s}{v_u} & \lambda^2 v_u v_s - G v_d \\ \lambda^2 v_d v_s - G v_u & \lambda^2 v_u v_s - G v_d & 2\kappa^2 v_s^2 + \frac{R_\lambda v_u v_d}{v_s} + R_\kappa v_s \end{pmatrix} \quad (4.2.9)$$

where we have defined

$$\begin{aligned} \bar{g}^2 &= \frac{1}{4}(g^2 + g'^2), & R &= \lambda\kappa, & R_\lambda &= \frac{1}{\sqrt{2}}\lambda A_\lambda, & R_\kappa &= \frac{1}{\sqrt{2}}\kappa A_\kappa \\ G &= R_\lambda + R v_s, & G_2 &= R_\lambda + R v_s/2. \end{aligned} \quad (4.2.10)$$

Note that the MSSM limit for the scalar masses⁴ can be recovered by $\lambda, \kappa \rightarrow 0$ (with the ratio κ/λ kept constant for a smooth approach) and keeping fixed the parameter $\mu = \lambda v_s/\sqrt{2}$, as well as the parameters A_λ and A_κ . In this limit one hence has $v_s \rightarrow \infty$.

Through an orthogonal transformation \mathcal{R}^S , the matrix M_S^2 is diagonalized in terms of the CP-even mass eigenstates H_i ($i = 1, 2, 3$) (paired indices implicitly summed),

$$H_i = \mathcal{R}_{ij}^S h_j^S, \quad j = d, u, s, \quad (4.2.11)$$

where, following SLHA2 conventions [142], $M_{H_1} \leq M_{H_2} \leq M_{H_3}$.

The CP-odd fields (a_d, a_u, a_s) can be, for later convenience, first rotated by an angle β_n in the subspace (a_d, a_u) , to separate a massless Goldstone boson G

$$\begin{pmatrix} a \\ a_s \\ G \end{pmatrix} = \begin{pmatrix} s\beta_n & c\beta_n & 0 \\ 0 & 0 & 1 \\ c\beta_n & -s\beta_n & 0 \end{pmatrix} \begin{pmatrix} a_d \\ a_u \\ a_s \end{pmatrix} \equiv \mathcal{R}_{ij}^{\beta_n} a_j, \quad (4.2.12)$$

⁴ In this limit the NMSSM is not rigorously mapped into the MSSM due to the non decoupling of the additional neutralino (see below).

with the abbreviations $c_x \equiv \cos x$ and $s_x \equiv \sin x$. In this way, starting from the tree-level CP-odd mass matrix squared in the basis $(a_d, a_u, a_s)^T$

$$M_P^2 = \begin{pmatrix} v_s G_2 \frac{v_u}{v_d} & v_s G_2 & (R_\lambda - Rv_s)v_u \\ v_s G_2 & v_s G_2 \frac{v_d}{v_u} & (R_\lambda - Rv_s)v_d \\ (R_\lambda - Rv_s)v_u & (R_\lambda - Rv_s)v_d & (R_\lambda + 2Rv_s)\frac{v_u v_d}{v_s} - 3R_\kappa v_s \end{pmatrix} \quad (4.2.13)$$

and using Eq. (4.2.12), one ends up with the mass matrix squared $M_P^{2\star}$ in the basis $h^P = (a, a_s, G)^T$, which reads

$$M_P^{2\star} = \begin{pmatrix} 2G_2 v_s \frac{c_{\Delta\beta}^2}{s_{2\beta}} & (R_\lambda - Rv_s)vc_{\Delta\beta} & G_2 v_s \frac{s_{2\Delta\beta}}{s_{2\beta}} \\ (R_\lambda - Rv_s)vc_{\Delta\beta} & (2R + R_\lambda/v_s)\frac{v^2 s_{2\beta}}{2} - 3R_\kappa v_s & (R_\lambda - Rv_s)vs_{\Delta\beta} \\ G_2 v_s \frac{s_{2\Delta\beta}}{s_{2\beta}} & (R_\lambda - Rv_s)vs_{\Delta\beta} & 2G_2 v_s \frac{s_{\Delta\beta}^2}{s_{2\beta}} \end{pmatrix} \quad (4.2.14)$$

with $\Delta\beta = \beta - \beta_n$ and $v^2 \equiv v_u^2 + v_d^2$. Here some care has to be taken to distinguish between the angle β_n parametrizing the rotation (which will not be subject to renormalisation) and the angle β defined through the ratio of the VEVs v_u, v_d , $\tan \beta = v_u/v_d$. They of course coincide at tree-level, whence $\Delta\beta = 0$ leading to a massless Goldstone boson (which decouples as it should), but the difference in their definitions will play a role when dealing with determination of the counterterms. It has to be noted that the first entry $(M_P^{2\star})_{11}$ at tree-level,

$$(M_P^{2\star})_{11} = \frac{2G_2 v_s}{s_{2\beta}}, \quad (4.2.15)$$

becomes the mass of the pseudoscalar Higgs boson in the MSSM limit⁵. Applying an orthogonal rotation $\mathcal{R}^{P\star}$ to $h^P = (a, a_s, G)^T$, the CP-odd mass eigenstates $A_i \equiv A_1, A_2, G$ ($i = 1, 2, 3$) are obtained,

$$A_i = \mathcal{R}_{ij}^{P\star} h_j^P, \quad (4.2.16)$$

⁵In the MSSM limit A_λ can be identified with the soft SUSY-breaking parameter B : $\mathcal{L}_{\text{soft, MSSM}} \supseteq m_{ud}^2 \epsilon_{ab} H_u^a H_d^b \equiv B\mu \epsilon_{ab} H_u^a H_d^b$.

where at tree-level $\mathcal{R}_{33}^{P\star} = 1$ and $\mathcal{R}_{3i}^{P\star} = \mathcal{R}_{i3}^{P\star} = 0$ for $i \neq 3$. The pseudoscalar masses are ordered by ascending mass, $M_{A_1} \leq M_{A_2}$. The net rotation transforming the gauge eigenstates (a_d, a_u, a_s) into the mass eigenstates A_i is therefore given by

$$\begin{aligned} A_i = \mathcal{R}_{ij}^{P\star} h_j^P &= \mathcal{R}_{ij}^{P\star} \mathcal{R}_{jk}^{\beta_n} a_k \\ \mathcal{R}_{ik}^P &\equiv \mathcal{R}_{ij}^{P\star} \mathcal{R}_{jk}^{\beta_n} \end{aligned} \quad (4.2.17)$$

The CP-even and CP-odd Higgs mass squared values at tree level are given by the eigenvalues of the respective mass matrices M_S^2 and M_P^2 , which are diagonalized numerically (for analytical results from expansion in special parameter regions see *e.g.* [137]). The situation is instead simpler for the charged Higgs boson, and quite similar to the MSSM case. After the massless charged Goldstone boson has been separated by an orthogonal rotation with a mixing angle β_c , at Born level we have $\beta_c = \beta$ and

$$M_{H^\pm}^2 = M_W^2 + \sqrt{2}\lambda \frac{v_s}{s_{2\beta}} \left(A_\lambda + \kappa \frac{v_s}{\sqrt{2}} \right) - \frac{\lambda^2 v^2}{2} = M_W^2 + (M_P^{2\star})_{11} - \frac{\lambda^2 v^2}{2}, \quad (4.2.18)$$

with M_W being the W -boson mass and where we have applied the definition given in Eq. (4.2.15).

4.3 Motivations for a study of the NMSSM bH_{light} associated production

Application of a pragmatic approach to possible direct signals of NP in the bottom sector seems to result in a paradox. Given that to be pragmatic one should stick to facts, it seems at least controversial to talk about direct signals of NP in their absence (here, maybe too rigorously, *direct signals* stands for detection of new particles). Here a pragmatic approach can drive the choice of NP to be analysed. It is well known [32, 33] that MSSM searches for light Higgs scalars has completely excluded this possibility in most appealing benchmark scenarios; contrarily, the well motivated NMSSM yet leaves open this possibility [138, 139]. And if it is allowed, rephrasing a well known Gell-Mann sentence, it is mandatory to study it. The question arise on which production channel.

Associated production of b -jets and Higgs scalars has been exhaustively studied in the context of the MSSM: it is indeed well known that a MSSM SM-like Higgs has enhanced couplings to bottom quarks in the high $\tan\beta$ regime. In this limit, resummation of $\tan\beta$ enhanced contributions through the redefinition of the relation between the bottom mass and its Yukawa couplings is necessary, both in SUSY-QCD and EW sectors (see [145]). In [140] an effective Born approximation was proposed, which takes into account universal such effects neglecting other relatively small contributions. In [141] it was shown that the situation in associated Higgs-bottom production is quite different: when the Higgs boson produced is not at rest in the center of mass frame, the improved Born approximation is no more sufficient, and a good approximation of the complete one-loop calculation is given by the so-called Reduced Vertex Approximation. So the reasons of the present calculation in the NMSSM are at least two: the first one is to investigate the existence of genuinely NMSSM enhancements in the b -quark couplings to a light Higgs scalar, *e.g.* driven by the ratio v_s/v_d . The second reason, related to the first, is to check the reliability of such kind of approximations in this new context.

4.4 Born Level cross section

At tree level the process is described by the s - and u -channel b -quark exchange diagrams depicted in Fig. 4.4. By usual Feynman rules prescriptions, the Born level amplitude is straightforwardly obtained as

$$\begin{aligned} \mathcal{M}_{bg \rightarrow bH_{\text{light}}} &= - \left(\frac{g_s}{s - m_b^2} \right) \bar{u}'_b(\lambda'_b) c_{bH_{\text{light}}} (\not{q} + m_b) \not{\epsilon}_g(\mu) u_b(\lambda_b) \\ &\quad - \left(\frac{g_s}{u - m_b^2} \right) \bar{u}'_b(\lambda'_b) \not{\epsilon}_g(\mu) (\not{q}' + m_b) c_{bH_{\text{light}}} u_b(\lambda_b) \end{aligned}$$

where s, u from the propagators are the usual Mandelstam variables, colors indices are implicitly understood, helicities are labelled by λ, μ , and u, \bar{u} are Dirac spinors while ϵ is the polarization vector of the gluon. The coupling $c_{bH_{\text{light}}}$

$$c_{bH_{\text{light}}} = \left(\frac{em_b}{2s_W M_W} \right) \frac{\mathcal{R}_{11}^S}{\cos\beta}, \quad H_i = \mathcal{R}_{ij}^S h_j^S, \quad h^S = (h_d, h_u, h_s) \quad (4.4.1)$$

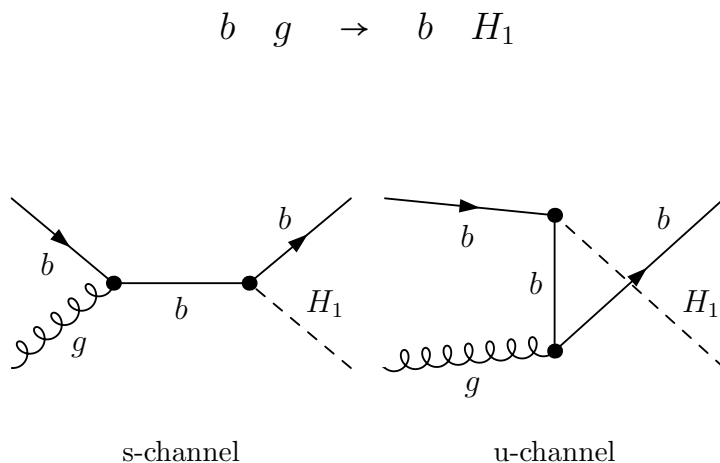


Figure 4.2. Relevant Feynman graphs at Born Level.

follows by the conventions $H_{light} \equiv H_1$, $h_1^S = h_d$.

4.5 One-Loop structure

The computation of one-loop corrections involves a huge number of diagrams: a brief list of classes of possible diagrams is shown in Figures 4.3, 4.4, 4.5. Hereafter the Dimensional Reduction regularisation scheme will be adopted, with a mixed OS- $\overline{\text{DR}}$ renormalisation scheme defined in [149]. A widely used classification of the different types of contributions will be applied in the following:

- Self Energies: two points one particle irreducible (1PI) insertions.
- Triangles: three points 1PI insertions. Here triangles will be further divided into Right/ Left and Up/Down Triangles depending on the vertex (bbh/bbg) and on the channel (s - or t -channel) the insertion is made.

- Boxes: four points functions.

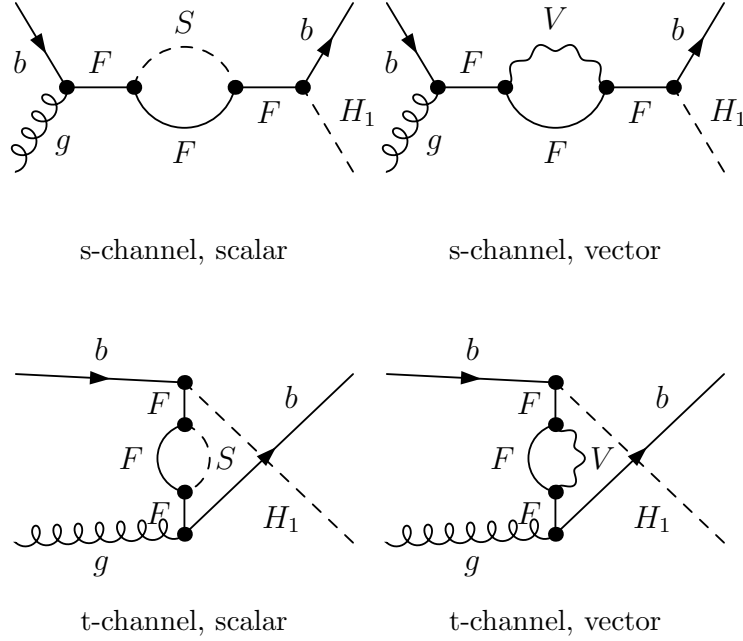


Figure 4.3. Internal Self Energies. Scalars, Fermions and Vectors are labelled as S , F and V .

4.5.1 Relevant Counterterms

The counterterms for the different amplitudes can all be derived from the ones renormalizing the vertices appearing at tree level, namely bbg and bbh , and from bottom propagator renormalisation. Dealing with EW corrections only (*i.e.* avoiding gluon and gluino insertions in the diagrams), the QCD coupling g_s and the gluon wave function gets not renormalized. This simplifies the QCD vertex counterterm to renormalisation of fermionic wave functions only :

$$\delta V_{bbg}^\eta = \frac{1}{2} (\delta Z_\eta^b + \delta Z_\eta^{b*}) \quad (4.5.1)$$

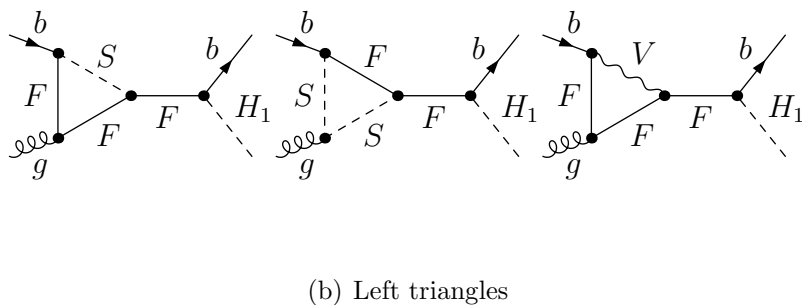
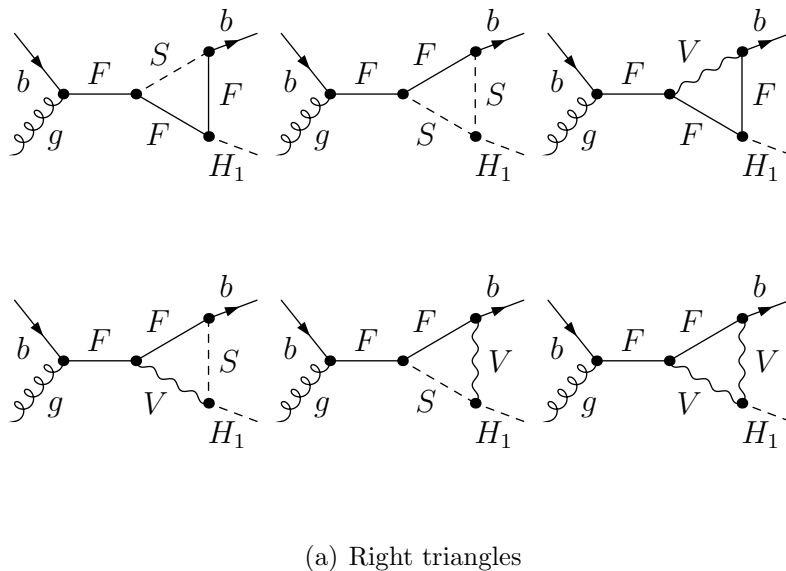
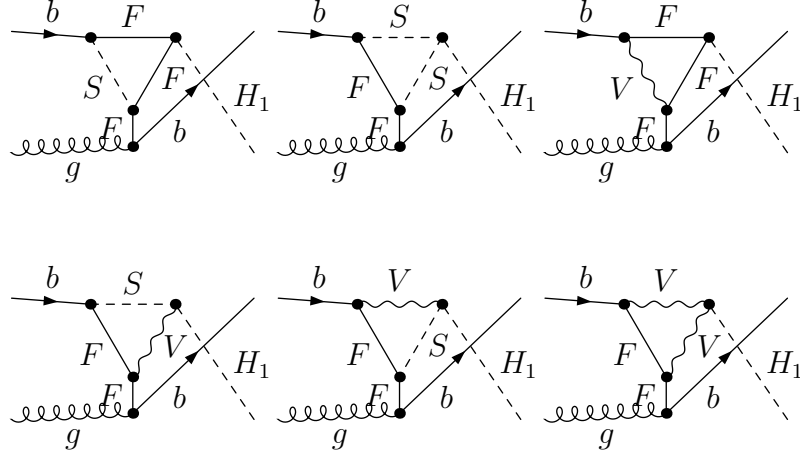
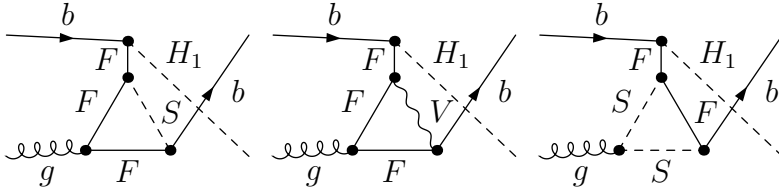


Figure 4.4. s -channel triangular diagrams contributing to EW one-loop corrections.

where η stands for the chirality projections L, R . The case of the bbh vertex is more interesting. Here also the bbh coupling 4.4.1 is subject to renormalisation, as it is



(a) Up triangles



(b) Down triangles

Figure 4.5. u -channel triangular diagrams contributing to EW one-loop corrections.

the case for the Higgs wave function:

$$\delta V_{bbh_1}^\eta = \frac{1}{2} (\delta Z_\eta^b + \delta Z_{\bar{\eta}}^{b*} + \delta Z^{h_1}) + \frac{\delta C_{bbh}}{C_{bbh}} \quad (4.5.2)$$

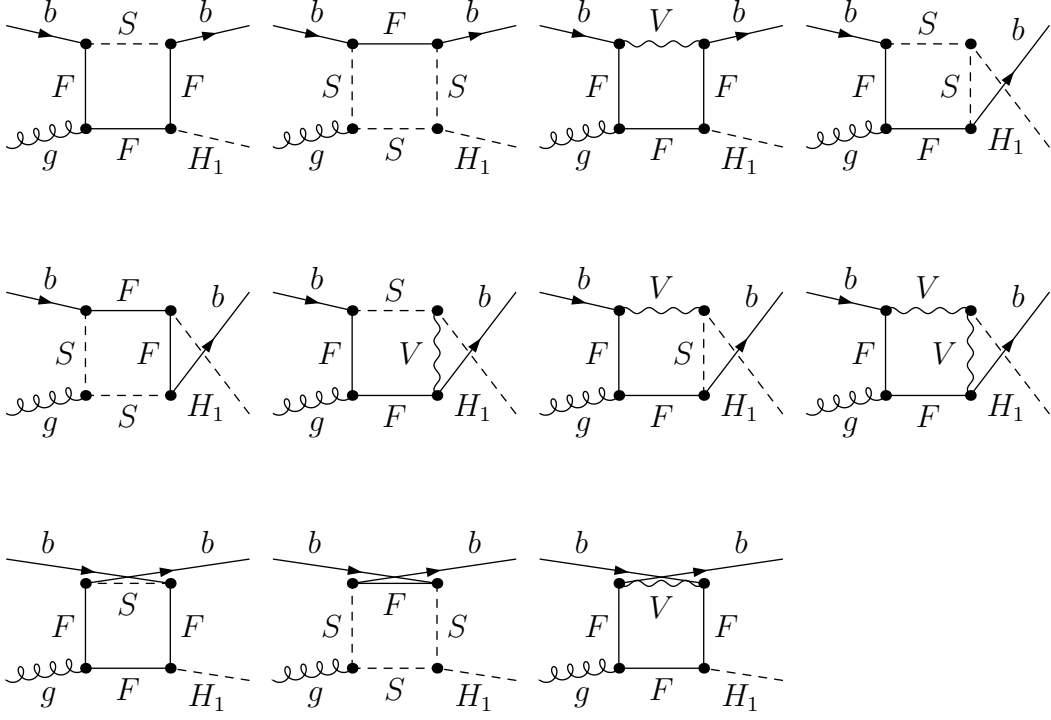


Figure 4.6. Boxes.

where $\bar{L} = R$ and viceversa, while

$$\begin{aligned}
 \delta Z^{h_1} &= \frac{1}{\mathcal{R}_{k1}^S} \sum_k \delta Z_{H_1 H_k} \mathcal{R}_{11}^S \\
 \delta Z_{H_j H_k} &= \sum_{\ell=d,u,S} \mathcal{R}_{\ell j}^{S*} \mathcal{R}_{k\ell}^S \delta Z_\ell \\
 \frac{\delta c_{bbh}}{c_{bbh}} &= \delta Z_e - \frac{\delta s\theta_W}{s\theta_W} + \frac{\delta m_b}{m_b} - \frac{\delta M_W^2}{2M_W^2} + \delta t\beta s\beta^2.
 \end{aligned}$$

The last ingredient needed is the internal b -exchange counterterm. This has to be decomposed into a counterterm assigned to the Lorentz vectorial part of the

propagator

$$\delta V_{bb}^{V,\eta} = \pm \frac{1}{2} (\delta Z_b^\eta + \delta Z_b^{\eta*}) \quad (4.5.3)$$

and one assigned to its scalar part

$$\delta V_{bb}^{S,\eta} = - \left[\frac{m_b}{2} (\delta Z_b^\eta + Z_b^{\bar{\eta}*}) + \delta m_b \right]. \quad (4.5.4)$$

With these basic counterterms all the derived ones associated to each particular one-loop amplitude can be computed: it suffices to substitute the actual 1PI insertion with the correspondent basic counterterm chosen between the three just mentioned. This procedure guarantees the UV finiteness of the singular amplitudes, but does not ensure well defined on-shell properties for external Higgs wave functions in case of non-OS renormalization schemes, as it is here the case. This follows from the fact that, if non-OS renormalization conditions are applied to the Higgs sector, the tree level mass eigenstates do not correspond automatically to the true one-loop ones, but get shifted by the higher order corrections. To properly take into account of this subtlety, one should take advantage of the procedure outlined *e.g.* in [149] to compute some (small) finite wave function normalization coefficients that allow to express the one-loop mass eigenstates in terms of the tree level ones. These coefficients in turn need the complete set of renormalization conditions of the whole Higgs sector, but resulting in a nearly negligible effect. For these reasons this part of the calculation will not be included in this work, but will be added in a forthcoming publication, also to allow the completion of some related checks. In the appendix the counterterms for the scalar squared mass matrix in gauge basis are explicitly derived, correcting some mismatch in related expressions in literature between [143] and [149].

4.6 Numerical Analysis

4.6.1 Numerical Checks

The renormalization procedure offers a good check of the model implementation, since cancellation of UV divergencies involves an intricate set of tree level relations

between different quantities. One of the most powerful virtues of having defined counterterms to single vertices is the fact that, in this way, UV finiteness can be checked in all subsets⁶ of amplitudes defined in Section 4.5. Boxes diagrams are finite by itself, so UV finiteness has to be checked only for Self Energies and Triangular diagrams. In order to do so, the parameter Δ regularizing the UV infinite terms

$$\Delta = \frac{2}{4-D} = \frac{2}{\epsilon}$$

has to be varied, checking that the sum of bare amplitudes and relative counterterms inside different subsets is indeed constant.

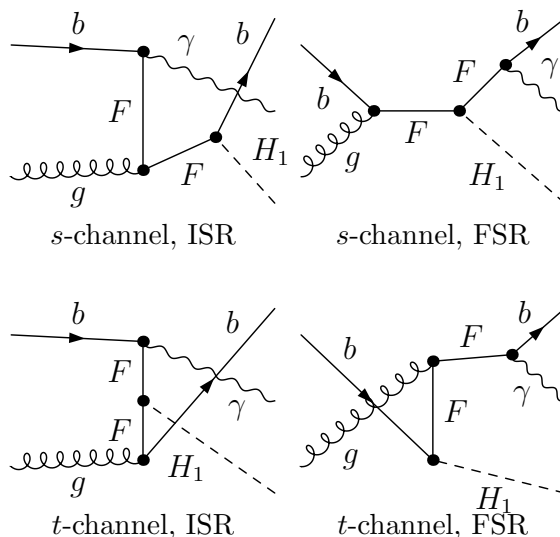


Figure 4.7. Soft photon radiation from external charged particles.

Infrared divergencies originate from exchange of virtual photons, and are regularized by a fictitious photon mass λ . IR finiteness is achieved after summing real soft photon emission (Fig. 4.7) from external charged particles to the virtual contributions, up to *unobservable* photon energies ΔE_{max} . Since the cancellation should be

⁶This, of course, does not means immediately that these subsets are automatically gauge independent, and in fact, as it will be shown below, the residual Infrared Divergencies do not cancel inside each subset, but in precise *combinations* among them and parts of the soft photon radiation.

exact, the regulator λ can be left to vary on arbitrary large ranges. The soft photon contribution, being a Born level quantity, clearly does not fall in any classification of the one-loop diagrams we gave (Triangles, Self Energies, Boxes): this means that IR finiteness will be achieved only after summation of all virtual subsets of diagrams, allowing IR divergencies cancellation *among* different virtual contributions and the soft photon real emission.

A third useful check of the model one-loop implementation, and in particular of the renormalization procedure in the Higgs sector, has to do with the Self Energies of the Goldstone bosons. In fact, since the Gauge Fixing Lagrangian is not renormalized, one expects, by custodial symmetry, that the neutral and charged Goldstone bosons Self Energies at zero external momentum equals one each other

$$\Sigma_{G_0}(0) = \Sigma_{G_{\pm}}(0) .$$

It has been checked numerically that indeed this is the case.

4.6.2 Benchmarks

A recent paper of S. King *et. al.* [138] has studied in great details the possibility of discovery of light scalar degrees of freedom in the contest of the NMSSM. It proposes several benchmark points that fulfil all present LHC and past experiments direct and indirect exclusions (limiting also from above the relic dark matter density using the upper bound of the PLANCK Collaboration precise measurement [144]). In particular, reduced signal rates μ_{XX} into different decay channels $H_i \rightarrow XX$

$$\mu_{XX}(H_i) = \frac{\sigma_{\text{prod}}(H_i)BR(H_i \rightarrow XX)}{\sigma_{\text{prod}}(H^{\text{SM}})BR(H^{\text{SM}} \rightarrow XX)} \equiv R_{\sigma_{\text{prod}}}(H_i) R_{XX}^{BR}(H_i) , \quad (4.6.5)$$

of the SM-like Higgs Boson $H_i \equiv h$

$$M_{H^{\text{SM}}} = M_{H_i} \equiv M_h = 124 - 127 \text{ GeV} \quad (4.6.6)$$

are fitted to their experimental values. They are defined as the production cross section σ_{prod} of the NMSSM Higgs boson H_i times its branching ratio BR into the final state XX , normalised to the corresponding SM values for a SM Higgs

boson H^{SM} . The approach used in that work is not only that of giving all possible parameters regions still safe under all these constraints, but also to suggest the benchmarks with best chances to be probed at the next LHC run. This kind of “pragmatism” is clearly well in accord with the spirit of the present work, and constitutes the main reason this has been chosen to provide benchmark points for the following numerical study. Here, if possible, an even more extreme attitude has been taken: among the proposed scenarios, only the ones in which the new, mostly singlet like, neutral scalar is *lighter* than the SM-like Higgs boson. With this additional constraint, the resulting benchmark points are three:

A.1 Scenario			
$M_{H_{\text{light}}}, M_{h_{\text{SM}}}, M_H$	90.3 GeV	126.8 GeV	341.3 GeV
$M_{A_1}, M_{A_2} = M_{A_s}, M_A$	118.5 GeV	346.7 GeV	
$ \mathcal{R}_{H_1 h_s}^S ^2, \mathcal{R}_{A_1 a_s}^{P\star} ^2$	0.97	0.94	
$\mu_{\tau\tau}, \mu_{bb}$	1.09	1.08	
$\mu_{ZZ}, \mu_{WW}, \mu_{\gamma\gamma}$	0.85	0.85	0.88
$\tan\beta, \lambda, \kappa$	1.66	0.64	0.11
$A_\lambda, A_\kappa, \mu_{\text{eff}}$	338.0 GeV	-71.2 GeV	162.8 GeV
A_t, A_b, A_τ	181.1 GeV	-1530 GeV	87.2 GeV
M_1, M_2, M_3	440 GeV	814 GeV	1710 GeV
$M_{Q_3} = M_{t_R}, M_{b_R}$	1827 GeV	3 TeV	
$M_{L_3} = M_{\tau_R}, M_{\text{SUSY}}$	1663.7 GeV	3 TeV	

Table 4.1. Relevant parameters defining scenario A.1. The values $|\mathcal{R}_{H_1 h_s}^S|^2, |\mathcal{R}_{A_1 a_s}^{P\star}|^2$ should be intended here, with a slight abuse of notation, as one-loop quantities, *i.e.* the absolute squares of the rotation matrices which relates tree level states to *one-loop corrected* states.

- **A.1 point:** Tab. 4.1. Both lightest scalar and pseudoscalar Higgs states are lighter than the SM-like Higgs Boson $H_1 \equiv h$. The lightest state is the CP even one, H_1 . Both scalars are nearly singlet like, while heaviest ones resembles the

heavy H and A scalars of the MSSM in the decoupling limit. The value chosen for $\tan\beta$ is quite small. The sign of μ_{eff} is positive.

- **A.2 point:** Tab. 4.2. Like in **A.1** point, both lightest scalar and pseudoscalar Higgs states are lighter than the SM-like Higgs Boson. Here the CP odd state is the lightest. The scalar is mostly singlet like, with increased mixing to doublets than **A.1** point. Also in this benchmark point the value of $\tan\beta$ is low, but here μ_{eff} is taken to be negative. This benchmark point could explain the LEP excess in SM Higgs boson searches [135]. Large values of the trilinear couplings in the third generation squark sector allow large mixings.
- **D.2 point:** Tab. 4.3. As **A.1** but moderately high value of $\tan\beta$.

A.2 Scenario			
$M_{H_{\text{light}}}, M_{h_{\text{SM}}}, M_H$	98.6 GeV	125.6 GeV	325.9 GeV
M_{A_s}, M_A	78.6 GeV	325.5 GeV	
$ \mathcal{R}_{H_1 h_s}^S ^2, \mathcal{R}_{A_1 a_s}^{P\star} ^2$	0.89	0.96	
$\mu_{\tau\tau}, \mu_{bb}$	1.05	0.93	
$\mu_{ZZ}, \mu_{WW}, \mu_{\gamma\gamma}$	0.86	0.87	0.90
$\tan\beta, \lambda, \kappa$	1.69	0.56	0.12
$A_\lambda, A_\kappa, \mu_{\text{eff}}$	-259.2 GeV	-22.8 GeV	-147.4 GeV
A_t, A_b, A_τ	1927.4 GeV	-948.9 GeV	1621.4 GeV
M_1, M_2, M_3	756 GeV	647 GeV	2425 GeV
$M_{Q_3} = M_{t_R}, M_{b_R}$	2468.3 GeV	3 TeV	
$M_{L_3} = M_{\tau_R}, M_{\text{SUSY}}$	1623.0 GeV	3 TeV	

Table 4.2. Relevant parameters defining scenario A.2.

D.2 Scenario			
$M_{H_{\text{light}}}, M_{h_{\text{SM}}}, M_H$	112.0 GeV	126.3 GeV	1288.2 GeV
M_{A_s}, M_A	61.5 GeV	1287.4 GeV	
$ \mathcal{R}_{H_1 h_s}^S ^2, \mathcal{R}_{A_1 a_s}^{P\star} ^2$	0.63	1	
$\mu_{\tau\tau}, \mu_{bb}$	0.73	0.62	
$\mu_{ZZ}, \mu_{WW}, \mu_{\gamma\gamma}$	0.90	1.03	1.06
$\tan\beta, \lambda, \kappa$	6.36	0.47	0.14
$A_\lambda, A_\kappa, \mu_{\text{eff}}$	1217.1 GeV	19.6 GeV	195.3 GeV
A_t, A_b, A_τ	-1804.6 GeV	-1196.8 GeV	1704.8 GeV
M_1, M_2, M_3	417.2 GeV	237.5 GeV	2362.2 GeV
$M_{Q_3} = M_{t_R}, M_{b_R}$	967.8 GeV	3 TeV	
$M_{L_3} = M_{\tau_R}, M_{\text{SUSY}}$	2491.6 GeV	3 TeV	

Table 4.3. Relevant parameters defining scenario D.2.

4.6.3 Results

In this section results for the different scenarios presented in previous sections are shown (Table 4.4). They refer to semi-inclusive bottom-light Higgs production at LHC, with 13 TeV in the center of mass of the colliding beams. For definiteness, a cut on the transverse momentum of the b -jet at $p_T > 25$ GeV has been applied,

Scenario	σ_{LO} (fb)	σ_{NLO} (fb)	K factors
A1	98.1	77.0	0.79
A2	46.0	35.8	0.78
D2	217	175	0.81

Table 4.4. Predictions for the semi inclusive NMSSM h_1^0 production cross sections in association with a $p_T > 25$ GeV b -jet at 13 TeV LHC, both at LO and EW NLO for benchmark points defined in the text.

accordingly to the flavour scheme adopted in the calculation. In order to investigate the possibility of an approximation of the complete results in term of different sources of one-loop corrections, every single contribution is here given in detail. As previously stressed, the various contributions are not all separately gauge independent, nor IR finite, so results are given as a function of the photon mass regulator λ . The K factor is conventionally defined as

$$K \equiv \frac{\sigma_{\text{NLO}}}{\sigma_{\text{LO}}} .$$

Figures 4.8, 4.9 and 4.10 describe the impact of one-loop electroweak corrections

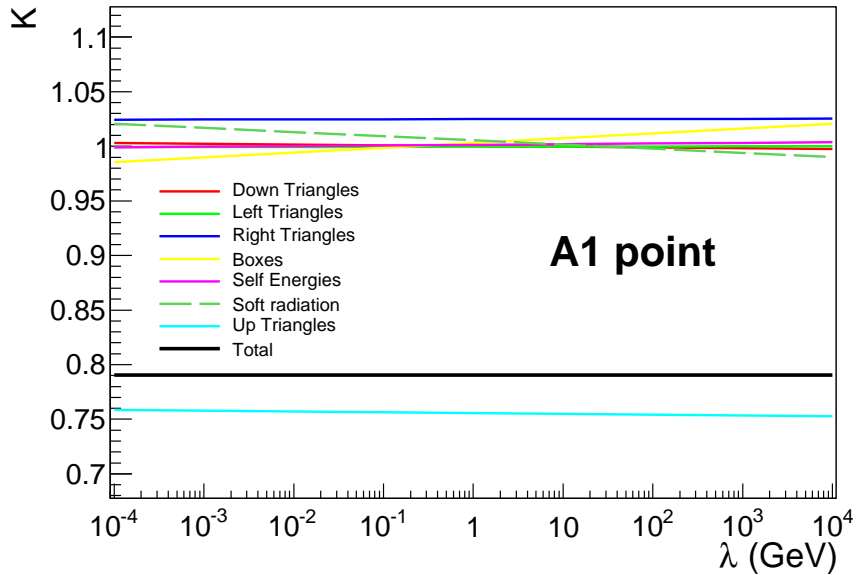


Figure 4.8. Results for case A.1 in terms of K factors. The dependence of the single virtual and real contributions on the soft photon mass regulator λ cancel in the total, UV and IR finite one-loop complete EW correction, shown in black.

for benchmark scenarios previously described. The several virtual contributions are displayed in different colors with a straight line, while the real soft photon correction is shown as a green dashed line. The complete correction is shown in black. The dominant contribution comes from Up Triangles, modifying the bbH_1 vertex in the t -channel. The second subdominant contribution is represented by Right Triangles, which also modify the bbH_1 vertex but in the s -channel. All other contributions are

completely negligible. It is important to stress that most of the IR dependence on the photon mass regulator λ in the virtual sector comes from Box diagrams, which alone approximately cancel the one given by the real contribution: the others indeed are roughly λ independent. This allows one to interpret the sum of the two bbH_1 vertex corrections as a genuine, well defined approximation to the complete result, in complete analogy to the Reduced Vertex Approximation defined in [141]. Here

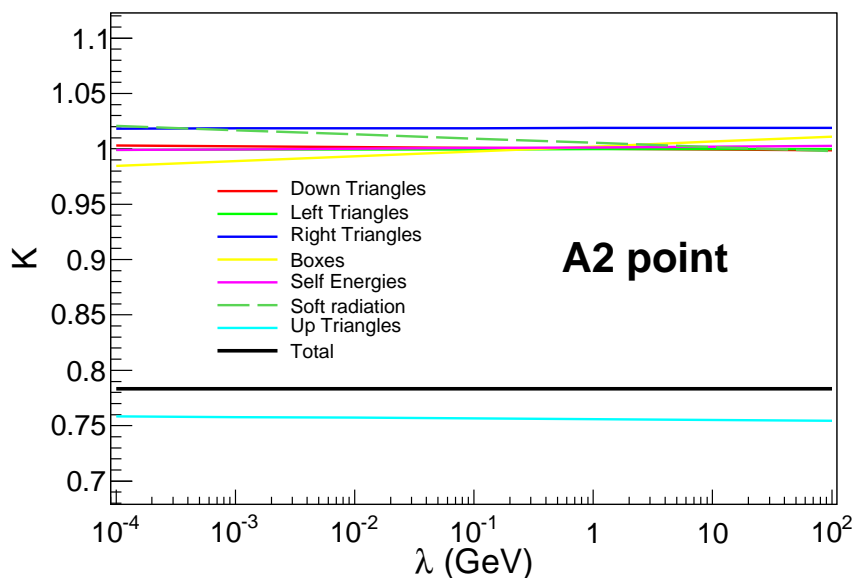


Figure 4.9. Results for case A.2 in terms of K factors.

one should notice, as it can be inspected from the figure, the magnitude of the total one-loop correction, which has a large impact on the result, roughly at the 20% level. Not surprisingly, results are similar one to each other: this follows from the fact that, in all scenarios, in order to pass present exclusion limits on light scalar states, the lightest Higgs boson is mostly singlet-like, as already stressed. This, in turn, constrains one-loop corrections to be genuinely NMSSM ones and, given the lightness of part of the scalar spectrum, not reducible to an effective approach.

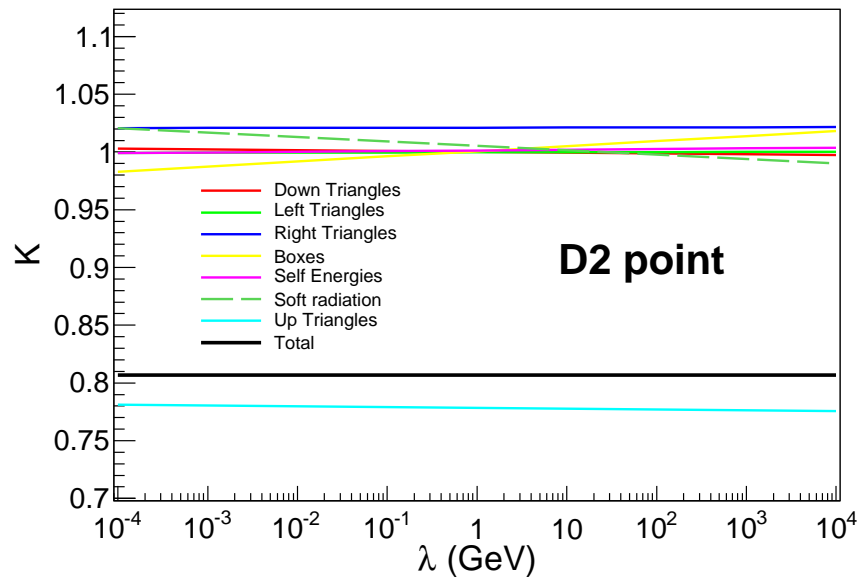


Figure 4.10. Results for case D.2 in terms of K factors.

Conclusions

In this thesis, new definitions and accurate predictions of measurable observables involving bottom quarks at the LHC have been given.

The first two have been theoretically conceived to try to furnish to the LHC experimental community the possibility to measure the \mathcal{A}_b parameter, whose value enters the SM theoretical prediction for A_{FB}^b , thus trying to address the outstanding LEP paradox.

At LHC, in the associated production of a b -quark and a Z -boson, the definition of $A_Z^{pol,b}$ is given through the formula

$$A_Z^{pol,b} \equiv \frac{\sigma(Z_R) - \sigma(Z_L)}{\sigma(Z_R) + \sigma(Z_L)}$$

where L, R refers to the helicity of the Z -boson. The candidate has computed its *theoretical* SM prediction at LO, and has proved its strong stability under scale variations and pdf set choices. Taking these as approximations to its theoretical uncertainties, $A_Z^{pol,b}$ at LHC has been predicted to be

$$A_Z^{pol,b} = -0.512 \pm 0.003_{\text{scale}} \pm 0.008_{\text{pdf}}.$$

This high level of theoretical precision should be compared to the remarkably larger deviation from its SM value $A_Z^{pol,b}$ could provide if found compatible to LEP measurements of A_{FB}^b , which could be as high as $\approx 8\%$.

The study of leptonic decays of the Z -boson in this same process has allowed the candidate to define a new asymmetry observable, called $A_{FB}^{b,\text{LHC}}$

$$A_{FB}^{b,\text{LHC}} \equiv \frac{\sigma(\mathcal{D}_F) - \sigma(\mathcal{D}_B)}{\sigma(\mathcal{D}_F) + \sigma(\mathcal{D}_B)},$$

where the reference axis defining the Forward-Backward (FB) directions is the b -quark momentum in the Z -rest frame. The candidate has exhaustively proved that this observable is proportional, at LO, to the LEP A_{FB}^b through a computable, completely kinematical factor k . He has studied the theoretical uncertainties associated to scale variations and pdf set choice also in this case, and found them again to be nearly negligible

$$A_{FB}^{b,\text{LHC}} = -0.0370_{-0.0006}^{+0.0003}{}^{\text{scale}} \pm 0.0002_{\text{pdf}}.$$

The candidate has also studied the concrete experimental procedure needed to measure $A_{FB}^{b,\text{LHC}}$: he has defined the mean Q_{FB} charge observable at LHC to be

$$\langle Q_{FB} \rangle \equiv \langle (-1)^{FB} Q_{\text{jet}} \rangle.$$

This has allowed the candidate to complete a feasibility study for a realistic measurement of $A_{FB}^{b,\text{LHC}}$, setting an upper bound to major experimental uncertainties affecting it. In particular he has shown that the relative statistical uncertainty at 14 TeV with an integrated luminosity of 3 ab^{-1} cannot be higher than 4%, while the upper bound on the systematic uncertainty, mainly coming from ISR, is 2%.

The last observable studied by the candidate has been the production cross section of a light Higgs boson in association with exactly one b -quark in the context of the NMSSM. This has been computed at one-loop accuracy, with related checks of UV and IR finiteness, enlightening a $\sim 20\%$ correction with respect to the Born prediction in allowed benchmarks scenarios. The related **Fortran** code, called *Beauty*, relies on updated computational tools, allowing an easy extension of this calculation to other processes including b -quarks and Higgs scalars as external particles.

This thesis has shown that these observables have the best chances to become little cornerstones in NP searches at the next and future Runs of LHC: they in fact give the particle physics community some means either to deepen our comprehension of the heart of the SM, through the study of one of its well known discrepancies, or to understand (or measure?) new features related to direct searches of Supersymmetric particles in most appealing benchmark scenarios of the well motivated NMSSM.

Appendix A

Useful results

The derivation of the counterterms to the CP-even and odd scalar matrices Eq. (4.2.9) need to re-express $M_{S,P}^2$ taking explicitly into account both tadpoles of the scalar (CP-even) fields and the difference between the definition of $\tan\beta = v_u/v_d$ and the angles $\beta_{n,c}$, which rotate away from, respectively, the CP-odd and charged Higgs scalar mass matrices the Goldstone degrees of freedom. This is done in terms of the difference

$$\Delta\beta \equiv \beta - \beta_n = \beta - \beta_c$$

The results of this work for the full $\Delta\beta$ dependence of $M_{S,P}^2$ agree well with [149] with two exceptions:

$$M_{S_{11}}^2 = \frac{ec_\beta c_{\beta_B}^2}{2M_W s_W c_{\Delta\beta}^2} [t_{h_d}(2t_\beta t_{\beta_B} + 1) - t_{h_u} t_\beta] + \frac{s_\beta^2}{c_{\Delta\beta}^2} [M_{H^\pm}^2 + (M_Z^2/t_\beta^2 - M_W^2)c_{\Delta\beta}^2] + 2 \left(\frac{\lambda M_W s_W s_\beta}{e} \right)^2 \quad (\text{A.0.1})$$

$$M_{P_{22}}^2 = -3A_k k \frac{v_s}{\sqrt{2}} + \frac{t_{h_s}}{v_s} - \frac{2M_W s_W s_\beta c_\beta^2 c_{\beta_B}^2}{e v_s^2 c_{\Delta\beta}^2} [t_{h_u} + t_{h_d} t_\beta t_{\beta_B}^2] + \left(\frac{M_W s_W s_{2\beta}}{e v_s c_{\Delta\beta}} \right)^2 [M_\pm^2 - M_W^2 c_{\Delta\beta}^2] + \frac{\lambda M_W^2 s_W^2 s_{2\beta}}{e^4 v_s^2} [2\lambda M_W^2 s_W^2 s_{2\beta} + 3ke^2 v_s^2] \quad (\text{A.0.2})$$

This results are confirmed by [143], which however has other mismatching results.

Given the complete dependence on $\Delta\beta$ of $M_{S,P}^2$, the related counterterms (CT) are easily derived by expanding the independent, bare observables through their own independent CTs, and imposing Born level relations only after having retained terms linear in these CTs. Results of this work regarding scalar mass CTs are completely in agreement with [143].

Appendix B

The code *Beauty*

Beauty is a collection of Mathematica [146] and Fortran routines written to compute EW 1 loop corrections for the cross section of the process $bg \rightarrow bh_0$ in the NMSSM at hadron colliders. It has been generated using FeynArts [148] and FormCalc, for which an NMSSM implementation with *explicit* EW counterterms for this process and for the Higgs sector, plus the possibility of hadronic cross section calculations (through a Fortran NMSSM model file), were not yet available.

B.1 FeynArts Model file [147]

The Mathematica model file `FullNMSSM_Z3.mod` follows from a tree level-only model file generated with `FeynRules` fed by a modified version of the `nmssm.fr` model file written by B. Fuks, to which the Z_3 discrete symmetry has been imposed from the beginning to avoid time consumption in one-loop calculations in this SUSY model. It contains complete counterterms for the EW and Higgs sectors, plus explicit counterterms for bbh and bbg vertices needed for EW one-loop corrections in the 5FNS process $bg \rightarrow bh$, in a mixed OS – $\overline{\text{DR}}$ renormalization scheme [149].

Before loading the model, if one is interested in a completely analytical computation, the variable `M$ExtParams` should be initialized to the empty set

$$\text{M\$ExtParams} = \{\}.$$

Of course, as usual in one-loop calculations, to obtain exact cancellations of UV

divergencies one should impose tree level relations between parameters of the model (Yukawa couplings and fermion masses, Higgs boson masses, Gauge boson masses and gauge couplings, etc.).

B.1.1 Checks of the model

Two kinds of checks has been verified. The first one is the usual UV finiteness check, which has been verified separately in different subsets of one-loop graphs relevant for the aforementioned process (Bottom quark Self Energy, Triangles modifying the bbh vertex, Triangles modifying the bbg vertex with only EW insertions). It has to be noted that, after this check, IR finiteness of $bg \rightarrow bh_0$ amplitudes was automatically achieved (this has been verified using the `FormCalc` intrinsic routines for soft photons factors). The second kind of checks, particularly useful to verify the correctness of the renormalization procedure of the Higgs Scalar Self Energies, has been to verify the equality between the neutral and charged Goldstone Bosons Self Energies at zero momentum. It has to be noted that these checks have not only allowed to test the present model and its one loop structure, but also to find small formal bugs present both in old versions of `FormCalc` and in the `FeynRules` routine `WriteFeynArtsOutput`, needed to export the `FeynRules` model in a `FeynArts` one. For details see Section 4.6.1.

B.1.2 Counterterms implementation

Here definitions of renormalization constants not genuinely of NMSSM type are skipped (since they are taken from other `FeynArts` models). This implementation follows conventions of [149].

Ren. Const.	Description	Ren. Scheme adopted
divdZH[1,j]	Diagonal Field RC for scalar mass eigenstates	$\overline{\text{DR}}$
dZHu,dZHd,dZHS	Field RC for scalar doublets H_u , H_d and singlet S	$\overline{\text{DR}}$
MaUS2	Auxiliary matrix of squares of entries of the mixing matrix U_S , useful to derive expression for scalar field CT	-
dZHH1[1,j ₁ ,j ₂]	General Field RC for scalar mass eigenstates, see also <code>divdZH</code>	$\overline{\text{DR}}$
dMHpsq	Mass RC for the charged scalar	OS
dThme	3d vector of tadpoles of scalar mass eigenstates	OS
dThgau	3d vector of tadpoles of scalar gauge eigenstates	OS
dSEPScaFull[i,j]	Redundant, Self Energies of the Pseudo Scalars mass eigenstates	-
dMPij _{sq}	CTs for the ij entry of $\mathcal{M}_{\mathcal{P}}$, the mass squared matrix obtained after rotating out the Goldstone boson from $\tilde{\mathcal{M}}_{\mathcal{P}}$	$\overline{\text{DR}}$
dtbovtb	$\delta \tan \beta / \tan \beta$	$\overline{\text{DR}}$
dNM1m	$\delta \lambda$	$\overline{\text{DR}}$
dMC22	CT for the 22 entry of the chargino mass matrix in gauge basis	$\overline{\text{DR}}$
dvs	δv_s	$\overline{\text{DR}}$
dMN55	CT for the 55 entry of the neutralino mass matrix in gauge basis	$\overline{\text{DR}}$
dNMk	δk	$\overline{\text{DR}}$
dNMAk	δA_k	$\overline{\text{DR}}$
dMS2[i,j]	CT for the ij entry of the scalar mass matrix in gauge basis \mathcal{M}_S	mixed

B.1.3 Restrictions

- **NoQuarkMixing**: ensures no mixing between generations both in the charged currents Vff , Sff (to be used only with $V_{CKM} = \mathbb{I}$) and in the neutral scalar Sff vertices.
- **NoQuarkSquarkMixing**: as before, but in the SUSY versions of the vertices $\chi f \tilde{q}$
- **NoSfermMixing**: no mixing between generations when two sfermions are involved in the vertex.

B.2 Fortran Model files

The files `modelNMSSM.F` and `modelNMSSM.h` are the fortran implementations of the NMSSM model with Z_3 symmetry of [86,142], with some additional useful definitions (where needed) when dealing with for one-loop calculations [149]. At present, only a diagonal Pontecorvo matrix can be used, which has to be directly imposed with the compiler directive

```
#define NO_PMNS.
```

The variable definitions are as follows:

B.2.1 Basic Parameters

Variable	Description	Equivalent variables
aEWM1	Inverse of α_{em}	
g1, g2	Gauge couplings of $U(1)_Y, SU(2)_L$	
yd, yu, ye	3x3 complex yukawa matrices	yd3x3=yd(3,3), etc. for 3rd family
vev	EW v.e.v ($= \sqrt{v_u^2 + v_d^2}$)	
vu, vd, vs	Vacuum expectation values of scalar doublets H_u, H_d and singlet S .	
tb,beta	$\tan \beta = v_u/v_d$	
PMNS	3x3 complex neutrinos Pontecorvo matrix	
Mino	3d vector of gauginos masses	RMx1, RMx2, RMx3

B.2.2 Intrinsic NMSSM parameters

Variable	Description	Equivalent variables
NM1m	Coupling λ	
NMk	Coupling k	
NMA1	Trilinear coupling A_λ	
NMAk	Trilinear coupling A_k	

B.2.3 Higgs sector masses and mixings

The code follows the convention that mass eigenstates are labelled by inverse mass order (basically to be coherent with the usual identification of the neutral Goldstone boson $G_0 \equiv A_3$). In any case the directive `MASSORDER` allows to change this convention (changing consequently the definition of G_0).

Variable	Description	Equivalent variables
MHiggs	Higgs scalar and pseudoscalar masses	MH0,MxA0; Mh01, Mh02, Mh03 and MxA01 ,MxA02
MHiggs1L	one-loop scalar masses	Mh03Loop
MShGauge	\mathcal{M}_S , 3x3 complex mass squared scalar matrix in gauge basis	
MPsq11,MPsq12,MPsq22	Entries of \mathcal{M}_P , the complex mass squared pseudoscalar matrix in gauge basis after rotating out the Goldstone Boson G_0	
US,UP	3x3 complex matrices diagonalizing the scalar and pseudoscalar mass squared matrices \mathcal{M}_S and $\tilde{\mathcal{M}}_P$	USixj; UP31,UP32
RP	3x3 complex matrix diagonalizing the pseudoscalar mass squared matrix \mathcal{M}_P obtained after rotating out the Goldstone Boson from $\tilde{\mathcal{M}}_P$	

B.2.4 Gauginos masses and mixings

Variable	Description	Equivalent variables
Mch	2d vector of chargino masses	Mch1,Mch2
MchGauge	Chargino mass matrix in gauge basis	
VV, UU	Complex matrices diagonalizing chargino mass matrix	
Mneu	5d vector of neutralino masses	Mneu1,Mneu2, ...
MneuGauge	Neutralino mass matrix in gauge basis	
NN	Complex matrix diagonalizing neutralino mass matrix	

B.2.5 Sfermions, soft SUSY breaking parameters

Variable	Description	Equivalent variables
td, tu, te	3x3 trilinear couplings matrices for down, up squarks and sleptons	
mQQ2, mLL2	3x3 soft squared masses matrices for squarks and sleptons $SU(2)_L$ doublets	
mUU2, mDD2, mEE2	3x3 soft squared masses matrices for squarks and sleptons $SU(2)_L$ singlets	

B.2.6 Sfermions, masses and mixings

Variable	Description	Equivalent variables
<code>Msn</code>	3d vector of sneutrino masses	<code>Msn1,Msn2,Msn3</code>
<code>Rn</code>	3x3 complex vector of sneutrino masses	
<code>Msl, Msu, Msd</code>	6d vectors of charged sleptons, up and down squarks masses	<code>Msl1,Msl2,...</code>
<code>Rl, Ru, Rd</code>	6x6 complex matrices diagonalizing squared mass matrices of charged sleptons, up and down squarks	<code>RlL, RlR,...</code> are 3x6 matrices parametrizing the L,R relative submatrices

B.2.7 Routines description

- `ModelDdefaults`: Calls `SMDefaults` and initialize NMSSM specific variables.
- `ModelConstIni`: Calls `SMConstIni` and sets some internal parameters. It reads also relevant NMSSM parameters from an input files (`spectr.dat`) following SLHA conventions (interfaced with `SLHALib`).
- `ModelVarIni`: Calls `SMVarIni` and relevant routines for diagonalization in different sectors.

It has to be noted that the routine `PHiggsMassesTree`, which diagonalizes the pseudoscalar mass matrix, makes use of a slightly modified version of the `FormCalc` intrinsic function `SEigensystem`, which orders eigenvalues by absolute value than by real part (in order to avoid possible ordering issues due to tiny negative masses assigned to the Goldstone Boson due to numerical precision). Also to be noted the fact that sfermion masses are not ordered, to keep track of the relative generation index already at the diagrammatic level.

B.3 Change of variables in lumi_hadron.F

In order to optimize the integration procedure when dealing with hadron cross sections calculations (in particular with gluon pdfs at modern hadron colliders, which increase rapidly at small x values), a simple change of variables has been found to be useful. Given the usual integration measure for hadron cross sections:

$$\int dx_1 dx_2 \frac{\tilde{f}_1(x_1)}{x_1} \frac{\tilde{f}_2(x_2)}{x_2},$$

the intrinsic `FormCalc` integration variable system, called (X,T) , can be interpreted as the following chain of changes of variables:

$$\begin{aligned} (x_1, x_2) &\xrightarrow[\tau = x_1 x_2]{x = x_1} (x, \tau) \xrightarrow[T = \sqrt{\tau}]{X = \frac{x-\tau}{1-\tau}} (X, T) & \text{(B.3.1)} \\ x &\in \{\tau, 1\}, \tau \in \{\tau_0, 1\} \\ X &\in \{0, 1\}, T \in \{T_0, 1\} \end{aligned}$$

after which the integration measure becomes (with a mixed variable set choice that renders it cleaner)

$$\propto \int dT dX (1 - \tau) \frac{\tilde{f}_1}{x} \frac{\tilde{f}_2}{T}. \quad \text{(B.3.2)}$$

From the numerical integration point of view, it would be very welcome to choose a variable set which can model the inverse power low behaviour in x and T of Eq. B.3.2. This is achieved recognising in the denominator xT a logarithmic Jacobian in these two variables, that suggests to substitute the third variable set of Eq. B.3.1 by

$$\begin{aligned} (x, \tau) &\xrightarrow[\tilde{T} = 1 - \frac{\ln \tau}{\ln \tau_0}]{\tilde{X} = 1 - \frac{\ln x}{\ln \tau}} (\tilde{X}, \tilde{T}) & \text{(B.3.3)} \\ \tilde{X} &\in \{0, 1\}, \quad \tilde{T} \in \{0, 1\} \end{aligned}$$

after which the integration measure becomes

$$\propto \int d\tilde{T} d\tilde{X} \ln \tau_0 \ln \tau \tilde{f}_1 \tilde{f}_2 = \int d\tilde{T} d\tilde{X} \ln^2 \tau_0 (1 - \tilde{T}) \tilde{f}_1 \tilde{f}_2. \quad \text{(B.3.4)}$$

With this variable choice a usual `Vegas` session computing the hadronic cross section for the process $b g \rightarrow b h_0$ has an increased efficiency of a factor $\simeq 15\%$. The variables \tilde{T}, \tilde{X} are called in the code as T, X with some kind of abuse of notation.

Bibliography

- [1] G. Aad *et al.*, ATLAS Collaboration, Phys. Lett. B **710** (2012) 49 [arXiv:1202.1408 [hep-ex]].
- [2] S. Chatrchyan *et al.*, CMS Collaboration, [arXiv:1202.1488 [hep-ex]].
- [3] [ALEPH and CDF and D0 and DELPHI and L3 and OPAL and SLD and LEP Electroweak Working Group and Tevatron Electroweak Working Group and SLD Electroweak and Heavy Flavour Groups Collaborations], arXiv:1012.2367 [hep-ex].
- [4] R. M. Barnett, H. E. Haber and D. E. Soper, Nucl. Phys. B **306** (1988) 697.
- [5] M. J. G. Veltman, Nucl. Phys. B **123**, 89 (1977).
- [6] Y. Fukuda *et al.*, Super-Kamiokande Collaboration, Phys. Rev. Lett. **81** (1998) 1562 [hep-ex/9807003].
- [7] L. Evans and P. Bryant, JINST **3** (2008) S08001.
- [8] G. Aad *et al.*, ATLAS Collaboration, JINST **3** (2008) S08003.
- [9] S. Chatrchyan *et al.*, CMS Collaboration, JINST **3** (2008) S08004.
- [10] A. A. Alves, Jr. *et al.*, LHCb Collaboration, JINST **3** (2008) S08005.
- [11] K. Aamodt *et al.*, ALICE Collaboration, JINST **3** (2008) S08002.
- [12] W. Lampl, S. Laplace, D. Lelas, P. Loch, H. Ma, S. Menke, S. Rajagopalan and D. Rousseau *et al.*, ATL-LARG-PUB-2008-002.
- [13] ATLAS Collaboration, ATLAS-CONF-2010-005.
- [14] M. Cacciari, G. P. Salam and G. Soyez, JHEP **0804** (2008) 063 [arXiv:0802.1189 [hep-ph]].
- [15] M. Cacciari, G. P. Salam and G. Soyez, Eur. Phys. J. C **72** (2012) 1896 [arXiv:1111.6097 [hep-ph]].

-
- [16] ATLAS Collaboration, ATL-PHYS-PUB-2014-014 (2014).
- [17] F. I. Olness and W. K. Tung, Nucl. Phys. B **308** (1988) 813.
- [18] D. A. Dicus and S. Willenbrock, Phys. Rev. D **39** (1989) 751.
- [19] J. M. Campbell, R. K. Ellis, F. Maltoni and S. Willenbrock, Phys. Rev. D **67** (2003) 095002 [hep-ph/0204093].
- [20] ALEPH Collaboration, CDF Collaboration, D0 Collaboration, DELPHI Collaboration, L3 Collaboration, OPAL Collaboration, SLD Collaboration, LEP Electroweak Working Group, Tevatron Electroweak Working Group, SLD electroweak heavy flavour groups, [arXiv:1012.2367v2 [hep-ex]] (2011).
- [21] The ATLAS Collaboration, ATLAS-CONF-2014-009.
- [22] CMS Collaboration, CMS-PAS-HIG-14-009.
- [23] ALEPH and DELPHI and L3 and OPAL and SLD and LEP Electroweak Working Group and SLD Electroweak Group and SLD Heavy Flavour Group Collaborations, Phys. Rept. **427** (2006) 257 [hep-ex/0509008].
- [24] M. S. Chanowitz, Phys. Rev. Lett. **87** (2001) 231802 [hep-ph/0104024].
- [25] X. -G. He and G. Valencia, Phys. Rev. D **68** (2003) 033011 [hep-ph/0304215].
- [26] L. Da Rold, JHEP **1102** (2011) 034 [arXiv:1009.2392 [hep-ph]].
- [27] J. Cao and J. M. Yang, JHEP **0812** (2008) 006 [arXiv:0810.0751 [hep-ph]].
- [28] R. Barbieri and A. Strumia, hep-ph/0007265.
- [29] W. J. Stirling and E. Vryonidou, JHEP **1207** (2012) 124 [arXiv:1204.6427 [hep-ph]].
- [30] D. A. Ross and M. J. G. Veltman, Nucl. Phys. B **95**, 135 (1975); M. J. G. Veltman, Nucl. Phys. B **123**, 89 (1977).
- [31] F. Jegerlehner, Prog. Part. Nucl. Phys. **27**, 1 (1991).
- [32] S. Lai, ATLAS and CMS Collaboration, EPJ Web Conf. **49** (2013) 09005 [arXiv:1303.4064 [hep-ex]].
- [33] S. Schael *et al.*, ALEPH and DELPHI and L3 and OPAL and LEP Working Group for Higgs Boson Searches Collaborations, Eur. Phys. J. C **47** (2006) 547 [hep-ex/0602042].
- [34] J. Beringer *et al.*, Particle Data Group Collaboration, Phys. Rev. D **86** (2012) 010001.

- [35] J. M. Campbell, R. K. Ellis, F. Maltoni and S. Willenbrock, Phys. Rev. D **69** (2004) 074021 [hep-ph/0312024].
- [36] E. Mirkes, Nucl. Phys. B **387** (1992) 3.
- [37] E. Mirkes and J. Ohnemus, Phys. Rev. D **51** (1995) 4891 [hep-ph/9412289].
- [38] J. Pumplin, D. R. Stump, J. Huston, H. L. Lai, P. M. Nadolsky and W. K. Tung, JHEP **0207** (2002) 012 [hep-ph/0201195].
- [39] A. Denner, S. Dittmaier, T. Kasprzik and A. Muck, JHEP **1106** (2011) 069 [arXiv:1103.0914 [hep-ph]].
- [40] S. J. Brodsky and X. -G. Wu, [arXiv:1204.1405 [hep-ph]].
- [41] A. D. Martin, W. J. Stirling, R. S. Thorne and G. Watt, Eur. Phys. J. C **63** (2009) 189 [arXiv:0901.0002 [hep-ph]].
- [42] R. D. Ball, V. Bertone, F. Cerutti, L. Del Debbio, S. Forte, A. Guffanti, J. I. Latorre and J. Rojo *et al.*, Nucl. Phys. B **849** (2011) 296 [arXiv:1101.1300 [hep-ph]].
- [43] G. Aad *et al.*, ATLAS Collaboration, Phys. Lett. B **706** (2012) 295 [arXiv:1109.1403 [hep-ex]].
- [44] M. Beccaria, C. M. Carloni Calame, G. Macorini, E. Mirabella, F. Piccinini, F. M. Renard and C. Verzegnassi, Phys. Rev. D **77** (2008) 113018 [arXiv:0802.1994 [hep-ph]].
- [45] M. Beccaria, C. M. Carloni Calame, G. Macorini, G. Montagna, F. Piccinini, F. M. Renard and C. Verzegnassi, Eur. Phys. J. C **53** (2008) 257 [arXiv:0705.3101 [hep-ph]].
- [46] A. Denner, S. Dittmaier, T. Kasprzik and A. Muck, JHEP **0908** (2009) 075 [arXiv:0906.1656 [hep-ph]].
- [47] M. Beccaria, F. M. Renard and C. Verzegnassi, LC-TH-2002-005 [hep-ph/0203254].
- [48] M. Beccaria, M. Melles, F. M. Renard, S. Trimarchi and C. Verzegnassi, Int. J. Mod. Phys. A **18** (2003) 5069 [hep-ph/0304110].
- [49] G. J. Gounaris and F. M. Renard, Acta Phys. Polon. B **42** (2011) 2107 [arXiv:1106.2707 [hep-ph]].

- [50] J. Baglio, M. Beccaria, A. Djouadi, G. Macorini, E. Mirabella, N. Orlando, F. M. Renard and C. Verzegnassi, Phys. Lett. B **705** (2011) 212 [arXiv:1109.2420 [hep-ph]].
- [51] M. Beccaria, G. Macorini, G. Panizzo and C. Verzegnassi, Phys. Lett. B **730** (2014) 149
- [52] M. Beccaria, N. Orlando, G. Panizzo, F. M. Renard and C. Verzegnassi, Phys. Lett. B **713** (2012) 457
- [53] A. Blondel, B. W. Lynn, F. M. Renard and C. Verzegnassi, Nucl. Phys. B **304** (1988) 438.
- [54] B. W. Lynn and C. Verzegnassi, Phys. Rev. D **35** (1987) 3326.
- [55] K. Abe *et al.*, SLD Collaboration, SLAC-PUB-6513 (94/05,rec.Aug.) 9 p
- [56] K. Abe *et al.*, SLD Collaboration, Phys. Rev. Lett. **84** (2000) 5945 [hep-ex/0004026].
- [57] M. Baak, M. Goebel, J. Haller, A. Hoecker, D. Kennedy, R. Kogler, K. Moenig and M. Schott *et al.*, Eur. Phys. J. C **72** (2012) 2205 [arXiv:1209.2716 [hep-ph]].
- [58] S. Schael *et al.*, ALEPH and DELPHI and L3 and OPAL and SLD and LEP Electroweak Working Group and SLD Electroweak Group and SLD Heavy Flavour Group Collaborations, Phys. Rept. **427** (2006) 257 [hep-ex/0509008].
- [59] A. Freitas and Y. -C. Huang, JHEP **1208** (2012) 050 [arXiv:1205.0299 [hep-ph]].
- [60] J. Stirling and E. Vryonidou, [arXiv:1302.1365 [hep-ph]].
- [61] A. Czarnecki and J. H. Kuhn, Phys. Rev. Lett. **77** (1996) 3955 [hep-ph/9608366].
- [62] A. Belyaev, N. D. Christensen and A. Pukhov, Comput. Phys. Commun. **184** (2013) 1729 [arXiv:1207.6082 [hep-ph]].
- [63] G. Aad *et al.*, ATLAS Collaboration, Phys. Lett. B **706** (2012) 295 [arXiv:1109.1403 [hep-ex]].
- [64] R. Akers *et al.*, OPAL Collaboration, Z. Phys. C **67** (1995) 365.
- [65] D. Krohn, M. D. Schwartz, T. Lin and W. J. Waalewijn, Phys. Rev. Lett. **110** (2013) 21, 212001 [arXiv:1209.2421 [hep-ph]].

- [66] R. D. Field and R. P. Feynman, Nucl. Phys. B **136** (1978) 1.
- [67] R. Barate *et al.*, ALEPH Collaboration, Phys. Lett. B **426** (1998) 217.
- [68] B. Nachman, ATLAS Collaboration, [arXiv:1409.0318 [hep-ex]].
- [69] J. Alwall, M. Herquet, F. Maltoni, O. Mattelaer and T. Stelzer, JHEP **1106** (2011) 128 [arXiv:1106.0522 [hep-ph]].
- [70] T. Sjostrand, S. Mrenna and P. Z. Skands, JHEP **0605** (2006) 026 [hep-ph/0603175].
- [71] J. de Favereau, C. Delaere, P. Demin, A. Giammanco, V. Lemaître, A. Mertens and M. Selvaggi, [arXiv:1307.6346 [hep-ex]].
- [72] ATLAS Collaboration, ATLAS-CONF-2011-141.
- [73] ATLAS Collaboration, ATLAS-CONF-2012-043.
- [74] ATLAS Collaboration, ATLAS-CONF-2012-100.
- [75] J. Baglio, M. Beccaria, A. Djouadi, G. Macorini, E. Mirabella, N. Orlando, F. M. Renard and C. Verzegnassi, Phys. Lett. B **705** (2011) 212 [arXiv:1109.2420 [hep-ph]].
- [76] ATLAS Collaboration, ATLAS-CONF-2013-014.
- [77] CMS Collaboration, CMS-PAS-HIG-13-005.
- [78] A. Djouadi, L. Maiani, G. Moreau, A. Polosa, J. Quevillon and V. Riquer, [arXiv:1307.5205 [hep-ph]].
- [79] M. Beccaria, G. Macorini, L. Panizzi, F. M. Renard and C. Verzegnassi, Phys. Rev. D **80** (2009) 053011 [arXiv:0908.1332 [hep-ph]].
- [80] T. Plehn, Phys. Rev. D **67** (2003) 014018; S. Zhou, Phys. Rev. D **67** (2003) 075006.
- [81] B. Batell, S. Gori and L. -T. Wang, JHEP **1301** (2013) 139 [arXiv:1209.6382 [hep-ph]].
- [82] J. A. Aguilar-Saavedra, R. Benbrik, S. Heinemeyer and M. Prez-Victoria, Phys. Rev. D **88** (2013) 9, 094010 [arXiv:1306.0572 [hep-ph]].
- [83] T. Peiffer, ATLAS and CMS Collaborations, PoS DIS **2014** (2014) 136.
- [84] A. Djouadi, G. Moreau and F. Richard, Nucl. Phys. B **773** (2007) 43 [hep-ph/0610173].
- [85] D. Choudhury, T. M. P. Tait and C. E. M. Wagner, Phys. Rev. D **65** (2002)

- 053002 [hep-ph/0109097].
- [86] U. Ellwanger, C. Hugonie and A. M. Teixeira, *Phys. Rept.* **496** (2010) 1
 - [87] E. Witten, *Nucl. Phys. B* **188** (1981) 513.
 - [88] S. Dimopoulos and H. Georgi, *Nucl. Phys. B* **193** (1981) 150.
 - [89] E. Witten, *Phys. Lett. B* **105** (1981) 267.
 - [90] R. K. Kaul and P. Majumdar, *Nucl. Phys. B* **199** (1982) 36.
 - [91] N. Sakai, *Z. Phys. C* **11** (1981) 153.
 - [92] J. R. Ellis, S. Kelley and D. V. Nanopoulos, *Phys. Lett. B* **260** (1991) 131.
 - [93] C. Giunti, C. W. Kim and U. W. Lee, *Mod. Phys. Lett. A* **6** (1991) 1745.
 - [94] U. Amaldi, W. de Boer and H. Furstenuau, *Phys. Lett. B* **260** (1991) 447.
 - [95] P. Langacker and M. x. Luo, *Phys. Rev. D* **44** (1991) 817.
 - [96] H. Pagels and J. R. Primack, *Phys. Rev. Lett.* **48** (1982) 223.
 - [97] H. Goldberg, *Phys. Rev. Lett.* **50** (1983) 1419.
 - [98] P. Fayet, *Nucl. Phys. B* **90** (1975) 104.
 - [99] P. Fayet and S. Ferrara, *Phys. Rept.* **32** (1977) 249.
 - [100] H. P. Nilles, *Phys. Rept.* **110** (1984) 1.
 - [101] S. P. Martin, *Adv. Ser. Direct. High Energy Phys.* **21** (2010) 1 [hep-ph/9709356].
 - [102] D. J. H. Chung, L. L. Everett, G. L. Kane, S. F. King, J. D. Lykken and L. T. Wang, *Phys. Rept.* **407** (2005) 1 [arXiv:hep-ph/0312378].
 - [103] J. E. Kim and H. P. Nilles, *Phys. Lett. B* **138** (1984) 150.
 - [104] P. Fayet, *Phys. Lett. B* **69** (1977) 489.
 - [105] L. E. Ibanez and G. G. Ross, *Phys. Lett. B* **110** (1982) 215.
 - [106] D. V. Nanopoulos and K. Tamvakis, *Phys. Lett. B* **113** (1982) 151.
 - [107] J. R. Ellis, L. E. Ibanez and G. G. Ross, *Phys. Lett. B* **113** (1982) 283.
 - [108] J. R. Ellis, L. E. Ibanez and G. G. Ross, *Nucl. Phys. B* **221** (1983) 29.
 - [109] G. F. Giudice and A. Masiero, *Phys. Lett. B* **206** (1988) 480.
 - [110] R. Barbieri, S. Ferrara and C. A. Savoy, *Phys. Lett. B* **119** (1982) 343.
 - [111] H. P. Nilles, M. Srednicki and D. Wyler, *Phys. Lett. B* **120** (1983) 346.
 - [112] J. M. Frere, D. R. T. Jones and S. Raby, *Nucl. Phys. B* **222** (1983) 11.

- [113] A. H. Chamseddine, R. L. Arnowitt and P. Nath, *Phys. Rev. Lett.* **49** (1982) 970.
- [114] P. Nath, R. L. Arnowitt and A. H. Chamseddine, *Phys. Lett. B* **121** (1983) 33.
- [115] S. Ferrara, D. V. Nanopoulos and C. A. Savoy, *Phys. Lett. B* **123** (1983) 214.
- [116] P. Nath, R. L. Arnowitt and A. H. Chamseddine, *Nucl. Phys. B* **227** (1983) 121.
- [117] R. L. Arnowitt, A. H. Chamseddine and P. Nath, *Phys. Rev. Lett.* **50** (1983) 232.
- [118] A. I. Veselov, M. I. Vysotsky and K. A. Ter-Martirosian, *Sov. Phys. JETP* **63** (1986) 489 [*Zh. Eksp. Teor. Fiz.* **90** (1986) 838].
- [119] N. Dragon, U. Ellwanger and M. G. Schmidt, *Phys. Lett. B* **154** (1985) 373.
- [120] U. Ellwanger, N. Dragon and M. G. Schmidt, *Z. Phys. C* **29** (1985) 209.
- [121] E. Cohen, J. R. Ellis, K. Enqvist and D. V. Nanopoulos, *Phys. Lett. B* **165** (1985) 76.
- [122] J. P. Derendinger, L. E. Ibanez and H. P. Nilles, *Nucl. Phys. B* **267** (1986) 365.
- [123] P. Binetruy, S. Dawson, I. Hinchliffe and M. Sher, *Nucl. Phys. B* **273** (1986) 501.
- [124] J. R. Ellis, K. Enqvist, D. V. Nanopoulos and F. Zwirner, *Nucl. Phys. B* **276** (1986) 14.
- [125] L. E. Ibanez and J. Mas, *Nucl. Phys. B* **286** (1987) 107.
- [126] G. Costa, F. Feruglio, F. Gabbiani and F. Zwirner, *Nucl. Phys. B* **286** (1987) 325.
- [127] I. Antoniadis, J. R. Ellis, J. S. Hagelin and D. V. Nanopoulos, *Phys. Lett. B* **194** (1987) 231.
- [128] B. A. Campbell, J. R. Ellis, J. S. Hagelin, D. V. Nanopoulos and R. Ticciati, *Phys. Lett. B* **198** (1987) 200.
- [129] I. Antoniadis, J. R. Ellis, J. S. Hagelin and D. V. Nanopoulos, *Phys. Lett. B* **205** (1988) 459.
- [130] J. R. Ellis, J. S. Hagelin, S. Kelley and D. V. Nanopoulos, *Nucl. Phys. B* **311**

- (1988) 1.
- [131] J. R. Ellis, J. F. Gunion, H. E. Haber, L. Roszkowski and F. Zwirner, Phys. Rev. D **39** (1989) 844.
- [132] M. Drees, Int. J. Mod. Phys. A **4** (1989) 3635.
- [133] M. Maniatis, [arXiv:0906.0777 [hep-ph]].
- [134] LEPSUSYWG, ALEPH, DELPHI, L3 and OPAL experiments, note LEPSUSYWG/01-03.1 (<http://lepsusy.web.cern.ch/lepsusy/Welcome.html>).
- [135] R. Barate *et al.*, LEP Working Group for Higgs boson searches and ALEPH and DELPHI and L3 and OPAL Collaborations, Phys. Lett. B **565**, 61 (2003) [hep-ex/0306033].
- [136] G. Belanger, U. Ellwanger, J. F. Gunion, Y. Jiang, S. Kraml and J. H. Schwarz, JHEP **1301** (2013) 069 [arXiv:1210.1976 [hep-ph]].
- [137] D. J. Miller, 2, R. Nevzorov, P. M. Zerwas, Nucl. Phys. **B681** (2004) 3 [hep-ph/0304049].
- [138] S. F. King, M. Muhlleitner, R. Nevzorov and K. Walz, Phys. Rev. D **90** (2014) 9, 095014 [arXiv:1408.1120 [hep-ph]].
- [139] M. Badziak, M. Olechowski and S. Pokorski, [arXiv:1406.1492 [hep-ph]].
- [140] S. Dittmaier, M. Kramer, 1, A. Muck and T. Schluter, JHEP **0703** (2007) 114 [hep-ph/0611353].
- [141] M. Beccaria, G. O. Davier, G. Macorini, E. Mirabella, L. Panizzi, F. M. Renard and C. Verzegnassi, Phys. Rev. D **82** (2010) 093018 [arXiv:1005.0759 [hep-ph]].
- [142] B. C. Allanach, C. Balazs, G. Belanger, M. Bernhardt, F. Boudjema, D. Choudhury, K. Desch and U. Ellwanger *et al.*, Comput. Phys. Commun. **180**, 8 (2009) [arXiv:0801.0045 [hep-ph]].
- [143] T. Graf, R. Grober, M. Muhlleitner, H. Rzehak and K. Walz, JHEP **1210** (2012) 122 [arXiv:1206.6806 [hep-ph]].
- [144] P. A. R. Ade *et al.*, Planck Collaboration, Astron. Astrophys. **571** (2014) A16 [arXiv:1303.5076 [astro-ph.CO]].
- [145] M. S. Carena, D. Garcia, U. Nierste and C. E. M. Wagner, Nucl. Phys. B **577** (2000) 88 [hep-ph/9912516].
- [146] Wolfram Research, Inc. 2008, <http://www.wolfram.com>

- [147] N. D. Christensen and C. Duhr, *Comput. Phys. Commun.* **180** (2009) 1614 [arXiv:0806.4194 [hep-ph]].
- [148] T. Hahn, *Comput. Phys. Commun.* **140** (2001) 418 [hep-ph/0012260].
- [149] K. Ender, T. Graf, M. Muhlleitner and H. Rzehak, *Phys. Rev. D* **85** (2012) 075024 [arXiv:1111.4952 [hep-ph]].